Charles University in Prague
Faculty of Science

Department of Physical Geography and Geoecology

Kristýna Flašarová

Multiproxy evidence of Late Pleistocene environmental changes in the loess/paleosol sequence of Bůhzdař

Rekonstrukce paleoenviromentálních změn v pozdním pleistocénu pomocí multiproxy záznamu ze sprašové série Bůhzdař

Master thesis

Supervisor: RNDr. Barbora Strouhalová, Ph.D.

Prague, 2016

Zadání diplomové práce ***Assignment of master thesis***

Název práce ***Title***

Rekonstrukce paleoenviromentálních změn v pozdním pleistocénu pomocí multiproxy záznamu ze sprašové série Bůhzdař

Multiproxy evidence of Late Pleistocene environmental changes in the loess/paleosol sequence of Bůhzdař

Cíle práce ***The aims of work***

Opuštěná cihelna v Bůhzdaři (kat. úz. Zájezd u Buštěhradu) je dosud velmi málo probádanou lokalitou. Vedle důkladného popisu sprašového profilu se práce zaměří na analýzu paleoenvironmentálních změn v pozdním pleistocénu ve středních Čechách. Studentka provede analýzu a interpretaci texturního, mineralogického a chemického složení a měření stabilních izotopů ^{13}C a ^{18}O ve spraši a fosilních půdních horizontech.

Abandoned brickyard in Bůhzdař (cadaster Zájezd u Buštěhradu) is so far very little explored locality. The work will focus on a detailed description of the loess profile and on the analysis of paleoenvironmental changes in the late Pleistocene in central Bohemia. The student will analyze and interpret textural, mineralogical and chemical composition and measurement of the stable isotopes ^{13}C and ^{18}O in the loess and the fossil soil horizons.

Použité pracovní metody, zájmové území, datové zdroje

Methods, study area, data sources

Terénní průzkum v lokalitě Bůhzdař, odebrání vzorků

Laboratorní měření: granulometrie, TOC, XRF, XRD, stabilní izotopy ^{13}C a ^{18}O

Field survey of the locality of Bůhzdař, sampling

Measurements in the laboratory: particle size distribution, *TOC, XRF, XRD, stable isotopes ^{13}C and ^{18}O*

Datum zadání ***Date of assignment***

22. 12. 2015

Autor ***Author***

Bc. Kristýna Flašarová .....

Vedoucí práce ***Supervisor***

RNDr. Barbora Strouhalová, Ph.D. ….....

Vedoucí katedry ***Head of the department***

Prof. RNDr. Bohumír Janský, CSc. .....

I declare that this thesis is my own work and all used sources of information and literature are properly acknowledged. Neither this thesis nor a substantial part of it was ever used to earn a different or the same academic degree.

In Prague, 15. 8. 2016

Signature:

Acknowledgments

I would like to thank my supervisor, Dr. Barbora Strouhalová, for providing valuable advice, dedicating her time to consult my work and guiding my research.

I would also like to express my gratitude to Professor Eric Verecchia of the University of Lausanne and his team for valuable advice and for providing me with an opportunity to condocut lab work and analyses at the University of Lausanne.

My thanks go to Associate Professor Petr Drahota for conducting the XRD analysis, Dr. Zbyněk Engel for the laser grain size distrubution analysis, Dr. Viktor Goliáš for the use of pulverizing equipment, Dr. Luděk Šefrna and Lukáš Vlček for help in the field.

Special thanks go to my family for immense emotional, mental and material support.

Very special thanks go to Petr for continued support and help.

Abstract: Loess-paleosol sequences preserve information that can be used to reconstruct paleoenvironement, specifically the climatic conditions and the vegetation present at the time of their formation. A dense network of reliably analyzed sequences from different geographic locations is crucial for representation of ecological and climatic trends during the Pleistocene (Frechen, 2011). The aim of this thesis is to fill the gap in the geographical distribution of well described loess-paleosol sequences in Central Europe. Therefore, it focuses on a loess-paleosol sequence in Bůhzdař, situated 9 km NW of Prague, Czech Republic. This profile was last studied in 1952 by naturalist Vojen Ložek. This thesis uses a number of analyses in order to get a multi-proxy record of local paleoenvironmental changes archived in a sequence of alternating loess sediments and paleosols in Bůhzdař. Geochemical approaches are combined with grain size distribution to define climatic conditions at the time of formation of the strata.

Key words: loess/paleosol sequences, Bůhzdař, Czech Republic, particle size distribution, total organic carbon, XRF, XRD, stable isotopes ^{13}C and ^{18}O

Abstrakt: Sprašové série disponují informacemi o přírodních podmínkách panujících v době jejich vzniku, které tak mohou být využity k rekonstrukci paleoklimatických podmínek a vegetace. K bližšímu poznání ekologických a klimatických změn v pleistocénu je nezbytná hustá síť detailně prozkoumaných profilů sprašových sérií z různých regionů (Frechen, 2011). Cílem této práce je vyplnit mezeru v geografickém rozložení detailně popsaných sérií moderními metodami ve střední Evropě. Zaměřuje se na sprašovou sérii na Bůhzdaři, která leží 9 km SV od Prahy. Tento profil byl naposledy studován v roce 1952 přírodovědcem Vojenem Ložkem. Tato práce používá řadu analýz k vytvoření multiproxy záznamu paleoenviromentálních změn, které jsou archivovány v sérii střídajících se spraší a paleopůd na Bůhzdaři. Ke zjištění klimatických podmínek panujících v době vzniku jednotlivých vrstev jsou použity geochemické analýzy v kombinaci se zrnitostní analýzou.

Klíčová slova: sprašové série, Bůhzdař, Česká republika, granulometrie, organický uhlík, XRF, XRD, stabilní izotopy ^{13}C a ^{18}O

Contents

List of figures 8
List of tables 10
1. Introduction 11
2. Literature overview 11
2.1. History of loess/paleosol sequences research 11
2.2. Previous investigations of the Bůhzdař profile 12
2.3. Loess 14
2.4. Paleosols 15
2.5. Loess/paleosols sequences 16
2.6. Quantitative methods 16
2.6.1. Grain size distribution 17
2.6.2. Mineralogical compositions (XRD) 17
2.6.2.1. Clay minerals 18
2.6.3. Chemical composition (XRF) 20
2.6.4. Stable isotopes 22
3. **Materials and methods** 24
3.1. Characterization of the study site and its environment 24
3.1.1. Geomorphology 25
3.1.2. Geology 26
3.1.3. Hydrology 27
3.1.4. Climatology 28
3.1.5. Pedology 29
3.1.6. Flora and fauna 30
3.1.7. Human settlement 31
3.1.8. Profile description 32
3.2. Sampling protocol 35
3.3. Methods 35
3.3.1. Particle size analysis 35
3.3.2. XRF, XRD 36
3.3.3. Stable isotopes 37
3.3.4. Total organic carbon 39
3.3.5. Color 39
3.3.6. Molecular weathering and pedogenesis ratios 39
3.3.7. Paleoclimate transfer functions 40

3.3.8. Principal component analysis (PCA) 41
4. **Results** 42
4.1. Grain size distribution analyses 42
4.2. Chemical composition (XRF) 46
4.3. Mineralogical composition (XRD) 51
4.3.1. Clay minerals 53
4.4. Total organic carbon 55
4.5. Color 55
4.6. Stable isotopes $\delta^{13}C$ and $\delta^{18}O$ 57
4.7. Total principal component analysis (total PCA) 58
4.8. Loess dolls 61
4.8.1. Color 61
4.8.2. Chemical and mineralogical composition 62
4.8.3. Stable isotopes $\delta^{13}C$ and $\delta^{18}O$ 62
4.9. Paleoclimate transfer functions 63
5. Discussion 64
5.1. Grain size distribution 64
5.2. Chemical composition (XRF) and mineralogical composition (XRD) 66
5.3. Total organic carbon (color) 71
5.4. Stable isotopes $\delta^{13}C$ and $\delta^{18}O$ 72
5.5. Paleoclimate transfer functions 74
6. Conclusion 76
7. References 77
7.1. Literature 77
7.2. Other sources 85
7.3. Software 86
8. Appendix 87

List of figures

Fig. 2.1: The first description of the Bůhzdař profile. 13
Fig. 2.2: Sketch of the Bůhzdař profile by Ložek in 1991. 14
Fig. 2.3: Distribution of loess in Eurasia. 15
Fig. 2.4: Mineralogical composition of the Haplic Chernozem and loess in Poland. 18
Fig. 2.5: Semi quantitative analyses of clay minerals in the studied soils. 20
Fig. 2.6: Molecular weathering and pedogenesis ratios in the soils. 21
Fig. 2.7: $^{13}CO_2$ discrimination among species in plant groups. 23
Fig. 2.8: Rainout effect on ^{18}O values. 24
Fig. 3.1: Location of the Bůhzdař profile (red spot). 25
Fig. 3.2: Geological map of the surroundings of the Bůhzdař profile. 27
Fig. 3.3: Hydrological situation of the surroundings of the Bůhzdař profile. 28
Fig. 3.4: Climograph of Praha, Ruzyně climatological station. 29
Fig. 3.5: Pedological map of the surroundings of the Bůhzdař profile. 30
Fig. 3.6: Panorama view on the Bůhzdař profile. 32
Fig. 3.7: Ice wedge, black loess dolls and krotovinas in the chernozemic paleosols in the Bůhzdař profile. 32
Fig. 3.8: Ice wedge polygons in the surroundings of the Bůhzdař profile (red spot). 33
Fig. 3.9: Cryoturbation and the layer of loess dolls in the western part of the Bůhzdař brickyard. 34
Fig. 3.10: Layout of the Bůhzdař profile. 34
Fig. 3.11: Collecting samples. 35
Fig. 3.12: Grain size and descriptive terms used for grain size division. 36
Fig. 3.13: Pressed pellets for XRF of trace elements. 37
Fig. 3.14: Forms of pedogenic carbonates in the study profile. 38
Fig. 3.15: Mollar masses of oxides/elements. 39
Fig. 4.1: Grain size distribution in the profile of Bůhzdař divided into groups with grain size bigger than 8 μm and smaller than 8 μm. 41
Fig. 4.2: Grain size density distribution of the profile of Bůhzdař. 44
Fig. 4.3: The Principal Component Analysis of grain size density distribution in the Bůhzdař profile. 46

Fig. 4.4: Distribution of selected elements and their proportions in the Bůhzdař profile. 48
Fig. 4.5: The proportions of elements showing the pedogenic processes in the Bůhzdař profile. 50
Fig. 4.6: The Principal Component Analysis of chemical composition of the samples form the study profile. 50
Fig. 4.7: Mineralogical composition of the Bůhzdař profile. 52
Fig. 4.8: Clay minerals composition of the Bůhzdař profile. 53
Fig. 4.9: A Principal Component Analysis of mineralogical composition of the Bůhzdař profile. 54
Fig. 4.10: Color, total organic carbon and FeO_3 content in the Bůhzdař profile. 56
Fig. 4.11: Stable isotopes composition of $\delta^{13}C$ and $\delta^{18}O$ in the Bůhzdař profile. 58
Fig. 4.12: A correlation circle distributing the total PCA variables according to their similar distribution in the profile Bůhzdař. 59
Fig. 4.13: A PCA dendrogram dividing the samples into groups based on the similarity of variables distribution in the Bůhzdař profile. 60
Fig. 4.14: Distribution of samples based on the similarity of variables distribution in the Bůhzdař profile and their division into groups according to the PCA dendrogram. 60
Fig. 4.15: The lightest (10 YR 8/1) and the darkest (5 YR 4/1) loess dolls. 61
Fig. 5.1: Comparison between coarse fraction (>63 μm) in loess profiles in Nussloch and Dolní Věstonice (DV) and NGRIP dust and $\delta^{18}O$ records. 65
Fig. 5.2: Grain size distribution of the Zeměchy profile and the Dobšice profile. 66
Fig. 5.3: Distribution of sand-sized grains in the Bůhzdař profile. 66
Fig. 5.4: The molar ratio Al/Si representing the clayeyness and the distribution of clay-sized particles in the Bůhzdař profile. 69
Fig. 5.5: Loess/paleosols sequences in the Czech Republic and Serbia. 70
Fig. 5.6: Stary Kaydaky (Ukraine) profile and the geochemical proxies. 71
Fig. 5.7: The $\delta^{13}C_{org}$ records in the European loess/paleosols sequences. 73
Fig. 6.1: Final description of the Bůhzdař profile with determined paleosols and pedocomplexes (PK). 77

List of tables

Table 3.1: Classification of the study site according to the Geomorphological regionalization of the relief of Bohemia. 25

Table 4.1: Grain size distribution in the Bůhzdař profile. 42

Table 4.2: Chemical composition of the study profile. 47

Table 4.3: Colors of loess dolls in the Bůhzdař profile. 61

Table 4.4: Chemical and mineralogical composition of loess dolls from the Bůhzdař profile. 62

Table 4.5: Stable isotopes $\delta^{13}C$ and $\delta^{18}O$ of loess dolls in the Bůhzdař profile. 62

Table 4.6: Approximations of mean annual precipitation (MAP) and mean annual temperatures (MAT) by the paleoclimate transfer functions based on data of XRF and $\delta^{13}C_{org}$. 63

1. Introduction

The loess/paleosol sequences in Europe display a close relationship with cooling and warming trends of the Northern Hemisphere during the Pleistocene and they record regional paleoclimatic and paleoecological changes, especially the Upper Pleistocene loess/paleosols sequences provide an excellent terrestrial archive with high-resolution of climate forcing (Frechen et al., 2003). Loess/palaeosol sequences in central Europe were deposited in the nonglaciated region between two glaciated regions: the ice advancing from the Alps on the south and the Fennoscandinavian ice sheet on the north (Shi et al. 2003). In general, loess is typical of cold and dry, periglacial climate and environment. The interleaved paleosols are indicators of warmer and more humid climate, representing interstadials or interglacials (Frechen et al. 1999). Loess/paleosol sequences in brickyard localities were studied by Ložek and Kukla in the 2nd half of the 20th century in the Czech Republic. Only a few of these brickyards, with profiles uncovering prehistory, were preserved until today and even fewer were studied by modern methods. A dense network of reliably analyzed sequences from different geographic locations is crucial for representation of ecological and climatic trends during the Upper Pleistocene (Frechen, 2011).

2. Literature overview

2.1. History of loess/paleosols sequences research

The research of loess/paleosols sequences used to be neglected for a long time. The first investigations of the loess/paleosol sequences were performed in the countries with flatlands such as Poland, Germany and Hungary in the 19th century. There were no other significant geological findings (Ložek, 1973). At the end of the 19th century archeological research was performed. The presence of paleosols was reported by Czech and Moravian researchers (Němeček et al. 1990). The first more detailed description of the paleosols was performed by Petrbok in the 20's of 20th century, and then in the Czech Republic by Pelíšek (1936) in the brickyards revealing the loess/paleosols sequences (Němeček et al., 1990). The specialized quaternary research was initiated in the period between two World Wars and after the Second World War. The quaternary research, including investigation of

loess/paleosols sequences was systematically studied by the Czechoslovak academic institutions (Ložek 1973). In 1950's and 1960's the detailed description of the loess/paleosols sequences was accomplished by Kubiena, Kukla, Ložek and Smolíková. The outcome of the research was published in numerous publications. The most extensive resources were by Kubiena (1953), Kukla (1969, 1975, 1977) and Ložek (1964, 1973). In 80's Smolíková revised the previous investigation by soil micromorphology analysis (Němeček et al., 1990). Hradilová (1994), Cílek (2001), Lisá and Uher (2006) were the recent Czech authors involved in the loess/paleosols sequences research. They were focused mostly on the loess provenance and rock geochemistry.

At present, due to new developments in the methods and analyses such as optically stimulated luminescence (OSL), magnetic susceptibility or stable isotopes composition, the loess/paleosol research is experiencing a rebirth, often supported by international cooperation. Recent publications on loess/paleosols sequences by Frechen et al. (1999), Bábek et al. (2011), Antoine et al. (2013), Vysloužilová et al. (2014) and Hošek et al. (2015) were focused mostly on the well-known profiles such as Zeměchy or Dolní Věstonice. On this account the multiproxy evidence of the Bůhzdař profile is unique.

2.2. Previous investigations of the Bůhzdař profile

The first cursory investigation in the Bůhzdař profile was carried by Petrbok (1948) who described paleomalacological findings of 8 terrestrial species and 4 aquatic species. This investigation was followed by more detailed research by Ložek (1952) who made the first profile description (Fig. 2.1) and analyzed the fossil malacofauna. He described the horizon under the paleosols as solifluction sediments of cretaceous rocks with no malacological findings. Above this horizon Ložek (1952) described brown loess horizon containing humus (number 4 in the Fig. 2.1) with xerothermic species such as *Chondrula tridens* Müll., *Helicella striata* Müll. and *Pupilla bigranata* Rsm., species occurring the semi-steppe environment and *Vallonia costata* Müll. and *Eulota fruticum* Müll. that lived in the foodplain forests and groves. The horizon above was described as buried chernozemic horizon (number 3 in the Fig. 2.1) possibly partly transported with xerothermic malacofauna: *Pupilla muscorum* L., *Vallonia costata* Müll., *Chondrula tridens* Müll., *Helicella striata* Müll., *Pupilla bigranata* Rsm., *Vallonia pulchella* Müll. characteristic for the steppe environment. The horizon above the paleosols was described by Ložek (1952) as a white-grey rusty-marbled layer with loess dolls on the surface (number 2 in the Fig. 2.1) that vanished in the western direction. This layer contained the aquatic malacofauna: *Galba truncatula* Müll., *Anisus leucostomus* Müll., *Gyraulus gredleri* Blz., *Pisidium obtusale* C. Pfr. and *P. cinereum* Ald.

and boreo-alpine species *Columella edentula columela* Mart. and *Vertigo genesii* Gredler that were completely extinct in Bohemia and demonstrated a very cold climate. The horizon above these particular horizons with loess dolls (number 1 in the Fig. 2.1) was described as light-brown loess that contained more humus in the eastern direction and the cold steppe malacofauna: *Pupilla muscorum* L. and *Helicella striata* Müll. A horizon of light-brown or yellow-brown loess with no malacological findings was described above that.

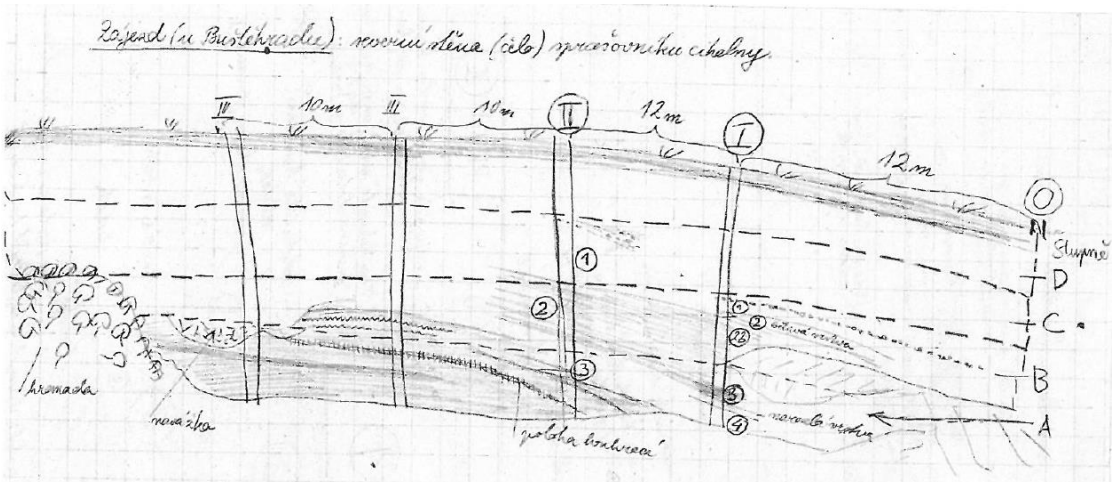

Figure 2.1: The first description of the Bůhzdař profile. Source: Ložek (1952).

Ložek (1952) was the last one who studied the Bůhzdař profile in detail. However, this survey was not very comprehensive, consisting only of a malacology analysis and a paleo geographical description. Since Ložek (1952), only a brief reference about archeological findings in the Bůhzdař profile was published by Žebera (1958). In 1962 the mayor of Zájezd wrote a letter to the Archeological institution demanding a detailed research of the Bůhzdař profile but it was never implemented (B. Vysloužilová, personal communication, 12 November, 2015). In 1990 a cursory description was made by Mašek for the purpose of the Czech Geological Survey who described sandy loess with rock fragments of Upper Pleistocene age within a loess buried soil and some frost deformational structures.

V. Ložek draw a sketch of the Bůhzdař profile in 1991 and recorded a paleosol between two loess horizons in the eastern part of the brickyard (Fig. 2.2) that was unfortunately already destroyed (V. Ložek, personal communication, 3 December, 2015). The last reference (photography) on the Bůhzdař profile was by Pokorný (2011) that documented the status as is it now-days.

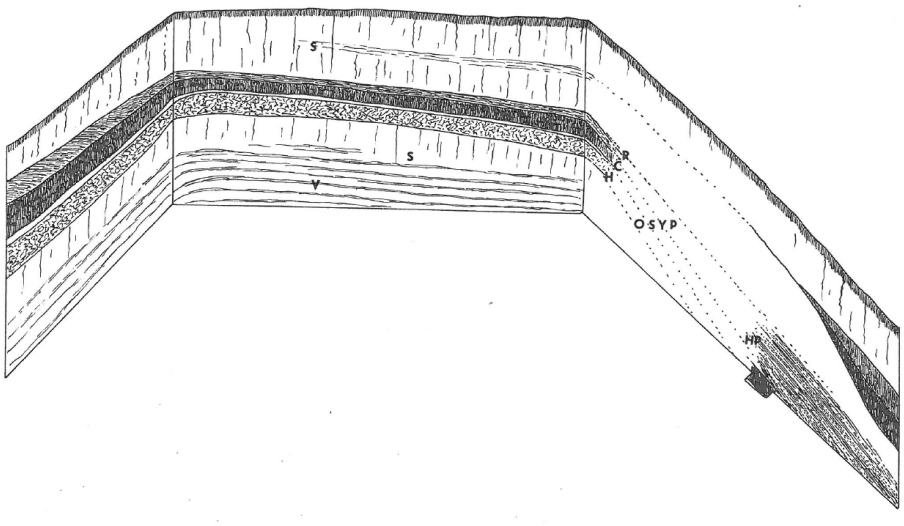

Figure 2.2: Sketch of the Bůhzdař profile by Ložek in 1991. Source: V. Ložek.

2.3. Loess

The term *loess* comes from the German word *löss* that was used for the friable and silty deposits along the Rhine Valley near Heidelberg in Germany (Kirchenheimer 1969 in Pye 1995). Lyell widespread the usage of this term when he observed the same deposits as along the Rhine Valley along the Mississippi Valley in North America in the 19th century (Pye, 1995).

Loess is a terrestrial deposit of aeolian dust composed predominantly of silt-size particles (Pye, 1995; Busacca and Sweeney, 2005; Muhs, 2007; Rousseau et al., 2007). Besides silt-sized particles loess contain also measurable amount of sand-sized particles and clay-sized particles that can reach up to 20 % (Muhs, 2007; Rousseau et al., 2007). The particles size in loess is changing with the wind intensity and the coarser grains correspond with stronger winds (Antoine et al., 2009). Loess is typically covering the preexisting landscape and it is recognizable in the field as a distinctive sedimentary body with thickness from few centimeters to hundreds of meters (Muhs, 2007). The mostly accepted sign of loess is its material strength that was formed by the process of loessification (Muhs, 2005). Loessification was first described by Ložek in 1960's as a soil forming process on the aeolian deposit (Pye, 1995). Commonly it is accepted that loessification is a post-depositional process such as cementation and aggregation. These processes have not been completely comprehended, yet (Spfrake and Obreht, 2015). Loess were formed under the semi-arid climate (Smalley et al., 2011), especially during the cold stages of Pleistocene (Spfrake and Obreht, 2015). More than 10 % of the earth's surface is covered by loess, mostly in the temperate zones (Pye, 1987) in the inner Eurasia (Fig. 2.3). Loess are located

in the low, warm and dry locations up to 300–400 m above the sea level in Central Europe (Ložek, 1973).

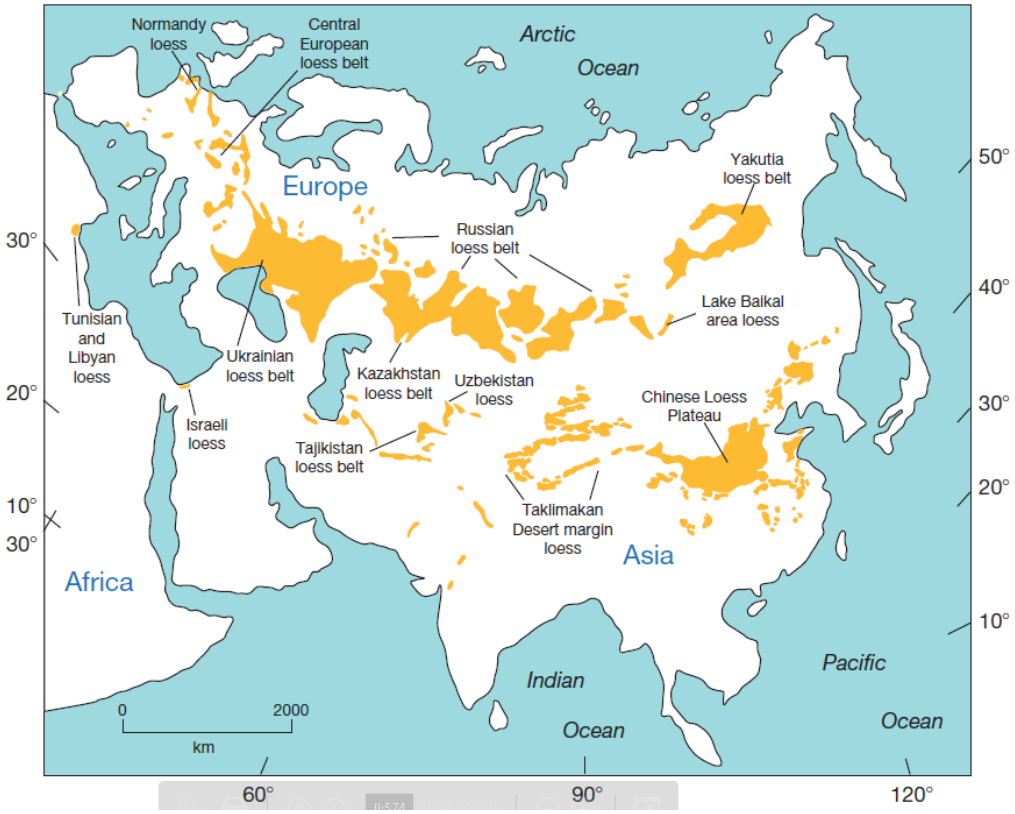

Figure 2.3: Distribution of loess in Eurasia. Source: Muhs (2007).

2.4. Paleosols

Paleosols are relict soils within thick deposits of loess. They can be used for simulating climate and ecological changes during the Pleistocene as one of the terrestrial proxies for reconstructing paleoclimate of the Quaternary Period (Kukla, 1975; Busacca and Sweeney, 2005; Muhs, 2007; Rousseau et al., 2007). Paleosols were formed during the period of low erosion and low sediments accumulation (Ložek, 1973). Preserved paleosols in loess/paleosol sequences are important paleoenvironment archives because of their long-term continuous paleoclimate record that equals that of marine proxy records or ice core records (Frechen et al., 2003; Muhs, 2007; Sheldon and Tabor, 2009). Paleosols formed at the Earth's surface were in direct contact with the climate and environment conditions prevailing at the time of their formation and they reflect the prevailing temperature and precipitation (Němeček et al., 1990; Sheldon and Tabor, 2009). The paleosol can be taken as an equivalent to the recent soil with the similar morphological signs (Němeček et al., 1990). However the resemblance between paleosols and recent soils is not identical

because the paleosols have undergone many changes over the time (Němeček et al., 1990). The most significant is degradation of organic matter in the paleosols (Vysloužilová et al., 2014).

Some properties of paleosols can provide insight to past climates including, by means of the following methods: stable isotopes in pedogenic carbonates and soil organic matter, soil morphology, magnetic susceptibility or plant pollen (Busacca and Sweeney, 2005).

2.5. Loess/paleosols sequences

Loess/paleosol sequences consist of altering loess and paleosols that represent a close relationship with cooling and warming trends during the Pleistocene (Kukla, 1975; Frechen et al., 2003; Ložek, 2007). Those alterations are widespread in the area of loess distribution and are reported worldwide (Jiamao et al., 1996; Dodonov, 2007; Muhs, 2007; Porter, 2007; Roberts et al., 2007; Frechen et al., 2003; Li and Liu, 2003; Kaakinen et al., 2006; Ning et al., 2006; Marković et al., 2008, 2013; Antoine et al., 2009, 2013; Rao et al., 2015; Ghafarpour et al., 2016). The number of paleosols interposed between loess corresponds to the age of whole sequence and depends on the local geomorphology and intensity of erosion and loess accumulation (Ložek 1973; Němeček et al., 1990; Frechen et al., 2003). In the 1960's Ložek and Kukla described the paleosols as pedocomplexes (PK). Those pedocomplexes usually represent several paleosols in one warmer period, in interglacial or in interstadial, as one pedocomplex (Ložek, 1973; Němeček et al., 1990). In most cases just 3–4 pedocomplexes are present: PK 0 represented by recent soils, PK 1 represented by the arctic slightly developed soils in the interstadial around 40 ka BP, PK 2 represented by mostly chernozemic paleosols at the beginning of the last glacial, the Weichselian glaciation around 70–90 ka BP, PK 3 represented by Luvisols and chernozemic paleosols from the most warm and humid period of the Eemian, the last interglacial around 115–130 ka BP (Ložek, 1973; Němeček et al., 1990; Frechen et al., 1999; Antoine et al., 2013). This classification based on the pedocomplexes was used only in the former Czechoslovakia.

2.6. Quantitative methods

The modern quantitative methods are based on comparison of the paleosols properties with the modern analogues from modern soils. Some techniques of these methods have been already used before like grain size distribution, clay mineralogy and rock geochemistry, whereas other techniques are relatively new innovation, for example isotope geochemistry (Němeček et al., 1990; Sheldon and Tabor, 2009). The new information about material provenance, weathering intensity, mean annual precipitation and temperature during

pedogenesis, the atmospheric composition of important gases including CO_2 and O_2, reconstructed vegetative covering, and paleoaltitude could permit to reconstruct the paleoenvironment and paleoclimatic conditions (Sheldon and Tabor, 2009).

2.6.1. Grain size distribution

Grain size distribution is a basic analysis used to characterize paleo-sedimentological changes. During the Upper Pleistocene, Glacial is characterized by silt-sized aeolian material, loess, whereas paleosols are typically enriched in clay. Clay contents refer to more robust pedogenic processes (Antoine et al., 2009; Obreht et al. 2014). For example, in Dolní Věstonice loess/paleosol sequence, paleosols samples are characterized by 10–17 % of fine sands, 25–35 % of coarse silts, and 50–65 % of particles <20 μm (clays). Loess is characterized by 20–45 % of fine sands, 25–40 % of coarse silts and 25–45 % of particles <20 μm (Antoine et al., 2013). Besides the soil formation processes the grain size distribution displays the information about the wind strength and the climate changes (Shi et al., 2003, Antoine et al., 2009). The stronger wind can transport coarser grains (Antoine et al., 2009). The grain coarseness is affected also by deflation susceptibility (affected by aridity, material and vegetation cover) and by the distance from the source area (Cílek, 2011; Antoine et al., 2009, 2013). The grains are coarser if the source area is closer (Antoine et al., 2009). Shi et al. (2003) likened the variation in the gain size distribution to the Heinrich event in the North Atlantic.

2.6.2. Mineralogical compositions (XRD)

Grain size distribution, mineralogical compositions can be used to characterize pedogenic processes. Some of clay minerals are present in paleosols as a product of pedogenesis. For analyzing paleoclimate and paleoenvironment conditions is important to analyze whole profile including the parent material. The comparison of geochemical composition of paleosols horizons and loess horizons, as a parental substrate of paleosols, is crucial in derivation of pedogenic processes (Sheldon and Tabor, 2009). For the analyses of mineralogical composition of material such as soil, X-ray diffractometry (XRD) is used. This method is used for the identification of unknown crystalline materials such as minerals or inorganic compounds. XRD can be used also for identification of clay minerals in the investigated material (Drewik et al., 2014; Kalm et al., 1996). The mineral composition of loess and paleosols consists up the following minerals in different proportions: quartz, K-feldspars, plagioclases, dioctahedral mica, biotite, calcite, chlorite, kaolinite, smectite, goethite and others (Fig. 2.4). Quartz is a dominant mineral in the soil on loess substrate

as well as in loess (40–80 % of quartz in European loess). Paleosols contain usually more quartz than loess (Rousseau et al., 2007; Drewink et al., 2014). The sign of weathering, specially leaching by the precipitation, is presence of calcite in the lower loess horizons and its absence in the paleosols (Sheldon and Tabor, 2009; Drewink et al., 2014). The relatively even distribution of clay minerals such as chlorite, kaolinite and smectite shows very low illuviation (Drewink et al., 2014; Tabor and Myers, 2015).

Horizon	Depth (cm)	Quartz	K-feldspars	Plagioclases	Di-mica	Biotite	Calcite	Chlorite	Kaolinite	Smectite	Goethite	Amorphous
		(%)										
Haplic Chernozem (Siltic)												
Ap	0–38	62.6	11.7	8.6	4.2	0.0	0.0	1.1	1.2	9.8	0.4	0.4
A	38–56	64.3	10.2	9.0	3.7	0.9	0.0	1.9	0.8	9.2	0.0	0.0
Bh/A	56–70	n.a.	n.a.	n.a.	n.a.	n.a.	n.a.	n.a.	n.a.	n.a.	n.a.	n.a.
Bh	70–95	63.4	6.9	9.9	5.7	1.3	0.2	2.0	1.6	9.1	0.0	0.0
C1	95–107	62.7	6.8	13.0	4.0	1.2	0.3	1.7	1.9	8.4	0.0	0.0
Ck2	107–240	n.a.	n.a.	n.a.	n.a.	n.a.	n.a.	n.a.	n.a.	n.a.	n.a.	n.a.
Ck3	240–370	n.a.	n.a.	n.a.	n.a.	n.a.	n.a.	n.a.	n.a.	n.a.	n.a.	n.a.
Ck4	370–400	57.3	9.2	9.0	4.4	0.4	5.4	2.9	0.3	10.7	0.0	0.3

Figure 2.4: Mineralogical composition of the Haplic Chernozem and loess in Poland. Source: Drewink et al. (2014).

2.6.2.1. Clay minerals

Clay minerals are very sensitive to environmental changes and they indicate very well the weathering and transformation of loess (Drewink et al., 2014). The amount of clay size particles increases with the increasing precipitation. The clay particles are leached out with high precipitation from the upper horizon and concentrate in the lower ones (Antoine et al., 2009; Sheldon and Tabor, 2009; Khormali and Kehl, 2011). Clay minerals are formed by alteration or weathering of primary minerals (olivine, pyroxene, feldspar, micas, quartz, and others) or by crystallization from solutions (Schulze, 2005; Chestworth, 2008) and reflect the climate factors such as temperature and precipitation, respectively the water availability in the soil (Sheldon and Tabor, 2009). It is well known that a weathering pattern for the clay minerals exists. It follows from hot and humid to cool and dry climate in order: kaolinite → smectite → vermiculite → chlorite and mixed-layer phyllosilicates → illite and mica (Sheldon and Tabor, 2009).

Kaolinite is present in more weathered soils, typically in Ferralsols and Acrisols (Schulze, 2005). Pedogenic kaolinites are formed in well-drained soils, under warm and humid climate. The soils rich in kaolinite are often associated with hematite, goethite and gibbsite (Sheldon and Tabor, 2009).

Mica in soils is generally inherited from igneous and metamorphic parent rock and sediments are derived from them. The clay-size mica is mentioned as illite in soils (Schulze, 2005). Mica minerals in rocks (muscovite, biotite) resemble the clay-size mica minerals in

soils. The muscovite, which is more resistant to the weathering than the other mica minerals, is the most common mica mineral in the soils. Micas weather to smectites and vermiculites (Schulze, 2005).

Smectites are common clay minerals in soils that are poorly drained with monsoonal and xeric climates which are characteristic by high seasonal precipitation (Sheldon and Tabor, 2009), typically Vertisols (Schulze, 2005). Smectite minerals are characteristic by their ability to shrink in dry conditions and swell when they get wet (Schulze, 2005). Smectites are present also in temperate-region soils. Smectite-dominated soils are rich in hematite and calcite (Schulze, 2005).

Soluble minerals such as carbonates, sulfates and soluble salts that are present in soils of semi-arid and arid regions (Schulze, 2005).

The origin of the clay minerals present in soils formed on argillaceous parent material such as alluvial or loessial deposits, marls, shales and claystone is often inherited which means that the clay minerals come from the parent material and they were not altered in the soil (Chestworth, 2008). Inheritance of clay minerals in the soil depends on the stable conditions in pedosphere. Unstable conditions provoke transformation of clay minerals to reach equilibrium of weathering (Yaalon et al. 1996 in Chestworth, 2008).

The information about weathering and probably the climate conditions, when the substrate was weathered (Sheldon and Tabor, 2009), is given by comparison of clay minerals composition in loess layers and paleosol layers.

The composition of clay minerals in the loess sequences can be also related to the time. Mica dominates in younger loess whereas the older loess is richer in vermiculite (McDaniel and Hipple 2010 in Khormali and Kehl, 2011). Khormali and Kehl discovered that soils on loess in aridic conditions (200 mm per year) are rich in illite and chlorite that are also present in parent material loess. These minerals are common in areas where the soil formation is limited (Wilson 1999 in Khormali and Kehl, 2011). Smectite content increases with higher soil moisture. In the humid regions (900 mm per year), vermiculite takes the primacy with the following illite (Khormali and Kehl, 2011). In the study of Kalm et al. (1996) the illite slightly indicates increasing aridity and it is dominant (55-75 %) throughout the profile in loess sequence in Chinese Loess Plateau. The amount of kaolinite is usually relatively constant (12-25 %). Increase of kaolinite could indicate increase of weathering or increase of delivery of kaolinite dust. The amount of kaolinite is significantly higher (>20 %) in the Red Clay layer only. Increase of chlorite-vermiculite characterizes weathering decrease and smectite higher amount (5-10 %) is typical for warm-temperate climate (Kalm et al., 1996).

Pedon	SMR	Hor.	Illite	Chlorite	Smectite	Kaolinite	Vermiculite	HIV
1	Aridic	A	++++	+++	+	++	–	–
		C	+++	+++	+	+	–	–
2	Dry Xeric	A	+++	++	+	+	–	–
		Bw	+++	++	+	+	–	–
		C	+++	++	+	+	–	–
3	Dry Xeric	A	+++	++	+	+	–	–
		Bk	+++	+++	+	+	–	–
		C	+++	+++	+	+	–	–
4, 5, 6	Xeric	A	++	++	++	+	–	–
		Bt	++	++	+++	+	+	–
		C	++	++	++	+	–	–
7	Udic	A	++	+	++	+	++	–
		Bt	++	+	++	+	++	–
		C	++	+	++	+	++	–
8	Udic	A	++	+	+	+	++	–
		Bt	++	–	+	+	+	++
		C	++	+	+	++	+	–

++++: >50%; +++: 30–50%; ++: 10–25%, +: <10%, –: not present.

Figure 2.5: Semi quantitative analyses of clay minerals in the studied soils. Pedon 1 refers mean annual precipitation 200 mm, pedon 2 350 mm, pedon 3 450 mm, pedon 4, 5, 6 630 mm, pedon 7 800 mm and pedon 8 900 mm. Source: Khormali and Kehl (2011).

2.6.3. Chemical composition (XRF)

Chemical analyses of the bulk fraction can also provide data to evaluate the rate of pedogenetic processes, for example by using weathering indices or variability in elemental components. X-ray fluorescence (XRF) is non-destructive method for analyzing the elemental composition of materials (Chesworth, 2008). Loess is typically composed of SiO_2 (55–65 %), Al_2O_3, Fe_2O_3, TiO_2, MgO and CaO, paleosol contains the same elements but in different proportion such as higher amount of SiO_2 and lower amount of bases (Muhs, 2007). The proportion of elements refers to weathering in soil, respectively to the pedogenic processes. Chemical weathering such as dissolution, hydrolysis and oxidation are the main weathering processes in the soil (Sheldon and Tabor, 2009). These pedogenic processes are defined by the proportion of elements in Figure 2.6. The hydrolysis proxies include ΣBases/Al and Al/Si as a measure for „clayeyness“ because Al is accumulated more in clay minerals (Sheldon and Tabor, 2009). The rate of salinization is given by proportion of alkali earth elements (Na and K), which are otherwise mobile, and Al that is under high pH stable (Chesworth, 2008; Sheldon and Tabor, 2009). The salinization ratio could be related to mean annual temperature. To verify salinization ratio results the other aridity indicators such as carbonate nodules should be considered (Sheldon and Tabor, 2009). The leaching ratio Bases/Ti provides relevant results in soils on mafic parent rocks. However this is not that much applicable for soils formed on limestone or on parent rocks/sediments relatively rich in quartz (Sheldon and Tabor, 2009). Ti/Al ratio is used mainly for the provenance indicator.

Mafic rocks are rich in Ti whereas Al is relatively constant, for example in granite versus basalt (Li 2000 in Sheldon and Tabor, 2009). At the near-neutral pH (5.5–8) are both elements relatively immobile and the ratio should be constant during the pedogenesis (Sheldon, 2006 in Sheldon and Tabor 2009).

Ratio	Formula	Rationale	Pedogenic process
Major elements			
ΣBases/Al	$\frac{\Sigma Bases}{Al}$	$\Sigma Bases = Ca + Mg + Na + K$ Common rock-forming alkaline and alkaline earth elements are lost relative to Al during pedogenesis	Hydrolysis
Base loss	Base/Ti	Base cations (Ca, Mg, Na, K) should be leached during weathering at normal pH conditions and Ti accumulated	Leaching
Clayeyness	Al/Si	Al accumulated as clay minerals form	Hydrolysis
Gleization	FeO/Fe_2O_3	Fe^{2+} is most common and mobile under reducing conditions, whereas Fe^{3+} is immobile under oxidizing conditions	Oxidation
Provenance	Ti/Al	Ti is most readily removed by physical weathering, Al by chemical weathering	Acidification (~pH)
Salinization	$\frac{K + Na}{Al}$	Alkali elements accumulate as soluble salts not removed	Salinization
Trace elements			
Leaching	Ba/Sr	Sr solubility >Ba solubility	Leaching/hydrolysis
Parent Material	La/Ce, Sm/Nd, U/Th	Different parent materials have different initial trace element ratios prior to pedogenesis, but most of those elements are immobile during weathering, so the paleosol ratio should approximate the parent material ratio	Acidification (~pH)

Figure 2.6: Molecular weathering and pedogenesis ratios in the soils. Source: Sheldon and Tabor (2009).

Trace elements ratio such as Ba/Sr and U/Th is used for measurement of weathering intensity (Kahmann et al. 2008, in Sheldon and Tabor 2009) and leaching (Sheldon 2006, Retallack 2001 a,b, 1999 in Sheldon and Tabor, 2009). Sr is under the same conditions more soluble than Ba (Vinogradov 1959 in Sheldon and Tabor, 2009) so the leached soil should have the ratio Ba/Sr relatively low in the upper part of the profile and relatively high lower in the profile (Sheldon 2006 in Sheldon and Tabor, 2009). U/Th is alternative ratio to Ba/Sr ratio where U is more soluble than Th under the same conditions. This ratio is most useful for soils with short-moderate forming time (Sheldon and Tabor, 2009).

Another weathering ratio using proportion of elements is called chemical index of alteration (CIA), first presented by Nesbitt and Young (1982). This index is defined by following formula:

$$\mathrm{CIA} = 100 \times \frac{\mathrm{Al}}{\mathrm{Al} + \mathrm{Ca} + \mathrm{Na} + \mathrm{K}}$$

The CIA provides data about weathering of feldspar minerals to form clay minerals. With the increasing clay and presumably Al should decreases amount of Ca, K and Na contents and the CIA values should be higher (McLennan, 1993). CIA is most useful for analyzes of soils formed on silicate rocks because they are rich in Al. For example limestone would

have very low amount of Al to start with and the CIA would have no convincing results (Sheldon and Tabor, 2009).

The weathering and soil forming ratios were used in the loess/paleosols sequences for example by Gallet et al. (1996), Chen et al. (1999), Zech et al. (2008), Bábek et al. (2011), Buggle et al., (2011), Hošek et al. (2015) and Obreht et al. (2015).

All the analyses comparing amount and proportions of elements depend on parent material. Sedimentary rocks and sediments can inherit clay minerals and the final results do not reflect the true pedogenesis (Sheldon and Tabor, 2009).

2.6.4. Stable isotopes

Stable isotopes analyses could help to discover climate conditions in the past. The stable isotopic composition of oxygen and carbon in loess/paleosol sequences provides valuable information about paleoenvironment situation and dynamics of the pedogenesis that affected the sediments. Stable isotopes values of pedogenic carbonates can be used as a proxy of climatic factors such as the temperature and the precipitation, respectively the water availability in the soil (Tabor and Myers, 2015). Carbon isotope values from the organic matter can be used to reconstruct the relative proportions of plants using C_3 and C_4 metabolic pathways (Kaakinen et al., 2006) or climate changes and changes in the atmospheric CO_2 concentration (Obreht et al., 2013). Both metabolic pathways (C_3 and C_4) discriminate $^{13}CO_2$ but in a different amount, which is specific for each group of metabolic pathways (Fig. 2.7) (Šantrůček et al., 2014). Plants with C3 photosynthesis have $\delta^{13}C$ values ranging from approximately -32 ‰ to -22 ‰ of VPDB (Vienna Pee Dee Belemnite) with mean values around -27 ‰ of VPDB, while those with C4 photosynthesis have $\delta^{13}C$ values ranging from about -17 ‰ to -9 ‰ with mean values around -13 ‰ of VPDB (Boutton et al., 1998).

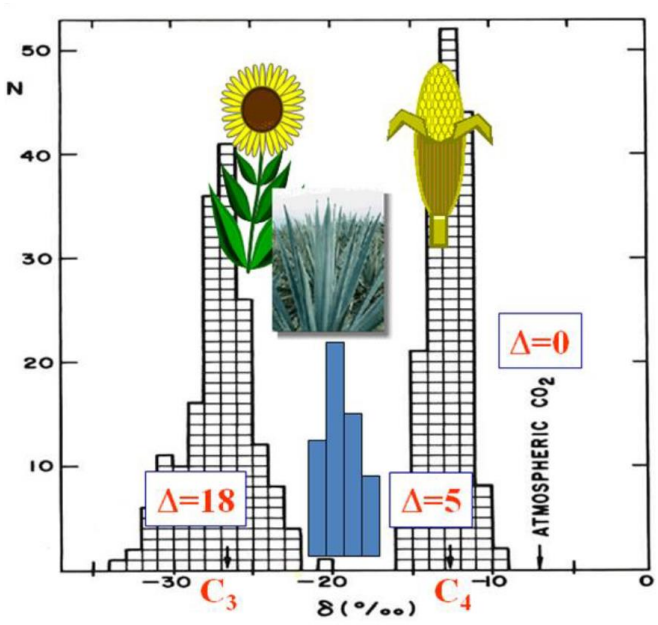

Figure 2.7: $^{13}CO_2$ discrimination among species in plant groups. Source: Šantrůček et al. (2014).

There is also variability in $^{13}CO_2$ discrimination among species in plant groups. A third group of metabolic pathway is called CAM (Crassulacean Acid Metabolism) and combines both metabolic pathways and its $^{13}CO_2$ discrimination values are between C_3 and C_4 plants (Šantrůček et al., 2014). In case that C_4 plants are not present, the data can be interpreted as a record of changes in soil respiration rate in C_3 plants resulting from changes in precipitation (Busacca and Sweeney, 2005). The level of $^{13}CO_2$ discrimination depends on available water. Plant incorporates more ^{13}C when moisture level is low because plant closes its stomata and cannot refresh CO_2 in the leaves (Šantrůček et al., 2014).

The amount of $\delta^{13}C$ from organic matter is usually around -24 ‰ of VPDB (Li and Liu, 2003; Kaakinen et al., 2006; Schatz et al., 2011; Antoine et al., 2013; Zech et al., 2013; Obreht et al., 2014) in loess and around -26 ‰ of VPDB in European paleosols (Hatté et al., 2013; Zech et al, 2013).

Oxygen isotopes retrieved from pedogenic carbonates and soil organic matter provide information on paleotemperatures (Busacca and Sweeney, 2005). Natural variation of the oxygen isotopic composition of water can be used to determine precipitation sources as well as evaporation effects. In addition, the oxygen isotope ratio of solid phases (e.g. from carbonate minerals) can record paleo-climate and paleo-hydrological information (Šantrůček et al., 2014). The proportion of ^{18}O depends on temperature and geographical location. Proportion of ^{18}O in water vapor or precipitation increases with growing

temperature. The distance from the ocean influences proportion of ^{18}O as well. With greater distance from the ocean (source of ^{18}O) the proportion of ^{18}O decreases because it condensates easier and falls in precipitation earlier than ^{16}O (Fig. 2.8). The amount of precipitation changes the proportion of oxygen isotopes. With stronger rain falls the proportion of lighter ^{16}O increases.

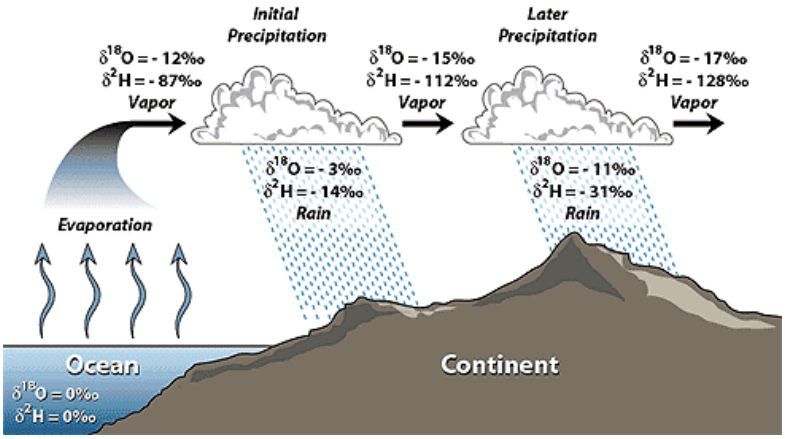

Figure 2.8: Rainout effect on ^{18}O values. Source: http://web.sahra.arizona.edu (downloaded on 27th of December 2015).

The stable isotopic composition of pedogenic carbonates is mostly influenced by the water availability and soil CO_2 that comes from the atmosphere and the decomposed organic matter (Tabor and Myers, 2015; Hasinger et al., 2015).

3. Materials and methods

3.1. Characterization of the study site and its environment

The Bůhzdař profile is situated 9 km northwest of Prague, Czech Republic, 50° 9' 54.481" N, 14° 12' 39.903" E (Fig. 1). The altitude of the profile is 300 m above sea level (at the top). The study profile is located in an old brickyard in the cadastral community Zájezd u Buštěhradu.

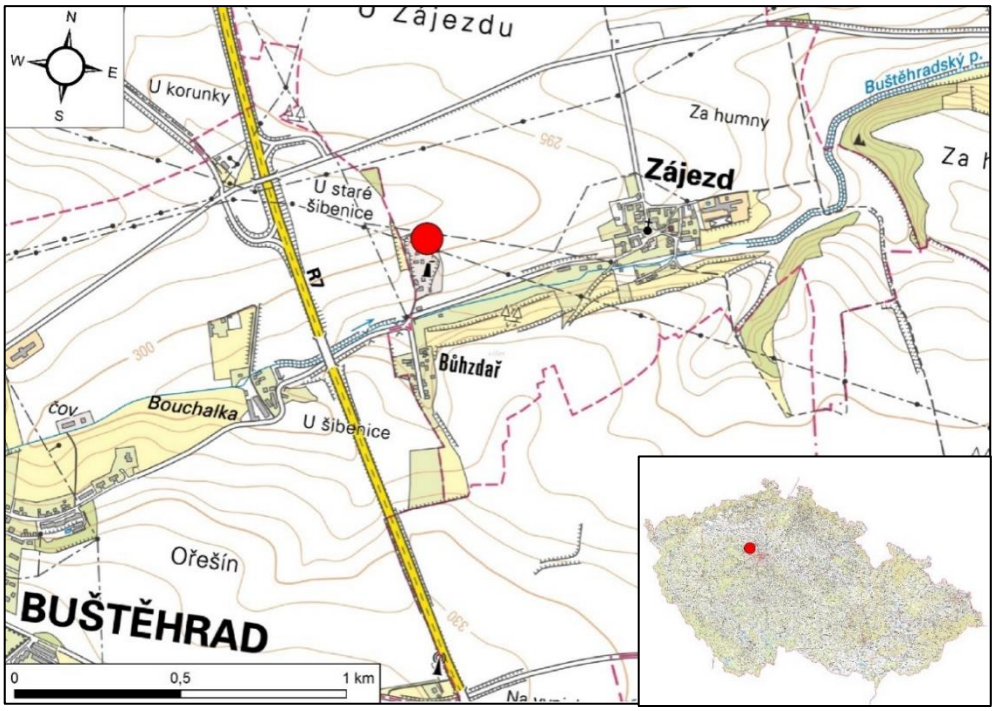

Figure 3.1: Location of the Bůhzdař profile (red spot). Source: ZM ČR (2016)

3.1.1. Geomorphology

The studied profile is located in Hostivice plateau (Hostivická tabule), a part of Kladno plateau (Kladenská tabule), itself a part of Prague plateau (Pražská plošina) that forms an integral part of Bohemian Massif (Table 3.1) (Balatka and Kalvoda, 2006).

Table 3.1: Classification of the study site according to the Geomorphological regionalization of the relief of Bohemia. Source: Balatka, Kalvoda (2006).

System/ *Systém*	Hercynian System/ Hercynský systém
Province/ *Provincie*	Bohemian Massif/ *Česká vysočina*
Subprovince/ *Subprovincie*	Beroun subprovince/ *Poberounská subprovincie*
Section/ *Oblast*	Brdy section/ *Brdská oblast*
Region/ *Celek*	Prague plateau/ *Pražská plošina*
Unit/ *Podcelek*	Kladno plateau/ *Kladenská tabule*
Subunit/ *Okrsek*	Hostivice plateau/ *Hostivická tabule*

Hostivice plateau is in an area of contiguous distribution of Upper Cretaceous rocks characterized by a large planed surface which is gently inclined from SW (380 – 410 m a. s. l.) to NE (340 – 350 m a. s. l.) (Balatka and Kalvoda, 2006). The lowest point of Prague plateau is in the valley of the river Vltava near the town of Kralupy nad Vltavou at 170 m above sea level and the highest point is Na rovinách near the town of Kladno at 435 m above sea level (Demek, 2006). The name Na rovinách can be translated as “on the plains” and expresses the flatland terrain of the surroundings of the study area.

A characteristic feature of these plateaus are loess accumulations (Ložek, 1973). The profile is situated 300 meters above sea level on the edge of a south-east oriented gentle slope above the Buštěhradský stream that flows about 15 meters of altitude lower. This position of the profile corresponds well with the leeward side in relationship to the prevailing direction of airflow during the last glacial period (Ložek, 1952). A significant landscape element in Central Bohemia are asymmetric north-south oriented valleys with gentle western slopes covered by loess and steep eastern slopes with rock outcrops (Ložek et al., 2003).

3.1.2. Geology

The geology of the surroundings of the study profile is very diverse (Fig. 3.2). Central Bohemia has one of the richest geological structures in Europe (Ložek et al., 2003). The study profile is situated in Central Bohemia in the Bohemian Massif in the Teplá-Barrandien Unit, which is made of the oldest rocks in the Czech Republic (Chlupáč et al., 2002; McCann, 2008). There are sedimentary rocks from the Neoproterozoic, the Kralupy – Zbraslav Group (phyllitic slates and phyllitic cherts) all around the study profile (Geologická mapa 1:50 000, 2013) and also under the loess in the study profile as a bedrock (Ložek, 1952). The thickness of Proterozoic sediments reaches up to 10 km in Central Bohemia. These rocks are slightly metamorphosed (Ložek et al., 2003). Paleozoic marine sediments such as Ordovician shales and quartzites, Silurian shales and Devonian limestones are no closer than 10 km S of the study profile and they are not present in the nearest surroundings of the study profile (Geologická mapa 1:50 000, 2013). Carboniferous sediments, the Kladno Formation, including conglomerates, sandstones, siltstones, mudstones, caustobioliths, breccias and tuffs are also typical for this region that are located 2 km NW of the study profile (Geologická mapa 1:50 000, 2013). Coal was mined in the 20th century in mines no closer than 3.5 km NW (Coalmine *Michael*) of the study profile (Hornictvi.info, 2016). The Mesozoic Era is present in Central Bohemia in the form of Cretaceous marine sediments of Bohemian Cretaceous Basin (spongilitic and silicified marl in the Bílá Hora

Formation, quartzitic, claye and glauconitic sandstones in the Peruc – Korycany Formation). These rocks can be found in the proximity of the study profile, eg. 750 m W of the profile (Geologická mapa 1:50 000, 2013). Volcanic activity is typical of the Neogene period. The closest manifestation of volcanic activity to the study profile is the stratovolcano Vinařická hora which is situated 10 km W of the study profile (Ložek et al., 2003). Larger volcanic formations are situated 45 km N (Central Bohemian Uplands) and 70 km W (Doupov Mountains) of the study profile (Geologická mapa 1:500 000, 2013). The youngest rocks from Quaternary; loess on the plateaus, alluviums near the watercourses and anthropogenic spoil tips which were stacked during coal exploration in the last century there, are the highest layer around the study profile (Geologická mapa 1:50 000, 2013).

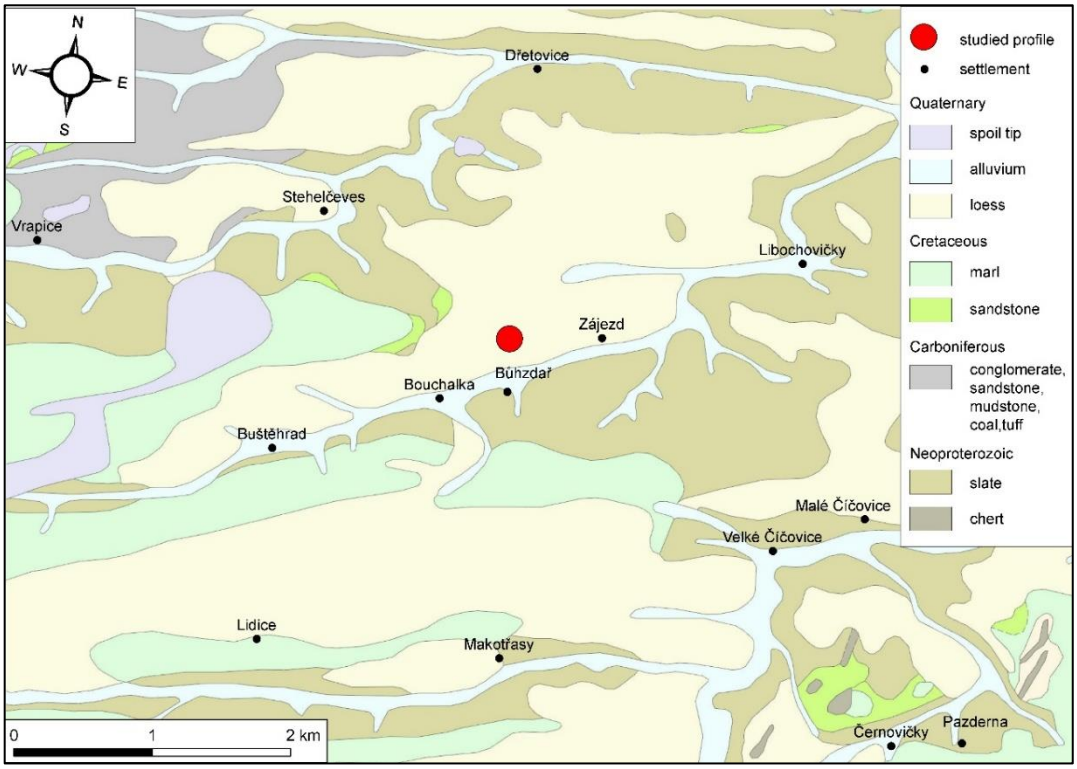

Figure 3.2: Geological map of the surroundings of the Bůhzdař profile. Source: Geologická mapa 1:50 000 (2013).

3.1.3. Hydrology

The study profile is situated in catchment of the Buštěhradský stream, which is a watercourse of 4th order in the absolute hierarchy according to Gravellius. The Buštěhradský stream springs 345 m above sea level. The length of the Buštěhradský stream is 7.87 km and its catchment area is 14.57 km^2 (DIBAVOD, 2007). The Buštěhradský stream is a left tributary of the Zákolanský stream (length 28.63 km, catchment area 265.77 km^2) which is

a left tributary of the river Vltava (DIBAVOD, 2007). The streams in the catchment of the Zákolanský stream flow mostly in NE direction (Fig. 3.3)

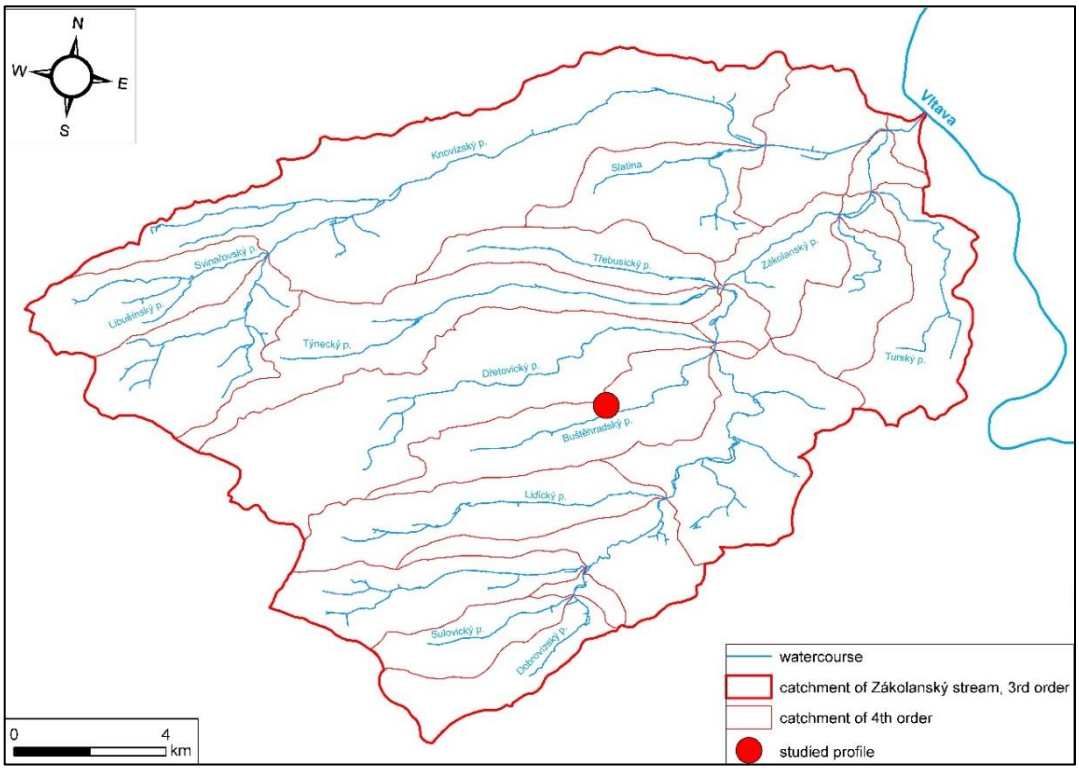

Figure 3.3: Hydrological situation of the surroundings of the Bůhzdař profile. Source: DIBAVOD (2007).

3.1.4. Climatology

The climate of the locality of the Bůhzdař profile according to the Köppen climate classification (1936) is Cfb: temperate climate without dry season and with warm summer. The nearest climatological station is in Prague, Ruzyně (374 m above sea level, 7 km SE of the study profile) with available temperature and precipitation data and their distribution during the year (Fig. 3.4). The mean annual temperature is 7.8 °C and the mean annual amount of precipitation is 526 mm (Klimadiagramme.de, downloaded on 7th of June 2016). According to the Quitt climate classification of climatic regions (1971), using data from years 1901-2000, the climate of the study locality is classified as warm with a long summer with 40 – 50 summer days, warm summer with average temperature 15 – 16 °C and summer precipitation 200 – 400 mm, 100 – 140 days with precipitation. The transition period is short with 100 – 140 frost days, the spring is moderately warm 7 – 8 °C and warm autumn with average temperature 8 – 9 °C. The winter is medium long with 50 – 60 frost days, moderately cold with average temperature from -2 to -3 °C, precipitation >400 mm and short period of snow cover 50 – 60 days (Hrnčiarová et al., 2009). The prevailing wind direction

is from the west, including winds blowing from the southwest and the northwest (Ložek et al., 2005).

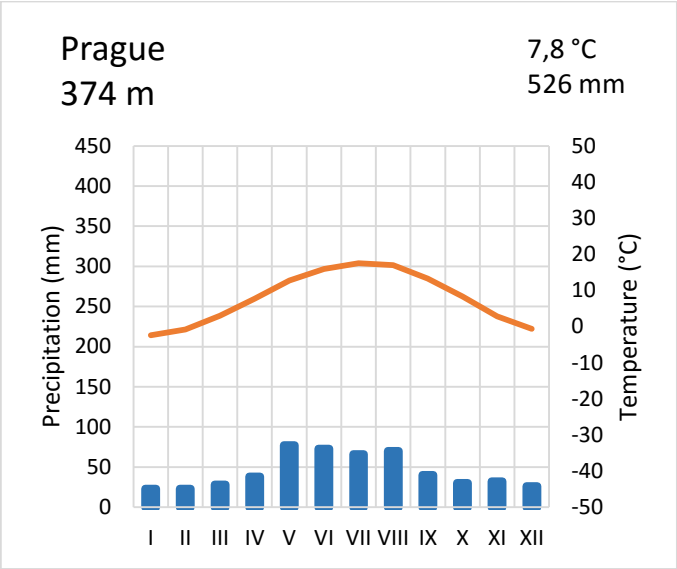

Figure 3.4: Climograph of Praha, Ruzyně climatological station. The station is situated in Prague plateau. Source: http://www.Klimadiagramme.de (downloaded on 7th of June 2016).

3.1.5. Pedology

The surroundings of the study profile (Fig. 3.5) abound in the most fertile soils in the Czech Republic, the Chernozems, specifically Haplic, and Calcic and Luvic ones. Luvisols are frequently present as well. Haplic Albeluvisols are rare. Chernozems and Luvisols formed on loess are typical for the plateau. Soils affected by water are common along watercourses: Haplic and Gleyic Fluvisols, Gleyic Chernozems and Gleysols. In the valleys, on the slopes leading to watercourses, there are often not well developed soils as Rendzic Leptosols and Haplic Leptosols. Haplic Kambisols are present in the surrounding of the study profile too with no specific distribution pattern (Hrnčiarová et al., 2009; Mapy.VÚMOP.cz, 2016).

It is important to mention paleosols besides the recent soils as well. Northern Central Bohemia is very rich in the findings of paleosol/loess sequences. These sequences are characterized by alternation of loess from the glacial periods, chernozemic paleosols from interstadials or early interglacial and early glacial periods and luvisols typical for the warm and humid climate of the interglacial periods (Ložek, 2007, 2011; Němeček et al., 1990). The most well-known localities are Prague-Sedlec, Jenerálka, Letky u Libčic nad Vltavou, Horky nad Jizerou and Zeměchy. Unfortunately, these profiles have mostly been destroyed

(Ložek, 2011). The nearest well-preserved profile is Zeměchy which is 8 km NE of the Bůhzdař profile and it is protected by the Czech law. Other profiles, uncovered due to brick production, have mostly been destroyed as well, the last active brickyard in the vicinity of the study profile is in Bratronice, 18 SW of the Bůhzdař profile.

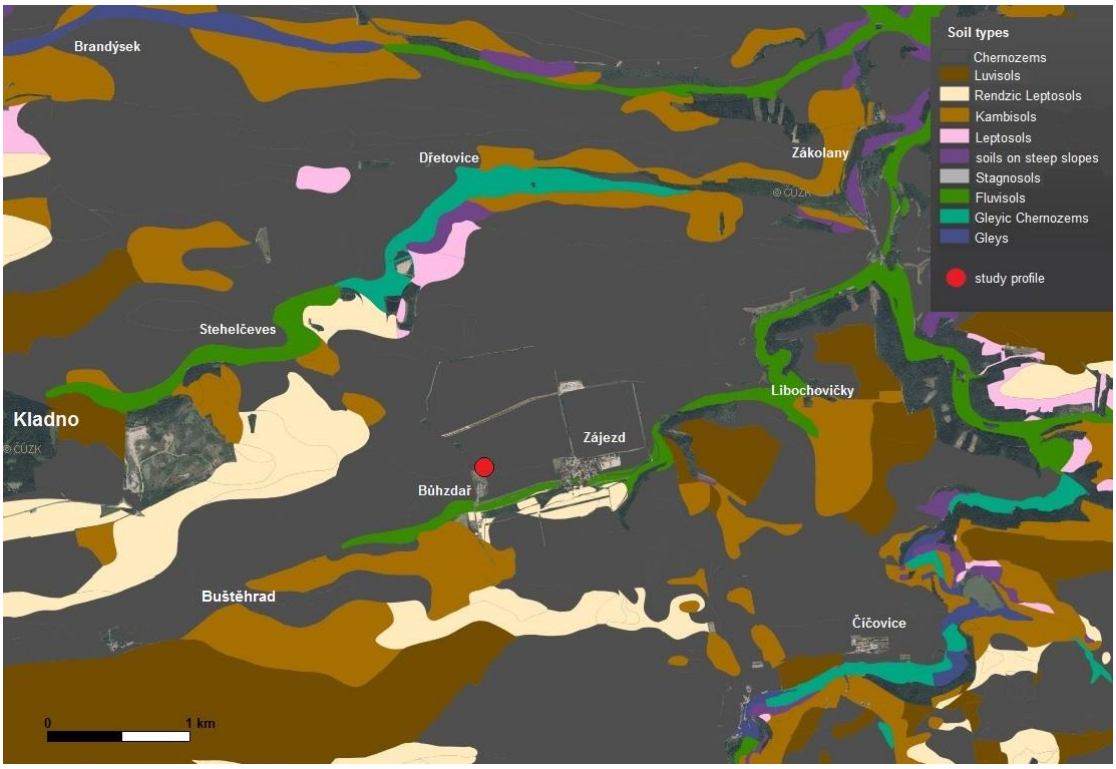

Figure 3.5: Pedological map of the surroundings of the Bůhzdař profile. Source: http://www.Mapy.VÚMOP.cz (downloaded on 7th of June 2016).

3.1.6. Flora and fauna

The study profile is situated in an agricultural landscape. Arable land is used intensively for cereal production, generally wheat. The typical wild flora around the study profile is ruderal vegetation and weeds such as *Lamium album, Viola arvensis, Elymus repens, Carduus, Tanacetum vulgare, Rubus franconicus, Sinapis arvensis, Prunus spinosa, Rosa canina, Sambucus nigra or Berberis.*

The representative fauna is, much like the flora, affected by human activity. There are virtually no exceptional or protected invertebrate species. Invertebrate species commonly found at the location include *Helix pomatia, Lumbricus terrestris, Forficula auricularia, Palomena viridissima, Pyrrhocoris apterus* and other common species of butterflies, moths, beetles and other insects. The vertebrate species of agricultural landscape are represented

by protected species including *Lacerta agilis* and *Cricetus cricetus* as well as common species such as *Mus musculus, Lepus europaeus, Microtus arvalis, Buteo buteo, Parus major, Emberiza citrinella* and others (Ložek et al., 2003). The potential natural vegetation would be oak-hornbeam woodland with *Melampyrum nemorosum* and oak woodland with *Potentilla alba* (Hrnčiarová et al., 2009).

3.1.7. Human settlement

Central Bohemia has been the preferred region for the humans since the first people came to Central Europe. The oldest archeological findings are from the Middle Paleolithic, from approximately 250 – 150 k years BP. The first human habitation was found in the vicinity of Kladno, Rakovník and Prague. The first Neolithic people came to Central Bohemia 5,500 years BC. The archeological findings of the Linear Pottery culture (the first Neolithic culture in Czechia) were found 12 km E of the study profile in Roztoky. Since the Neolithic people came to this region the landscape has been developed under continuous human influence which affected the primarily soils and biota (Ložek et al., 2003). The Bronze Age (2,400 – 750 BC) is characterized by the Únětice culture (10 km E of the study profile) with characteristic open settlements, fortified settlements were common in the Younger Únětice culture (Ložek et al., 2003). Besides villages, scattered settlement units in the form of fortified or unfortified farmhouses are known from the La Tène culture (540 - 370 BC) of the Iron Age, representing a notable change in land use. The human impact on landscape grew until the 1st century BC, especially the felling of forests, iron mining, stone mining as well as agriculture. Around the year 20 BC many Celtic settlements were abandoned. Bohemia was inhabited by Germanic peoples between the 1st and 6th centuries AD who settled in the warmest regions around watercourses and whose presence was marked by large scale iron production and the felling of forests around their settlements (Ložek et al., 2003). The Slavs came in the 6th century and settled down alongside Germanic peoples. Their agriculture was simple and from the 8th century they started to build the Slavonic fortified settlements, known as gords (Levý Hradec, 12 km E of the Bůhzdař profile; Budeč, 4 km NE of the study profile). Since this time the human impact on the landscape has grown steadily and continues to this day without any major interruptions (with the exception of the Thirty Years' War in the 17th century). In the 13th century, the cultural landscape reached the altitude of 500 m above sea level. The rise in mining activity, construction, glass production and general development led to increased rates deforestation as well (Ložek et al., 2003).

The first written record of Zájezd, the cadastral community in which the study profile is situated, dates back to 1316 (http://www.obeczajezd.iprostor.cz , 2016).

3.1.8. Profile description

The brickyard is not used for brick production anymore, last bricks were made in 2003 there. Despite that, the profile is still well visible and no big interventions were needed to clean the profile (Fig. 3.6).

Figure 3.6: Panorama view on the Bůhzdař profile. Photo: B. Vysloužilová

The uncovered profile is 5 m in height (Fig. 3.10). The recent humus horizon of chernozem is not present in the profile because it was taken away as it is conventional in raw material extraction. Only a layer of approximately 30 cm of the recent soil remains. Below these upper 30 cm, there is 2.6 m of loess, which is divided into 4 horizons (Loess I, II, III and IV). The deepest of these horizons (Loess IV) is further extended into a paleosol layer by a 70 cm long ice wedge, likely formed during the Last Glacial (Fig. 3.7).

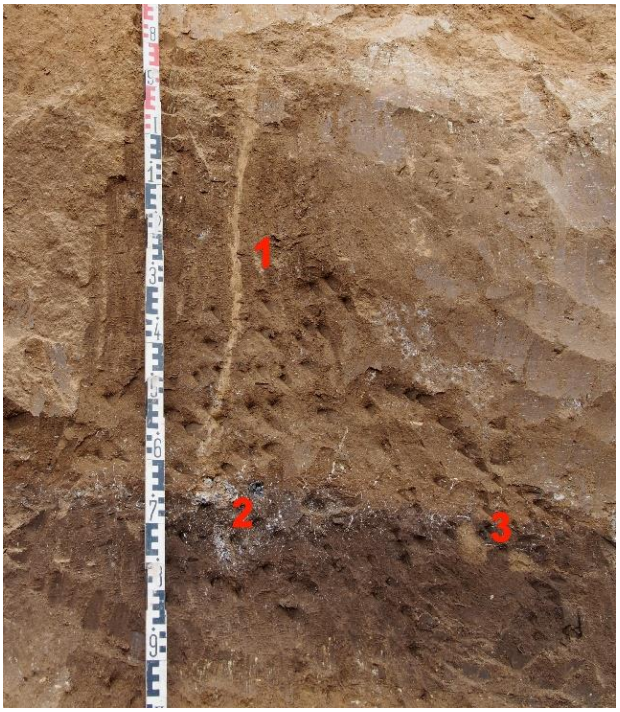

Figure 3.7: Ice wedge (1), black loess dolls (2) and krotovinas (3) in the chernozemic paleosols in the Bůhzdař profile. Photo: L. Šefrna

The presence of ice wedges is documented by ice wedge polygons in the nearest surroundings of the Bůhzdař profile that are visible on the aerial photography in the Figure 3.8 (Křížek et al., 2011; Bertran et al., 2014).

Figure 3.8: Ice wedge polygons in the surroundings of the Bůhzdař profile (red spot). Source: http://www.Mapy.cz (downloaded on 7th of June 2016).

The upper paleosol (Chernozemic paleosol I) seems to be made of redeposited chernozem or poorly developed chernozem. Between 3.65 m and 3.95 m in depth, there is a Chernozemic paleosol II with numerous dark loess dolls, arranged in one layer, which are distributed inside the middle part of this chernozemic horizon. There are also pseudomycelia and krotovinas present in this horizon (Fig. 3.7) Krotovinas are filled with loess (Fig. 3.7). The horizon of Chernozemic paleosol II displays a marble pattern, black and beige in color, in some parts. Under the Chernozemic paleosol II is buried probably another paleosol (Loess/paleosol) with slight signs of Luvisol as the slight eluviation. The upper part of this paleosol appearing lighter than the lower one. The Loess/paleosol is brown in color with a sharp boundary with the underlying loess (Loess V), which is enriched in marl fragments arranged mostly in layers. The marl flakes are sometimes aggregated and their layer forms a united block. The soil texture is characterized by the presence of marl gravels (coarse grains > 2 mm), with fine-grained material (loess). These marl gravels are distributed mostly in layers throughout the profile. In some parts of the outcrop, for

example in the western part of the brickyard, layers with gravels are more visible and form “waves”, perhaps as a result of cryoturbation (Fig. 3.9).

Figure 3.9: Cryoturbation and the layer of loess dolls in the western part of the Bůhzdař brickyard. Photo: B. Vysloužilová.

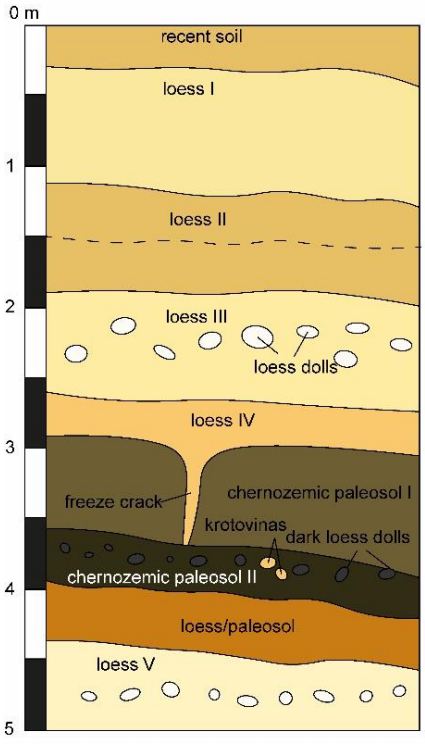

A/C: 0 - 30 cm:	10YR 7/6 - 7/4, texture silt loam, lot of live roots, quite a lot of compact carbonated roots and pseudomyceliums present, planty of earthworm tunnels
C: 30 - 110 cm:	10YR 7/3, texture silt loam, roots present, quite a lot of carbonated roots, some of them fragile,planty of earthworm tunnels, iron concrecions present, around depth of 80 cm loess very compact
C: 110 - 190 cm:	10YR 7/6 upper part, 10 YR 7/4 lower part, the transition 10YR 7/3 - 7/4 texture silt loam (160 - 180 texture silt), very fragile carbonated roots present, planty of earthworm tunnels, around the depth of 160 cm loess dolls, concretions present
C: 190 - 260 cm:	10YR 7/4, texture silt loam, lack of carbonated roots present, big loess dolls with like chalky surface present between the depths of 200 cm and 240 cm, concretions present
C: 260 - 290 cm:	10YR 6/6, texture silt loam (from 280 begins texture silty clay loam and under the binocular microscope little bit of dark soil is visible), carbonated roots present, concretions present
IIA: 290 - 365 cm:	10YR 5/4 - 5/3, texture silt loam or silty clay loam, pseudomycelium and carbonated roots present, some of them very fragile, loose structure, freeze crack going through whole horizon present
IIIA: 365 - 395 cm:	10YR 4/3, texture silt loam or silty clay loam, from depth of 380 cm parts of loess (pedoturbation), compact carbonated roots and pseudomycelium present, dark loess dolls present
IIA/C: 395 - 435 cm:	10YR 6/4 in the upper part, 6/6 in the lower part, sligtly signs of eluviation, texture silt loam, fragile carbonated roots present, loose structure
IIC: 435 - 500 cm:	10YR 8/2, texture silt loam, carbonated roots present, some of them fragile, some compact, loose structure, loess dolls, lot of marl flakes, concretions present

Figure 3.10: Layout of the Bůhzdař profile.

3.2. Sampling protocol

The samples were collected in 10 cm intervals form cleaned profile on 10th Dec 2015 (Fig. 3.11). The weather conditions were cloudy, air temperature around 2 °C, 90 % of air humidity, no precipitation and air pressure 1035 hPa. The first sample was collected in the depth of 20 cm under the top. The total amount of each sample was around 400 g of bulk material. The collected samples were dried in an oven at 40 °C for at least two days.

Then the samples were divided in two parts. One part which was visibly rich in pedogenic carbonates was left without any other preparation for the analyses of pedogenic carbonates and the second one was sieved at 2 mm to separate the coarser particles that were abundantly present in the study profile. Part of the sieved material was treated for the particle size analyses and part was ground with the laboratory sample pulverizer with different duration for loess samples and paleosols samples. Those preparations were carried out with equipment of laboratory of Institute of Geochemistry, Mineralogy and Mineral Resources, Faculty of Science, Charles University in Prague. The sieved and ground samples were taken to University of Lausanne where they were used for geochemical analyses.

Figure 3.11: Collecting samples. (Photo: L. Šefrna)

3.3. Methods

3.3.1. Particle size analysis

The sieved samples for the particle size analysis were treated with HCl and H_2O_2 to break up the bonded particles with $CaCO_3$ and organic matter. The residual chemicals were

washed after the treatment with warm distilled water. The treated samples were than measured with Laser granulometer Helos/KF (Sympatec). The treatment and the particle size analysis were carried out in laboratory of Department of Physical Geography and Geoecology. The measured values were divided into size scale descriptive terms (Fig. 3.12) and converted into percentages by the program GRADISTAT Version 8.0 (Blott and Pye, 2001).

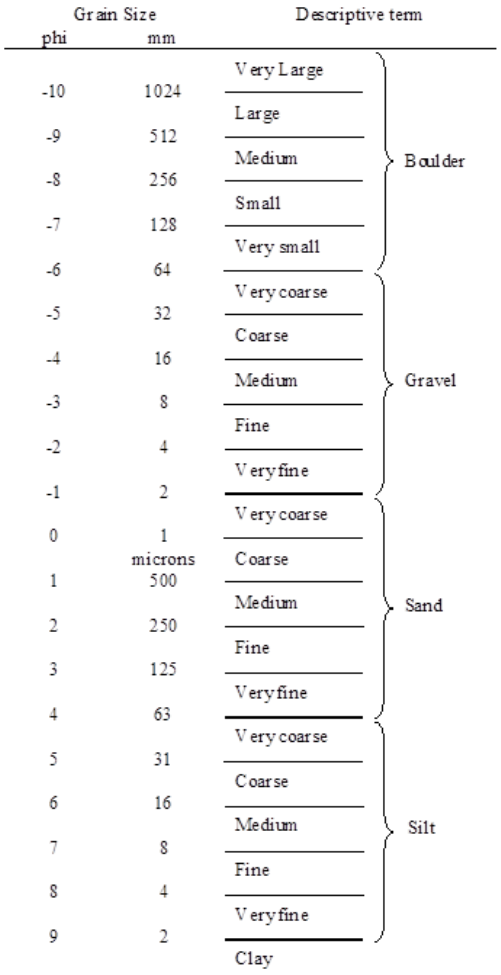

Figure 3.12: Grain size and descriptive terms used for grain size division. Source: Blott and Pye (2011).

3.3.2. XRF, XRD

Chemical composition of studied samples was measured using X-ray fluorescence (XRF). The preparation of samples for XRF analyses was different for XRF analysis of trace elements and for major elements. For the trace element analysis, pressed pellets were used (Fig. 3.13) that were made of 12 g of ground sample and 3 g of wax as a binder. This mixture was shaken for 3 minutes in an automatic sample shaker. Then the mixed sample was pressed together with a force 100 kN. Samples for the major elements were prepared as

fused beads. First, the ground samples were heated over the night in an oven at 1000 °C and then 1.2 g of each sample was mixed with 6 g of $Li_2B_4O_7$. This mixture was ground in a grinding glass bowl for 3 minutes. Then the homogenous mixture was heated to 900–1000 °C in a platinum crucible. The sample was dissolved in the flux and cast into a mold with a flat bottom. The chemical composition of such prepared samples was measured using FRX Philips PW2400 spectrometer at the University of Lausanne. Loss on ignition (LOI) was measured by weighing before and after 1 h of calcination at 950 °C.

Mineralogical composition and clay mineral composition was determined using X-ray diffraction (XRD) on ground samples using ARL Xtra diffractometer (Thermo) at the University of Lausanne and calculated by Thierry Adatte.

Figure 3.13: Pressed pellets for XRF of trace elements. (Photo: K. Flašarová)

3.3.3. Stable isotopes

The preparation and treatment of samples for stable isotopes composition measurement was different for the $\delta^{13}C$ stable isotope composition of the soil organic matter (SOM) and for the $\delta^{13}C$ and $\delta^{18}O$ stable isotopes of pedogenic carbonates.

The $\delta^{13}C$ stable isotope composition of SOM ($\delta^{13}C_{org}$) was measured from ground samples which were treated by HCl (10%) for decarbonation. Because of a lack of soil organic matter in the samples, 2000–3000 µg of treated material was used for the paleosols and 5000–10 000 µg for the loess samples. The $\delta^{13}C_{org}$ values were determined by elemental analysis–isotope ratio mass spectrometry (EA–IRMS) with a Carlo Erba 1108 connected to a Thermo Fisher Delta V IRMS (Bremen, Germany) at the University of Lausanne. Carbon isotope compositions are reported in the delta (δ) notation as the per mil (‰) deviation relative to the Vienna Pee Dee Belemnite limestone (VPDB) standard.

The pedogenic carbonates were separated under a binocular microscope from bulk samples with no previous treatment. The pedogenic carbonates (Fig. 3.14) were often very fragile (with the exception of small loess dolls) and the samples were mixed together with loess or paleosol. Because of this fact, only pure compact carbonated roots were used for the stable isotope composition analyses or in a few cases, when the carbonates were too fragile for separation, they had to be scraped to for analyzing. The $\delta^{13}C$ and $\delta^{18}O$ stable isotopes of pedogenic carbonates ($\delta^{13}C_{carb}$ and $\delta^{18}O_{carb}$) were determined using a Thermo Fisher (former ThermoQuest/Finnigan, Bremen) GasBench II connected to a Delta Plus XL isotope ratio mass spectrometer (IRMS) at the University of Lausanne. The values of $\delta^{13}C_{carb}$ and $\delta^{18}O_{carb}$ are reported in ‰ VPDP as the $\delta^{13}C_{org}$.

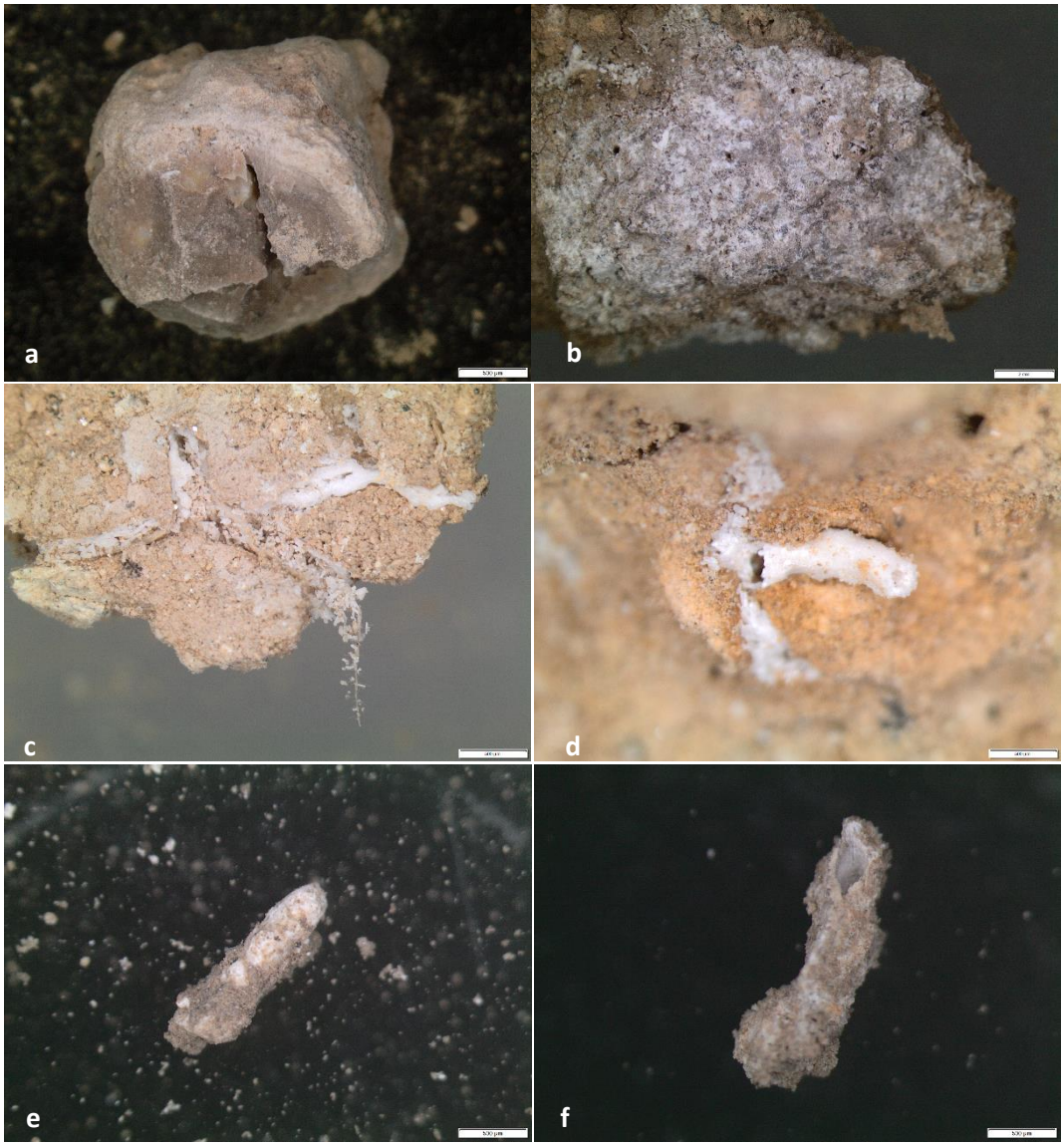

Figure 3.14: Forms of pedogenic carbonates in the study profile, a: loess doll, b: pseudomycellium, c and d calcified root cells, e: rhizolith and f: carbonate coating, by Barta (2011, 2014). Photo: K. Flašarová

3.3.4. Total organic carbon

Total organic carbon (TOC) was measured as part of the measuring of the stable isotope $\delta^{13}C$ from organic matter from the samples treated with HCl (10%) by the mass spectrometry (EA–IRMS) with a Carlo Erba 1108 connected to a Thermo Fisher Delta V IRMS (Bremen, Germany) at the University of Lausanne.

3.3.5. Color

Colors were determined on the dry samples in laboratory using the Munsell Soil Color Charts.

3.3.6. Molecular weathering and pedogenesis ratios

The geochemical ratios providing information about pedogenic processes in the study profile were calculated using formulas that use converted values from XRF (Sheldon and Tabor, 2009). The conversion of values means that the value (in weight percentage or ppm) measured by XRF was divided by its molecular mass (Fig. 3.15) to eliminate the differences between weight and volume among study elements/oxides (Sheldon and Tabor, 2009).

Molecular masses of common oxides and elements	
Oxide/element	Molar mass ($g\ mol^{-1}$)
Al_2O_3	101.96
Ba	137.3
CaO	56.08
Ce	140.12
K_2O	94.2
La	138.91
Lu	175
MgO	40.32
MnO	60.94
Na_2O	61.98
Nb	92.9
Nd	144.2
P_2O_5	189.94
Rb	85.47
SiO_2	60.09
Sm	150.4
Sr	87.6
Th	232.04
TiO_2	79.9
U	238
Yb	173
Zr	91.22

Figure 3.15: Mollar masses of oxides/elements. Source: Sheldon and Tabor (2009).

The pedogenic process of hydrolysis was calculated using following formula:

$$\frac{(Ca + Mg + Na + K)}{Al}$$

The pedogenic process of leaching was calculated using following formula:

$$\frac{(\mathrm{Ca}+\mathrm{Mg}+\mathrm{Na}+\mathrm{K})}{\mathrm{Ti}}$$

The pedogenic process of acidification was calculated using following formula:

$$\frac{\mathrm{Ti}}{\mathrm{Al}}$$

The pedogenic process of salinization was calculated using following formula:

$$\frac{(\mathrm{Na}+\mathrm{K})}{\mathrm{Al}}$$

The pedogenic process of hydrolysis showing the clayeyness was calculated using following formula:

$$\frac{\mathrm{Al}}{\mathrm{Si}}$$

The pedogenic process of leaching was calculated from the rare elements using following formula:

$$\frac{\mathrm{Ba}}{\mathrm{Sr}}$$

The chemical index of alteration (CIA) was calculated by the program Chemical weathering index calculations spreadsheet, developed by Babechuk et al. (2013).

3.3.7. Paleoclimate transfer functions

The paleoclimate transfer functions from XRF data were provided by Sheldon et al. (2002) and by Tabor and Myers (2015). The values from XRF were divided by their molecular mass (Fig. 3.15). The mean annual precipitation (MAP) was calculated using following formulas:

$$\mathbf{MAP1} = -130.93 \ln\left(\frac{\mathrm{Ca}}{\mathrm{Al}}\right) + 467.4,$$

$$\mathbf{MAP2} = -259.34 \ln\left(\frac{\mathrm{Ca+K+Mg+Na}}{\mathrm{Al}}\right) + 759.05,$$

$$\mathbf{MAP2} = 14.265(\mathrm{CIA}-\mathrm{K}) - 37.632,$$

where CIA-K is the chemical index of alteration without potassium was calculated by the program Chemical weathering index calculations spreadsheet, developed by Babechuk et al. (2013).

The mean annual temperatures (MAT) were calculated using following formulas:

$$\mathbf{MAT1} = -2.74 \ln \mathrm{PWI} + 21.39,$$

where

$$PWI = -100(4.2\mathrm{Na} + 1.66\mathrm{Mg} + 5.54\mathrm{K} + 2.05\mathrm{Ca}),$$

$$\mathbf{MAT2} = 46.9\left(\frac{\mathrm{Al}}{\mathrm{Si}}\right) + 4,$$

$$\mathbf{MAT3} = -18.516\left(\frac{\mathrm{Na+K}}{\mathrm{Al}}\right) + 17.298.$$

The paleoclimate transfer functions based on data from $\delta^{13}C$ from organic matter were calculated by using following formulas by Hall and Penner (2013):

$$\mathbf{MAT4} = -6.751 + (0.809 \times \text{mean July temperature}),$$

$$\mathbf{MAP4} = 1208.220 - (38.76 \times \text{mean July temperature}),$$

where

$$\text{mean July temperature} = 34.9 + (0.685 * \delta 13\mathrm{Corg}).$$

3.3.8. Principal component analysis (PCA)

The PCA was calculated in MATLAB 7.8.0 software using a script (Appendix 1) by E. Verrecchia (personal communication, 20 May, 2015).

4. Results

4.1. Grain size distribution analyses

Silt-sized grains (2–63 μm), as the dominant particle size in the loess, dominate in the study profile with 61.39–82.06 %, followed by clay (> 2 μm) with 11.47–35.33 % and sand (64–2000 μm) with 0–16.05 % (Tab. 4.1). Loess horizons are richer in silt sized particles (70.20–82.02 %) than the horizons of paleosols (61.39–71.63 %). Clay sized particles are more frequently present in horizons of paleosols (24.21–35.33 %) compared to the loess horizons, especially the upper part of the profile, Loess I–III (Fig. 3.10), (11.47–18.73 %). The Loess V horizon is quite rich in clay sized particles (21.50–23.89 %). Loess horizons in the depth of 2.2 m to 2.4 m (11.06–16.05 %) have distinctly higher amount of sand, this can be seen in Figure 2. On the contrary, the paleosol horizons in the depths of 3.3 m and 3.7 m have no sand sized particles, nor very coarse silt sized particles.

Table 4.1: Grain size distribution in the Bůhzdař profile (calculated by GRADISTAT analysis software).

DEPTH (m)	FINE SAND (%)	VERY FINE SAND	SAND (%)	VERY COARSE SILT	COARSE SILT (%)	MEDIUM SILT (%)	FINE SILT (%)	VERY FINE SILT	SILT (%)	CLAY (%)
0,2	0,00	4,30	**4,30**	16,75	18,67	14,88	15,84	15,92	**82,06**	**13,65**
0,6	0,00	5,49	**5,49**	14,81	16,08	14,52	16,25	17,20	**78,85**	**15,66**
0,8	0,00	3,81	**3,81**	11,21	13,99	15,33	18,37	19,28	**78,18**	**18,02**
1,2	0,00	5,97	**5,97**	19,64	20,59	14,44	13,64	13,52	**81,83**	**12,20**
1,4	0,20	6,89	**7,09**	18,09	19,96	15,29	13,80	13,30	**80,45**	**12,46**
1,6	0,13	6,06	**6,19**	18,05	21,21	15,70	14,06	13,24	**82,26**	**11,56**
1,8	0,00	7,32	**7,32**	19,87	19,67	14,53	13,99	13,14	**81,21**	**11,47**
2	0,13	5,31	**5,44**	15,39	20,65	16,48	14,79	14,24	**81,56**	**13,00**
2,2	2,60	13,46	**16,05**	16,10	14,80	13,61	13,85	13,33	**71,69**	**12,25**
2,4	0,44	10,63	**11,06**	10,61	9,97	13,20	17,28	19,14	**70,20**	**18,73**
2,8	0,00	4,72	**4,72**	7,40	5,23	10,02	18,41	26,84	**67,90**	**27,38**
3	0,00	6,93	**6,93**	4,15	1,41	8,52	18,78	28,53	**61,39**	**31,68**
3,2	0,00	2,69	**2,69**	0,74	1,94	9,37	24,41	34,08	**70,54**	**26,77**
3,3	0,00	0,00	**0,00**	0,00	1,36	9,33	25,57	34,93	**71,19**	**28,81**
3,4	0,03	4,13	**4,16**	1,86	1,14	7,76	28,10	32,77	**71,63**	**24,21**
3,7	0,00	0,00	**0,00**	0,00	1,76	11,35	21,03	30,53	**64,67**	**35,33**
3,8	0,00	3,67	**3,67**	3,33	3,63	9,12	22,67	31,37	**70,12**	**26,21**
4	0,13	6,96	**7,10**	10,89	10,01	13,45	20,63	20,55	**75,54**	**17,36**
4,2	0,00	1,66	**1,66**	3,20	6,28	12,45	23,98	28,53	**74,44**	**23,89**
4,4	0,00	2,25	**2,25**	9,03	13,92	16,00	17,61	19,69	**76,25**	**21,50**
4,6	0,00	2,30	**2,30**	5,49	10,56	15,22	19,73	22,98	**73,98**	**23,71**

The values were divided in two groups according to their grain size: grains under 8 μm (clay,

very fine silt and fine silt) and coarser grains over 8 μm (medium silt, coarse silt, very coarse silt, very fine sand and fine sand) (Fig. 4.1). The differences between loess and paleosols in grain size are can be seen in Figure 4.1. Loess (Loess I, II and III) in depth from 0.2 m to 2.2 m has coarser grains (grains > 8 μm) that reach up to 61 %. The finer part (grains < 8 μm) dominates in the paleosol samples (depths from 2.8 m to 3.8 m) with 79–89 % of finer grains. The samples from 2.4 m and from 2.8 m have a higher amount of finer grains even though they are part of loess horizons (Loess III and Loess IV). That can signify slow transition between the formation of paleosol and loess. The loess situated under the horizons of paleosols, i.e. Loess V (samples in depth 4.4–4.6 m), shows higher values of finer grains (up to 66 %). This loess horizon (Loess V) with higher values of finer grains can be affected by pedoturbation that brought the finer grains from the upper paleosol as well as the loess under the recent soil (Loess I, samples in the depth from 0.2 to 0.8 m) with proportion of finer grains up to 56 %).

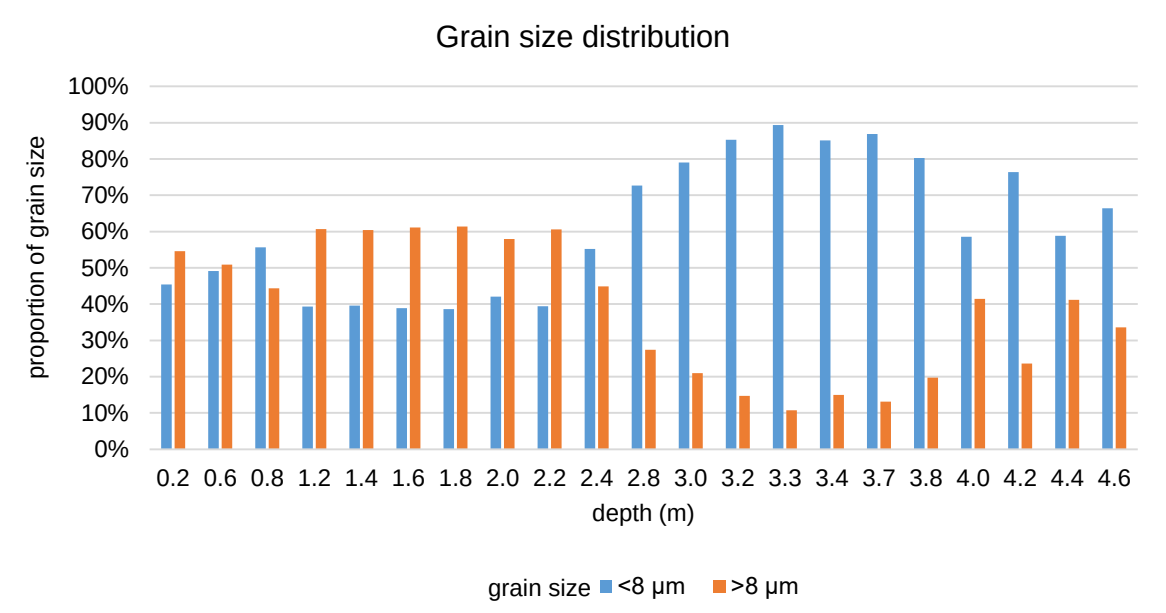

Figure 4.1 Grain size distribution in the profile of Bůhzdař divided into groups with grain size bigger than 8 μm and smaller than 8 μm.

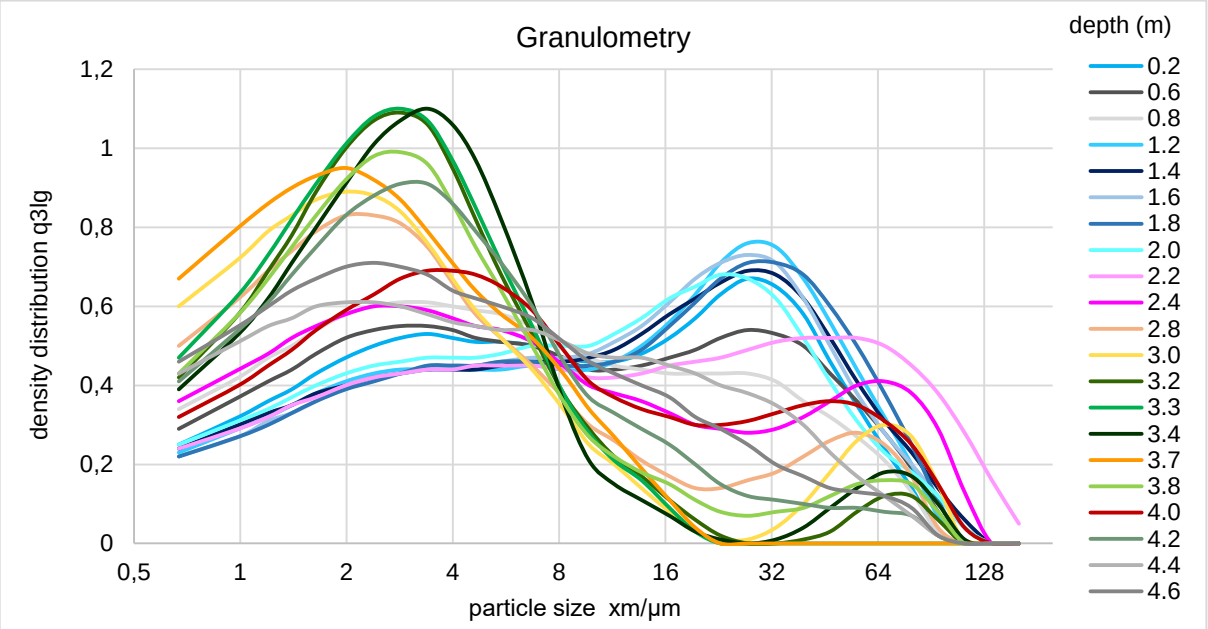

Figure 4.2: Grain size density distribution of the profile of Bůhzdař.

Figure 4.2 shows the grain size density distribution of all samples in the study profile. Each color represents a different shape of curve of grain size density distribution of study samples that were divided visually. There are 6 principal groups with colors: blue, grey, pink, orange, green and red.

The first group is characterized by the peak of grain size density distribution of coarse and very coarse silt sized grains (up to 40 % of the total amount) and it is marked by blue color. This group has the lowest proportion of finer grains < 8 µm (less than 45 %) out of all groups from the study profile. The samples displaying characteristics of this group form, with the exception of two samples (depth 0.6 m and 0.8 m), a continuous section in the upper loess horizons (Loess I, II and III) between 0.2 m and 2.0 m of depth.

The samples from the depth 0.6 and 0.8 show signs of a different group, which contains mostly the samples from the deepest loess horizon, Loess V. These samples have fewer coarse and very coarse silt sized grains (less than 25 %) and more of finer grains < 8 µm (over 55 %) than the samples of Loess I, II and III. This group is represented by grey color in the Figure 4.2. The sample from the depth of 0.6 m forms a transition between these two groups and is represented by a dark grey color.

The third group, with a specific shape of the grain size density distribution curve, is represented by pink color and contains samples from the Loess III horizon, i.e. from the depths between 2.2 m and 2.4 m. These samples have a significantly higher proportion of

sand sized grains (11.06–16.05 %) than the other samples. The proportion of finer grains (< 8 μm) is similar to the other loess samples (40–55 %).

The fourth group (green color) consists of samples that have two notable peaks in the grain size density distribution. The first peak is a high proportion of very fine silt sized grains (over 30 %). The second one shows a slightly higher proportion of very fine sand sized grains. These samples are from the horizons of chernozemic paleosols, from the depth between 3.2 m and 3.8 m, except for the sample from the depth of 3.7 m which displays signs of a different group.

The sample from the depth of 3.7 m is part of the last large group, represented by yellow-orange color, very rich in clay sized grains (around 30 %) and with a secondary peak of very fine sand sized grains. Apart from the abovementioned sample this group contains samples from the depths of 2.8 m and 3.0 m that are part of the Loess IV and Chernozemic paleosol I horizons, respectively.

The sample from the depth of 4.2 m, horizon of Loess/paleosol, displays characteristics of both the “green group” and the “grey group” that is represented by green-grey color.

The 4.0 m sample has a curve shaped similarly to the “pink group” of samples but has a lower proportion of sand sized grains (7.1 % compared to 11.06–16.05 % in the “pink group”). This sample is part of the Loess/paleosol horizon and is marked by red color.

Using the Principal Component Analysis (PCA), the samples were divided into 6 groups (Fig. 4.3). The PCA division corresponds very well with the visual division mentioned above. “Blue group”, “orange group”, “grey group” and “green group” are identical. Samples 0.6 and 4.2 are placed in a different group according to the PCA than by visual classification, but they are located next to groups whose signs they show in Figure 4.3. The PCA put the sample 2.2 away from other samples. Samples 2.4 and 4.0 were included in one group by the PCA.

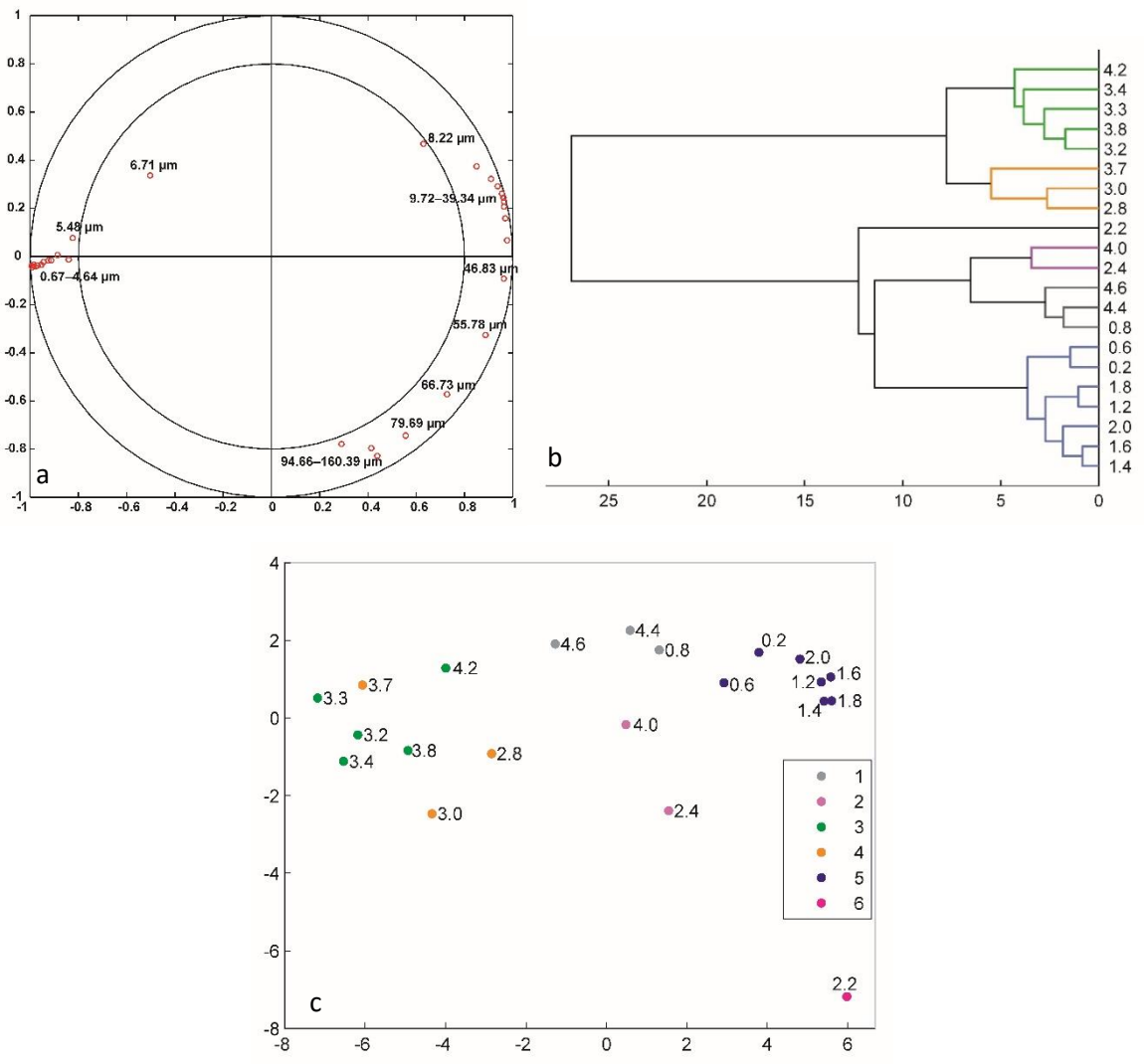

Figure 4.3: The Principal Component Analysis of grain size density distribution in the Bůhzdař profile, a: a correlation circle distributing the grain size according to their similar distribution in the study profile, b: a dendrogram dividing the samples into groups based on the similarity of grain size proportions, c: the distribution of samples groups based on the similarity of grain size proportions and their division into groups according to the dendrogram.

4.2. Chemical composition (XRF)

X-ray fluorescence analysis (XRF) provides the proportions of major (SiO_2, TiO_2, Al_2O_3, Fe_2O_3, MgO, CaO, Na_2O and K_2O) as well as trace (Mn, Rb, Sr, Zr, Br, La and Ce) element composition of samples from the study profile (Tab. 4.2).

Table 4.2: Chemical composition of the study profile.

Sample depth (m)	Major elements composition (% weight total)									Trace elements composition (ppm)						
	SiO_2	TiO_2	Al_2O_3	Fe_2O_3	MgO	CaO	Na_2O	K_2O	CO_3	Mn	Rb	Sr	Zr	Ba	La	Ce
0.2	57.76	0.69	9.30	3.48	1.45	10.83	0.68	1.81	13.89	418	73	198	332	330	31	61
0.3	58.53	0.71	9.52	3.49	1.45	9.61	0.72	1.84	13.72	427	76	192	351	346	33	60
0.4	60.10	0.73	9.63	3.55	1.49	9.44	0.78	1.86	11.98	437	77	196	365	357	41	59
0.5	59.59	0.71	9.60	3.54	1.48	9.65	0.75	1.86	12.47	409	78	202	338	352	34	64
0.6	58.33	0.67	9.53	3.57	1.43	10.41	0.60	1.84	13.33	432	79	225	299	354	31	54
0.7	58.57	0.65	9.73	3.53	1.42	10.28	0.56	1.85	12.98	421	80	229	265	353	30	59
0.8	59.36	0.67	9.77	3.63	1.42	9.60	0.62	1.92	12.64	406	83	219	279	359	29	57
0.9	58.62	0.68	9.69	3.67	1.44	10.05	0.66	1.94	12.92	419	84	221	296	368	36	62
1	57.24	0.67	9.61	3.60	1.35	10.86	0.60	1.93	13.91	412	85	226	288	359	31	59
1.1	58.90	0.72	9.76	3.62	1.39	10.03	0.65	2.07	12.57	441	88	224	335	372	29	59
1.2	59.90	0.76	9.99	3.75	1.44	9.05	0.73	2.17	11.83	487	92	206	356	385	33	60
1.3	60.00	0.77	10.32	3.92	1.47	8.55	0.75	2.20	11.69	453	95	205	346	389	30	62
1.4	59.58	0.77	10.29	3.96	1.49	8.76	0.74	2.17	11.90	449	94	199	331	377	35	57
1.5	60.39	0.77	10.45	3.88	1.46	7.98	0.74	2.22	11.67	428	96	192	348	381	32	62
1.6	59.91	0.77	10.36	3.96	1.53	8.61	0.80	2.19	11.38	485	95	183	342	377	32	60
1.7	61.59	0.79	10.57	3.81	1.53	7.69	0.77	2.27	10.60	448	97	200	352	384	33	63
1.8	62.38	0.74	10.13	3.58	1.42	7.76	0.76	2.07	10.94	367	92	200	332	350	30	57
1.9	60.36	0.67	9.51	3.46	1.35	8.97	0.62	1.92	12.87	394	87	228	285	337	32	55
2	62.84	0.77	10.43	3.75	1.48	7.11	0.81	2.14	10.44	465	96	192	356	364	30	62
2.1	62.42	0.74	10.18	3.68	1.49	7.50	0.79	2.09	10.82	402	93	196	340	351	29	62
2.2	60.93	0.62	9.24	3.34	1.32	9.29	0.52	1.83	12.55	434	84	242	253	325	34	54
2.3	60.61	0.51	8.26	3.08	1.10	10.56	0.32	1.63	13.64	451	74	277	197	291	23	48
2.4	61.43	0.52	8.45	3.20	1.12	10.05	0.34	1.60	13.01	333	75	274	206	287	25	52
2.5	64.06	0.59	9.49	3.62	1.19	7.36	0.36	1.70	11.36	354	85	245	227	317	29	58
2.6	66.90	0.65	10.22	3.83	1.21	4.90	0.39	1.81	9.92	362	93	216	244	332	31	60
2.7	67.84	0.65	10.41	3.95	1.22	3.80	0.39	1.83	9.71	325	94	209	247	326	31	61
2.8	70.28	0.63	10.28	3.88	1.17	2.70	0.36	1.81	8.19	327	95	204	243	323	28	58
2.9	70.50	0.61	9.64	3.68	1.10	2.63	0.34	1.80	9.54	529	101	212	259	366	30	55
3	72.81	0.60	9.72	3.60	1.07	1.86	0.32	1.83	7.78	491	95	198	231	327	29	52
3.1	72.96	0.58	9.50	3.44	1.01	1.68	0.29	1.79	8.16	834	94	201	235	354	25	51
3.2	73.18	0.57	9.41	3.41	1.00	1.31	0.28	1.79	8.41	475	95	201	220	324	27	52
3.3	73.50	0.60	9.82	3.51	1.05	1.31	0.30	1.83	7.84	404	98	203	227	321	24	55
3.4	74.41	0.55	9.06	3.24	0.96	1.06	0.27	1.73	8.60	483	95	203	233	329	28	52
3.5	73.81	0.53	9.37	3.20	1.01	1.45	0.26	1.86	8.31	588	94	218	212	339	25	43
3.6	66.51	0.74	10.60	3.86	1.15	3.45	0.46	1.93	10.61	690	109	192	266	395	28	59
3.7	70.96	0.60	9.65	3.40	1.06	2.23	0.33	1.73	9.78	422	106	211	226	334	26	53
3.8	72.86	0.61	9.84	3.48	1.05	1.19	0.34	1.79	8.58	435	105	201	235	337	32	56
3.9	73.63	0.60	9.68	3.41	1.04	0.93	0.32	1.76	8.46	329	101	203	222	320	24	49
4	71.37	0.57	10.17	3.71	1.17	1.09	0.30	1.71	9.33	337	94	219	212	307	25	47
4.1	70.49	0.60	10.76	4.03	1.25	0.92	0.33	1.77	9.70	430	95	223	215	326	26	55
4.2	69.94	0.64	11.41	4.29	1.35	1.60	0.42	1.90	8.22	438	94	217	221	342	32	64
4.3	61.73	0.57	9.50	3.50	1.19	8.26	0.38	1.71	12.93	405	80	250	205	327	40	48
4.4	56.90	0.48	8.01	2.90	1.07	13.22	0.30	1.48	15.39	336	67	257	169	287	25	43
4.5	53.23	0.42	6.98	2.45	0.95	16.52	0.25	1.32	17.62	275	59	251	154	247	21	40
4.6	57.56	0.53	8.36	2.99	1.06	11.79	0.35	1.61	15.31	243	74	219	201	287	28	44
4.7	60.29	0.60	9.21	3.34	1.18	9.78	0.41	1.80	13.03	317	81	214	225	315	30	52
C 2.4	7.99	0.08	1.13	0.41	0.63	49.33	0.05	0.17	40.05	94	12	143	32	74	14	7
C 3.6	19.22	0.25	3.28	1.23	0.68	40.23	0.16	0.53	34.02	465	37	266	79	209	19	21
C 4.5	17.04	0.14	2.29	0.81	0.67	42.87	0.09	0.38	35.52							

Some of the elements appear to have similarly shaped chart curves throughout the profile. When this is the case only one out of a given group of elements with similarly shaped curves is shown in Figure 4.4. However, it should be noted that the actual proportion of respective elements in a given group can (and does) differ. Fe_2O_3 has a curve shaped rather similarly to Al_2O_3. However, the proportion of Fe_2O_3 fluctuates between 2.45–4.29 % (Fig. 4.10)

which is lower than the actual proportion of Al_2O_3 (6.98 - 11.41 %). Both elements have peaks in comparable depths (around 1.5 m, 2 m, 2.7 m, 3.6 m and 4.2 m) with the most significant peak in the depth of 4.2 m: 11.41 % of Al_2O_3 and 4.29 % of Fe_2O_3, that are the highest values in the study profile. The lowest values are in the depths of 1.9 m, 2.3 m and in 4.5 m. TiO_2 has a similar shape of curve in Figure 4.4 to Al_2O_3 and Fe_2O_3. The bases (MgO, Na_2O and K_2O) represented in Figure 4.4 by K_2O have a similar shape of curve as the previous elements. The highest values are in the depth around 1.5 m (Loess II) reach up 1.53 % of MgO, 0.80 % of Na_2O and 2.27 % of K_2O. The lowest values are in the depths of 4.5 m and in 2.3 m where loess dolls were found. Some rare elements, such as Zr, Ba and Rb have a curve shaped similarly to the curve of bases. Higher values of Zr, Ba and Rb are found in the horizon of Loess II in the depth of around 1.5 m, 2.9 m and in the depth of 3.6 m. The lowest values are in the depths of 2.3 m, much like the previous elements. Sr has an inverse shape of curve of the graph: peaks in depths of 2.3 and 4.5 m and minimums in the depths of 1.6 m and 3.6 m. CaO has an inverse shape of curve to SiO_2. CaO has highest values in the horizons of Loess I, II, III and V, from 7.98 % to 16.52 %, (where SiO_2 has the minimums, at 53.23–62.84 %) and the minimums in the horizons of paleosols (0.92–3.45 %) where SiO_2 has the highest values (66.51–74.41 %). Loss on ignition (LOI) is connected to the amount of carbonates and organic matter in the samples.

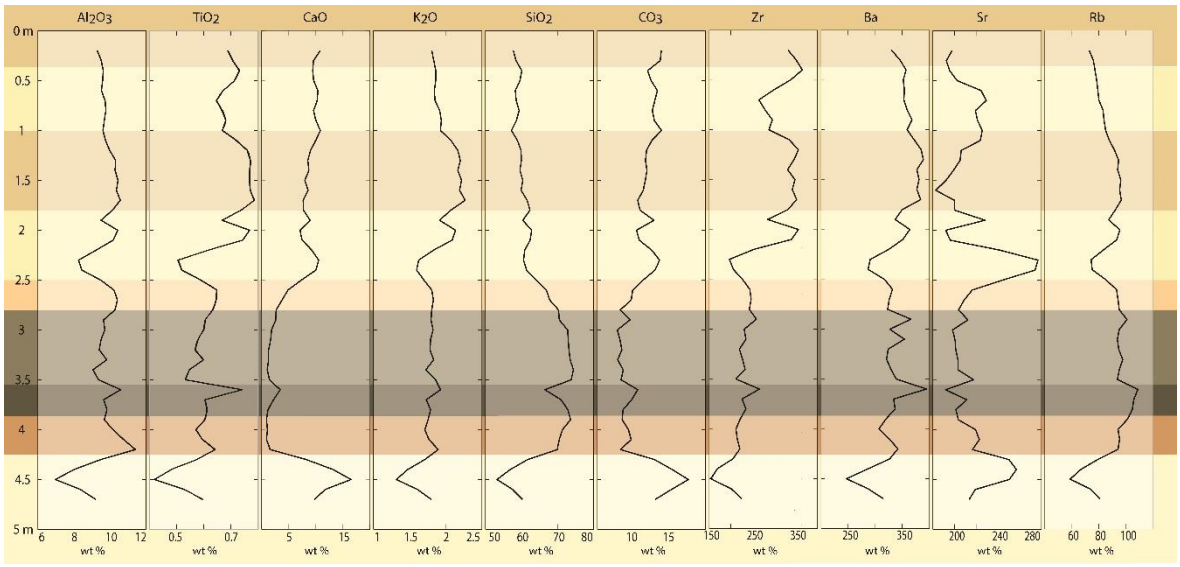

Figure 4.4: Distribution of selected elements and their proportions in the Bůhzdař profile.

Molecular weathering and pedogenesis ratios shown in Figure 4.5 present information about pedogenic processes in the study profile. Hydrolysis and leaching, represented by ratio of ∑Bases/Al and ∑Bases/Ti, respectively, have the similar curve shapes in the graph. The highest values (low leaching and low hydrolysis) are in the horizons of Loess I, III and

V and the lowest values in the horizons of paleosols with a gentle peak of higher values in the depth of 3.6 m. The ratios of Ti/Al, representing acidification, and (K+Na)/Al, representing salinization, have remarkably similar curve shapes. High values suggest low acidification or salinization while low values suggest the opposite. These curves have peaks in the depths of 0.4 m (Loess I), 1.2–2.1 m (Loess II and Loess III) and 3.6 m (boundary between Chernozemic paleosol I and II). The minimums are in the depths of 2.8–3.5 m (Chernozemic paleosol I) and 4.0–4.2 m (Loess/paleosol). The ratio Al/Si shows the clayeyness as Al is accumulated in clay minerals. High values are recorded in horizons of Loess I, II and III, a marked decrease can be seen from 2.6 m (Loess IV) to approximately 3.4 m, followed by a notable increase at about 3.6 m of depth. An interesting peak can be seen rising throughout the Paleosol/loess horizon (3.9–4.3 m), possibly signalizing a higher accumulation of clay minerals (Sheldon, Tabor, 2009). Another ratio comparing leaching is the proportion of rare elements Ba and Sr. The highest values are in the horizon of Loess II, especially in the depth of 1.6 m, and in the horizons of paleosols (from 2.9 m to 4.3 m, with the peak in 3.6 m) and represent high rates of leaching. The minimums are in the depths of 1.9 m, 2.3 m and 4.5 m.

Last curve shows the values of the chemical index of alteration (CIA) which compares the proportions of major elements. This index corresponds to the alteration intensity, higher values mean higher intensity of alteration. There can be seen a notable difference between the loess horizons (Loess I, II, III and V) and the paleosols (Chernozemic paleosol I, II and Loess/paleosol) in Figure 4.5. The lowest values of CIA were recorded in the depths of 2.3 m (Loess III) and 4.5 m (Loess V) while the highest ones between 3.9 m and 4.1 m of depth (Paleosol/Loess). Slightly higher values can be found in the depth from 1.5 m to 2.1 m (Loess II and III). The CIA curve in Loess IV (depth from 2.6 m to 2.9 m) rises steadily and this increase continues into the paleosol horizon.

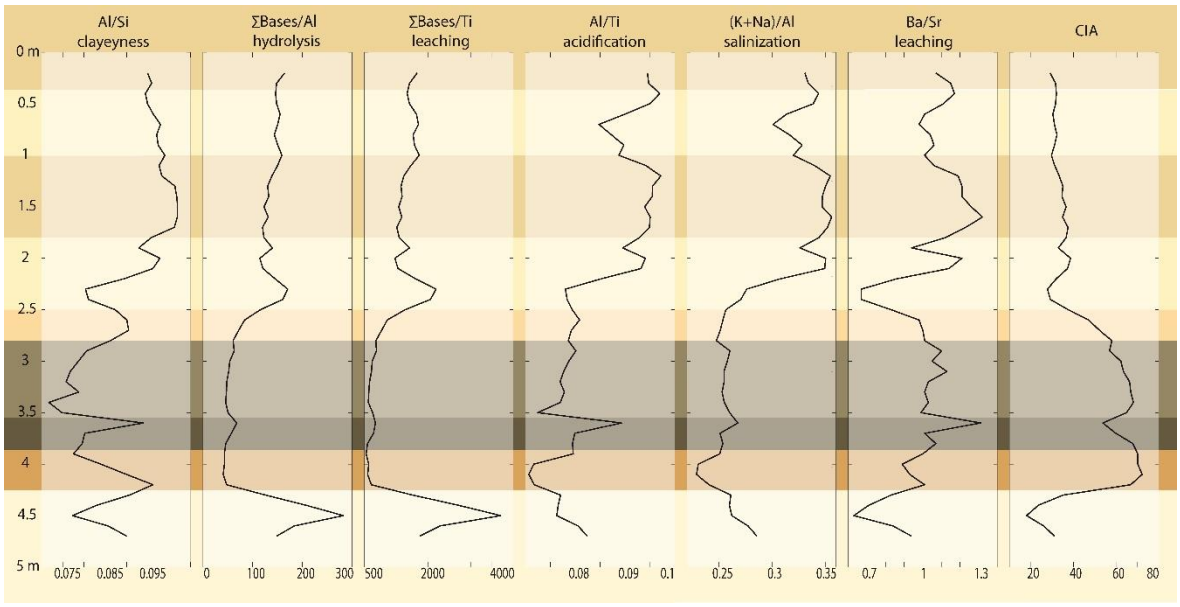

Figure 4.5: The proportions of elements showing the pedogenic processes in the Bůhzdař profile.

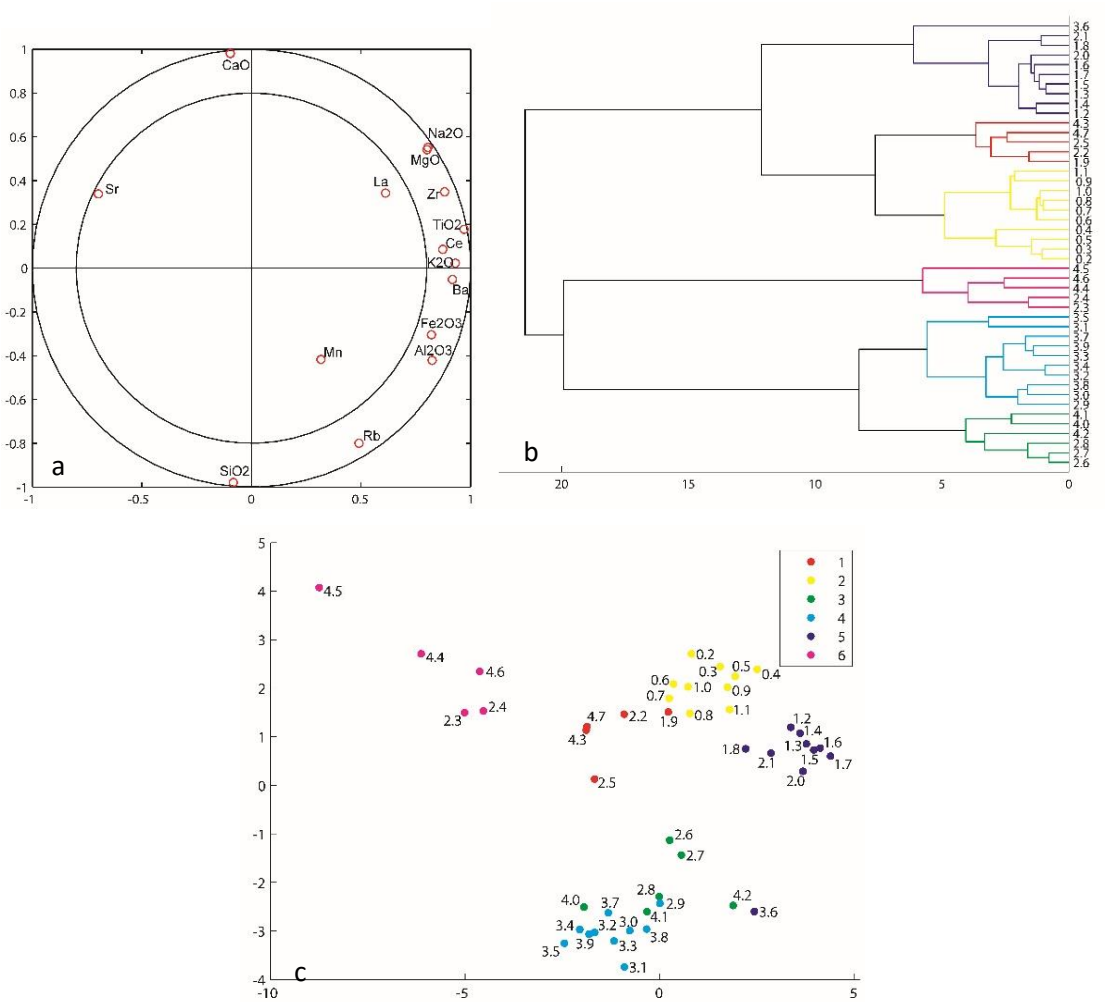

Figure 4.6: The Principal Component Analysis of chemical composition of the samples form the study profile, a: a correlation circle distributing the elements based on the

similarity of distribution in the study profile, b: a dendrogram dividing the samples into groups based on the similarity of their chemical composition, c: the distribution of samples based on the similarity of their chemical composition and their division into groups according to dendrogram.

A Principal Component Analysis was used to divide the samples into groups with a similar element composition (Fig. 4.6). There are six groups in total. Group number 1 is marked in red color and includes samples from the horizon of Loess III and V and a sample from the transition zone between Loess/paleosol. Yellow color represents group number 2 which contains samples from the top part of study profile, 0.2–1.1 m of depth (Recent soil and Loess I). Those samples are close to one other in the graph. Group number 3, marked by green color, represents samples from the horizons both above and below the chernozemic paleosols (2.6–2.8 m and 4.0–4.2 m). Group number 4, marked by light blue color, is situated next to the third group in the chart, signifying a similar geochemical composition, and contains samples from both Chernozemic paleosol horizons (2.9–3.9 m). Group number 5 (marked by dark blue color) that is compact in the chart much like group number 2 and is made up of samples from the Loess II horizon (1.2–2.1 m). However, this group contains a sample from the depth of 3.6 m (boundary between Chernozemic paleosol I and II). The last group, number 6, has pink color and represents the samples from Loess III and Loess V (2.3–2.4 m and 4.4–4.6 m) and has a large spread in the graph of sample distribution (Fig. 4.6).

4.3. Mineralogical composition (XRD)

The mineralogical composition of the study profile is shown in the Figure 4.7. The most common mineral in the study profile is quartz (39.77–59.87 %). Phyllosilicates, including clay minerals, are abundantly present as well (17.09–44.23 %). The mineralogical composition of the ancillary minerals consists of calcite (0–25.01 %), K-feldspar (0–17.90 %), plagioclase-Na (0–10.32 %), dolomite (0–5.41 %), ankerite (0–0.88 %), goethite (0–2.60 %) and non-quantified fraction (0.20–8.35 %).

The loess horizons contain less quartz (39.77–49.78 %) than the paleosol horizons (49.09–59.87 %). A similar situation can be seen with the phyllosilicates, the loess horizons are less rich in those minerals (17.09–39.56 %) than the paleosol horizons (27.09–44.23 %). On the other hand, the loess horizons are richer in calcite (5.96–25.01 %) than the paleosol horizons (0–3.45 %). The highest value of calcite in the paleosol horizons at 3.45 % was recorded at the depth where the dark loess dolls were found. The presence of (dark) loess

dolls explains the higher value. Plagioclase-Na shows similar distribution to calcite. The loess horizons contain more plagioclase-Na (3.18–10.32 %) than the horizons of paleosols (1.13–5.49 %). K-feldspar does not show any relation to diagnostic horizons in its distribution. Dolomite is abundantly present in the horizons of Loess 1 and 2 (1.28–5.41 %). The dolomite mineral is not present in Loess 5 that is very rich in calcite (over 20.96 %). Ankerite is present in only 3 samples, in depths of 0.5 m, 0.6 m and 3.1 m. Out of those three, the amount of ankerite is noticeable just in the depth of 0.5 m (0.88 %), in the other two samples it is negligible (0.26–0.30 %). Goethite is present in two samples, in the horizon of Chernozemic paleosol II, depth of 3.8 m (2.60 %), and in the rusty horizon of Loess/paleosol in the depth of 4.2 m (2.31 %). Small undeterminated amount of amphibole is present in the depths of 0.4 m, 0.8 m and 1.0 m that are in the horizon of Loess 1. Amphibole is further present in the depths of 3.5 and 3.9 m that are part of the Chernozemic paleosol I and II.

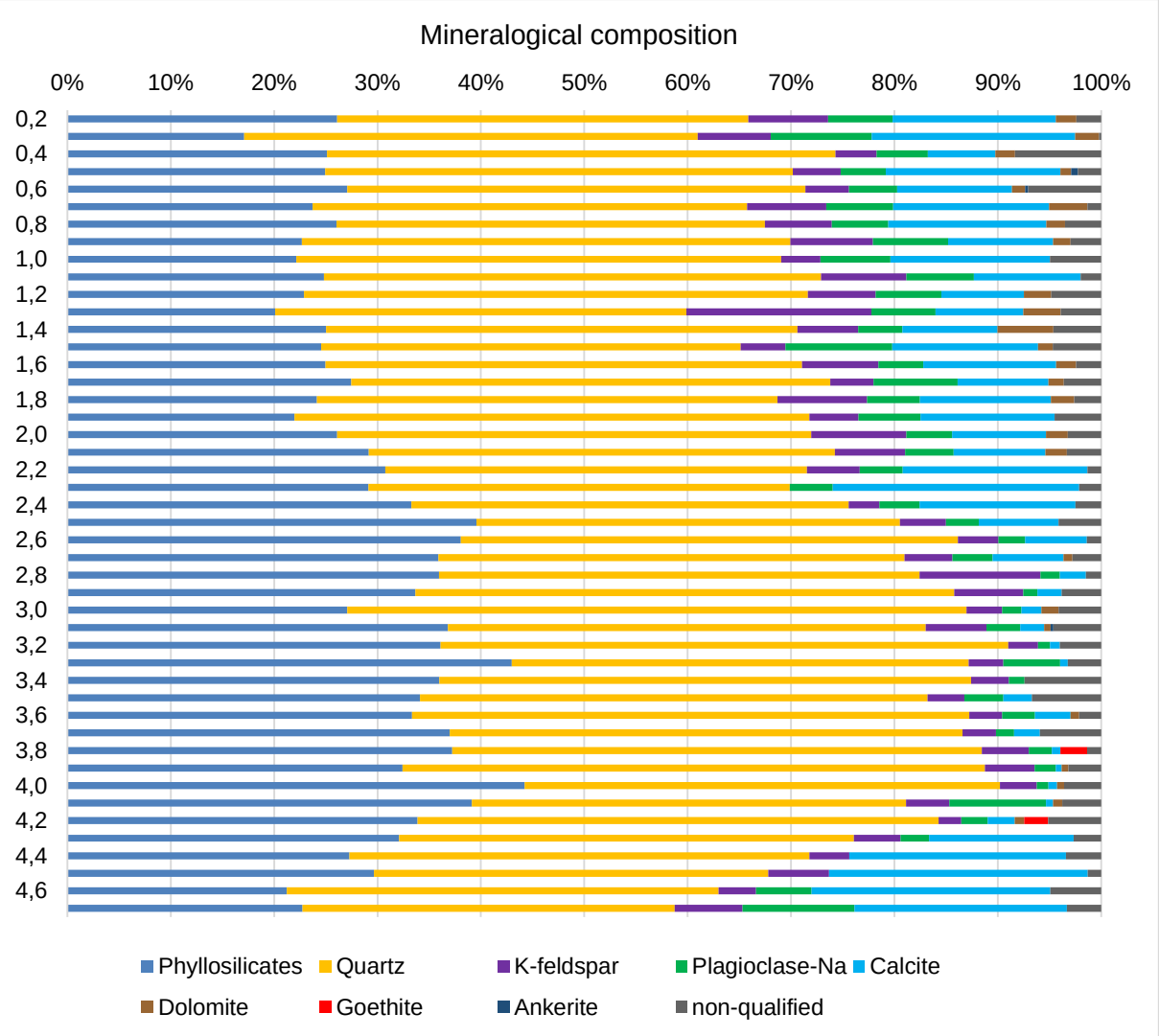

Figure 4.7: Mineralogical composition of the Bůhzdař profile.

4.3.1. Clay minerals

The proportion of clay minerals (phyllosilicates) fluctuates between 17.09 % in loess and 44.23 % in the horizons of paleosols (Fig. 4.7). The proportion of clay minerals rises considerably from the depth of 2.5 m (39.56 %) which is in the transition zone between Loess III and Loess IV. The proportion of phyllosilicates then oscillates to the beginning of the horizon of Loess V (32.09 % in the depth of 4.3 m) where the amount of clay minerals starts to decrease. The principal clay mineral composition (Fig. 4.8) consists of micas (7.24–16.36 %), chlorite (3.83–16.63 %), kaolinite (4.08–13.16 %) and smectite (0–8.44 %). The presence of smectite is mostly limited to horizons affected by pedogenesis. The total amount of the individual clay minerals is related to the total amount of clay minerals in the respective samples, i. e. the percentages of chlorite, micas and kaolinite in a given sample increase with an increasing proportion of clay in that sample.

The results of clay mineral composition are calculated from the XRD of ground samples and they are just informative and the values are not exact. For more precise determination of clay mineral composition and the proportions of clay minerals in the study profile, a different kind of XRD analysis with specific treatment of the samples including separation of clay sized particles and their treatment with various chemicals to distinguish diverse clay minerals would have to be carried out (Brindley, 1952).

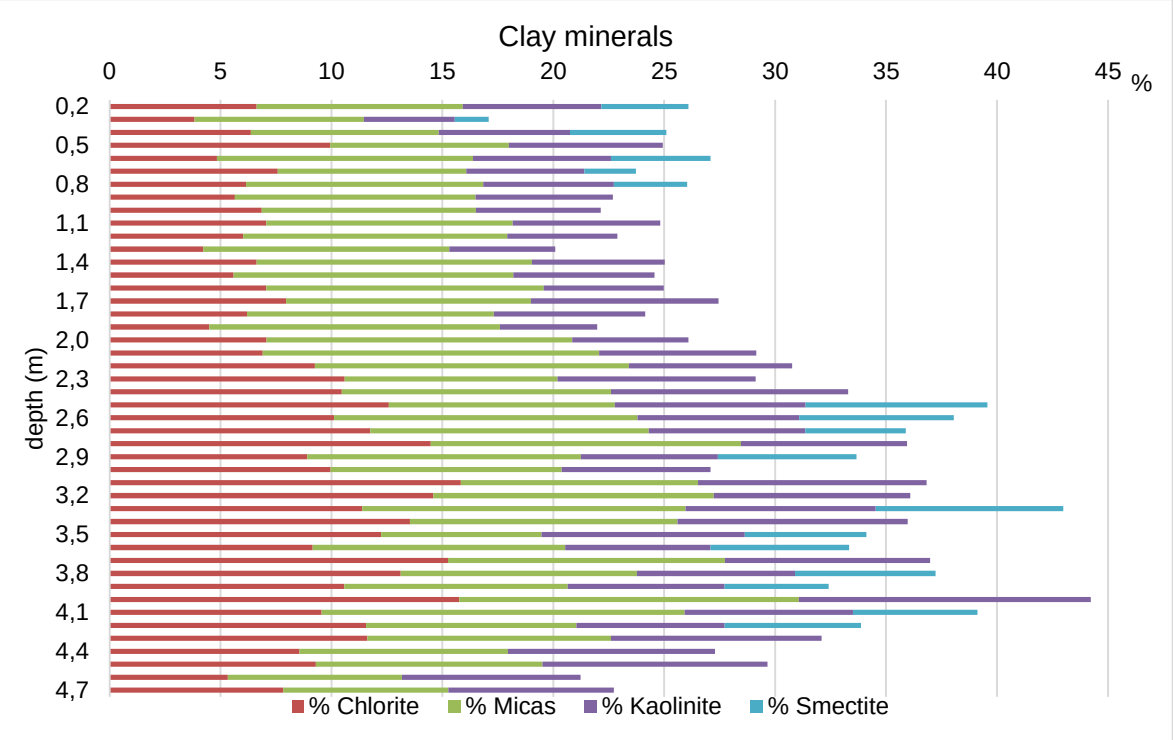

Figure 4.8: Clay minerals composition of the Bůhzdař profile (counted from the XRD of mineralogical composition).

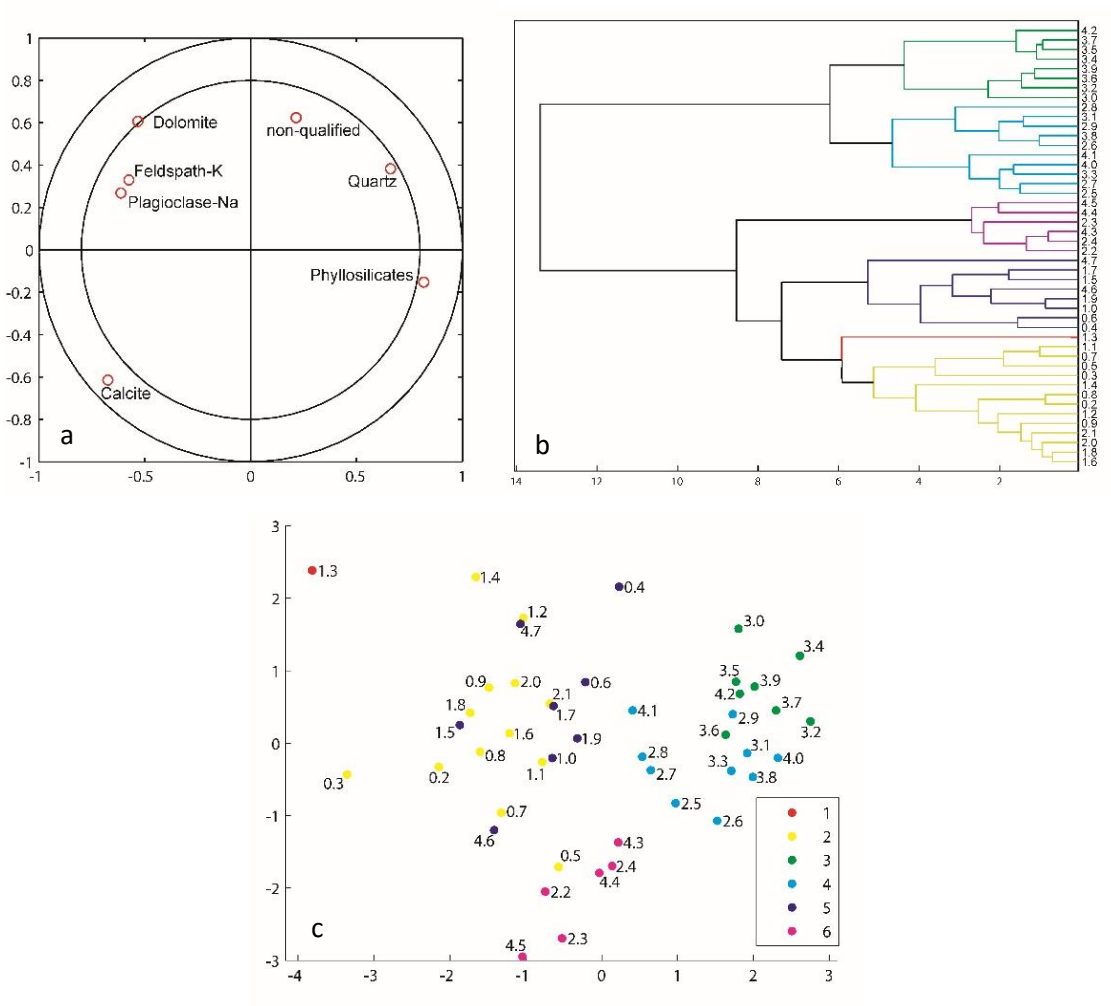

Figure 4.9: A Principal Component Analysis of mineralogical composition of the Bůhzdař profile, a: a correlation circle distributing the minerals according to their similar distribution in the study profile in the study profile, b: a dendrogram dividing the samples into groups based on the similarity of their mineralogical composition, c: the distribution of samples based on the similarity of their mineralogical composition and their division into groups according to the dendrogram.

A Principal Component Analysis (Fig. 9) divided the samples into 6 groups with similar mineralogical composition. Group number 1 is marked by red color and consists of a single sample (depth of 1.3 m) that is enormously rich in K-feldspar (17.90 %). Yellow color represents group number 2 which contains samples from the top part of the study profile 0.2–2.1 m (Recent soil and Loess I, II and III). Those samples are distributed on the left side of the chart. Some samples from this depth (0.4 m, 0.6 m, 1.0 m, 1.5 m and 1.7 m) form group number 5 (dark blue color) and they are distributed among the yellow group.

Group number 3, marked by green color, contains some samples from the paleosol horizons of Chernozemic paleosol I and II as well as Loess/paleosol (3.0–4.2 m). The next group, number 4, marked by light blue color, has similar properties to group number 3 and contains a number of samples from the depth 2.5–4.1 m. Group number 6 has the color pink and represents samples from Loess III and Loess V (2.2–2.4 m and 4.3–4.5 m) and can be seen at the bottom of the chart (Fig. 4.9).

4.4. Total organic carbon

The total organic carbon (TOC) is a basic index of input of organic matter into the soil and its stocking. The values from the study profile range from 0.27 % in the depth of 2.9 m to 0.71 % at 3.7 m (Fig. 1). The two uppermost samples represent horizon A/C of recent soil and the amount of TOC ranges between 0.29 and 0.26 %. The loess that is the parent material of recent soil (Loess I) can be affected by recent vegetation and its long roots (Vysloužilová, 2014) as well because the amount of TOC decreases from 0.23 % to 0.17 % in the horizon Loess I. The loess layers above the paleosols have values of TOC between 0.11 to 0.14 %. Chernozemic paleosol I exhibits TOC values between 0.27 % and 0.44 % and Chernozemic paleosol II shows TOC values from 0.52 % to 0.71 %. The loess layers found under the paleosol display values between 0.15 % and 0.27 %, considerably more than the upper loess layers (see above). Increasing amount of TOC in the loess layer from the depth of 2.6 m (0.18 % of TOC) down (Loess IV) is of interest as this can indicate a slow transition between soil and loess accumulation (Fig. 4.10). The horizon of Loess/paleosol, located under the chernozemic paleosols, shows similar values to the abovementioned transition horizon (Loess IV) between the Chernozemic paleosol I and Loess III. There is 0.19 % of TOC in the upper part (4.0 m) of the Loess/paleosol horizon and 0.16 % of TOC between 4.1 and 4.3 m of depth.

4.5. Color

Generally, the amount of TOC in individual samples seems to be linked to their color. This is apparent in the horizon of recent soil (color 10 YR 7/6 and almost 0.3 % of TOC) and in the horizons of paleosols (color from 10 YR 5/6 to 4/3 and TOC from 0.27 to 0.71 %) that are the darkest in the study profile (Fig. 10). On the other hand, the deepest loess horizon (4.35–5 m) that is the lightest horizon in the profile, color 10 YR 8/2, contains quite a lot of TOC (up to 0.27 %). This fact could be caused by a high content of white colored $CaCO_3$ content (20.96 – 25.01 % of calcite). Generally, the loess in the study profile has color ranging from 10 YR 7/3 to 10 YR 7/6, i.e. fairly consistent throughout the profile. The

differences in the color of study samples were often negligible and the classification of dry samples was very hard. It is possible that the difference between 10 YR 7/6 and 10 YR 7/4 is not so apparent in the horizon Loess III.

Another factor affecting color is iron content. As can be seen in Figure 4.10, there is no major difference between the amounts of TOC (around 0.13 %) in the loess from 1.1 m to 2.5 m of depth but the color around 1.3 m and 1.7 m is darker (10 YR 7/6 – 7/4) than in the loess above (10 YR 7/3). A comparison of iron content and color (Fig. 4.10) appears to show a relation between chroma and iron content. The horizons of Loess IV above and Loess/paleosol below the chernozemic paleosols contain the highest amount of iron in whole profile (3.83 to 4.29 % of FeO_3) and have a characteristic “rusty” color (10 YR 6/6).

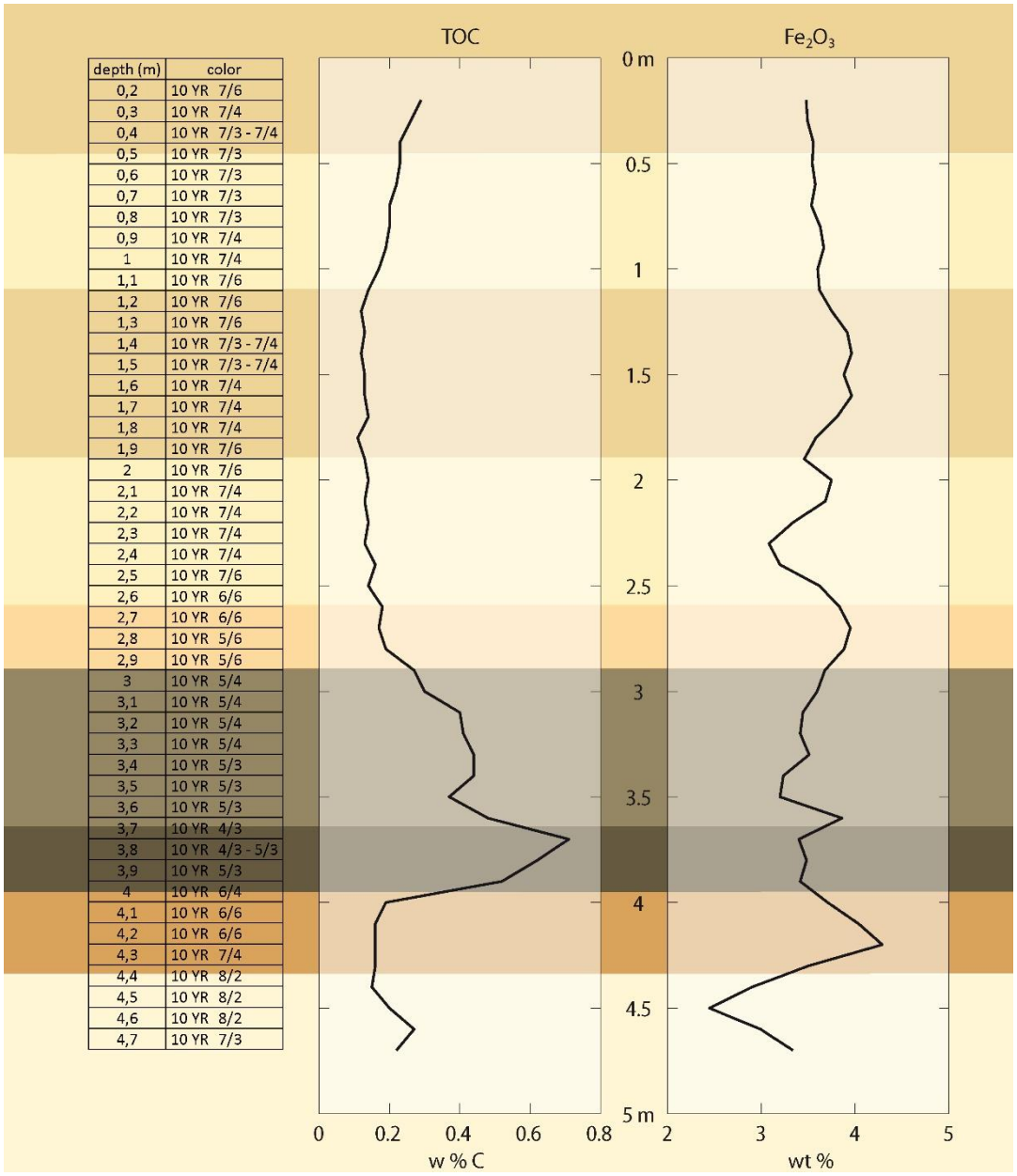

depth (m)	color
0,2	10 YR 7/6
0,3	10 YR 7/4
0,4	10 YR 7/3 - 7/4
0,5	10 YR 7/3
0,6	10 YR 7/3
0,7	10 YR 7/3
0,8	10 YR 7/3
0,9	10 YR 7/4
1	10 YR 7/4
1,1	10 YR 7/6
1,2	10 YR 7/6
1,3	10 YR 7/6
1,4	10 YR 7/3 - 7/4
1,5	10 YR 7/3 - 7/4
1,6	10 YR 7/4
1,7	10 YR 7/4
1,8	10 YR 7/4
1,9	10 YR 7/6
2	10 YR 7/6
2,1	10 YR 7/4
2,2	10 YR 7/4
2,3	10 YR 7/4
2,4	10 YR 7/4
2,5	10 YR 7/6
2,6	10 YR 6/6
2,7	10 YR 6/6
2,8	10 YR 5/6
2,9	10 YR 5/6
3	10 YR 5/4
3,1	10 YR 5/4
3,2	10 YR 5/4
3,3	10 YR 5/4
3,4	10 YR 5/3
3,5	10 YR 5/3
3,6	10 YR 5/3
3,7	10 YR 4/3
3,8	10 YR 4/3 - 5/3
3,9	10 YR 5/3
4	10 YR 6/4
4,1	10 YR 6/6
4,2	10 YR 6/6
4,3	10 YR 7/4
4,4	10 YR 8/2
4,5	10 YR 8/2
4,6	10 YR 8/2
4,7	10 YR 7/3

Figure 4.10: Color, total organic carbon and FeO_3 content in the Bůhzdař profile.

4.6. Stable isotopes $\delta^{13}C$ and $\delta^{18}O$

The stable isotope analysis provides data about the isotopic composition of the study profile, shown in Figure 4.11. The values are reported in per miles as deviation from the VPDB. The values of proportion of $\delta^{13}C$ in the soil organic matter ($\delta^{13}C_{org}$) are higher in the loess horizons (from -25.2 ‰ to -23.0 ‰) than in the paleosol horizons (from -26.1‰ to -24.6 ‰). The highest value reaches -23.0 ‰ in the depth of 1.8 m (Loess II) which is in the middle of the loess horizons. From this depth the values gradually decline until the depth of 3.6 m (-26.0 ‰) and 3.9 m where the value reaches the minimum in whole profile at -26.1 ‰ of $\delta^{13}C_{org}$. Thence the values rise again, ranging from -25.1 ‰ to -24.8 ‰ in the horizon of Paleosol/loess. At the bottom of the study profile, at a depth of 4.7 m (Loess V), the value is -24.5 ‰.

The values of $\delta^{13}C$ and $\delta^{18}O$ from pedogenic carbonates ($\delta^{13}C_{carb}$ and $\delta^{18}O_{carb}$) do not reflect the horizons (Fig. 4.11). The values of $\delta^{13}C_{carb}$ in the upper half of the study profile (0.2–2.5 m, Loess I, II and III horizons) fluctuate between -18.25 ‰ and -8.63 ‰, nearly covering the total range of values in the study profile. From the depth of 2.5 m (Loess III) to 3.4 m (Chernozemic paleosol I) the values of $\delta^{13}C_{carb}$ fluctuate between -12.67 ‰ and -9.39 ‰. The highest values were recorded in the horizons of Chernozemic paleosol II and Paleosol/loess (3.6–4.2 m), from -9.78 ‰ to -8.36 ‰, the latter being the highest value in the study profile. Relatively high values (-10.72 to -8.37 ‰) can also be found in the Loess V horizon (4.3–4.7 m).

The values of $\delta^{18}O_{carb}$ fluctuate in the upper half of the study profile (between -10.14 ‰ and -7.05 ‰), much like the abovementioned values of $\delta^{13}C_{carb}$. The range narrows between the depths of 2.5 m and 3.7 m (Loess III and IV and Chernozemic paleosol I and II) to -9.41 ‰ to -7.62 ‰. The highest values can be found in the bottom part of the study profile (3.8 m and below) in the horizons of Chernozemic paleosol II, Paleosol/loess and Loess V between -7.61 ‰ and -6.06 ‰.

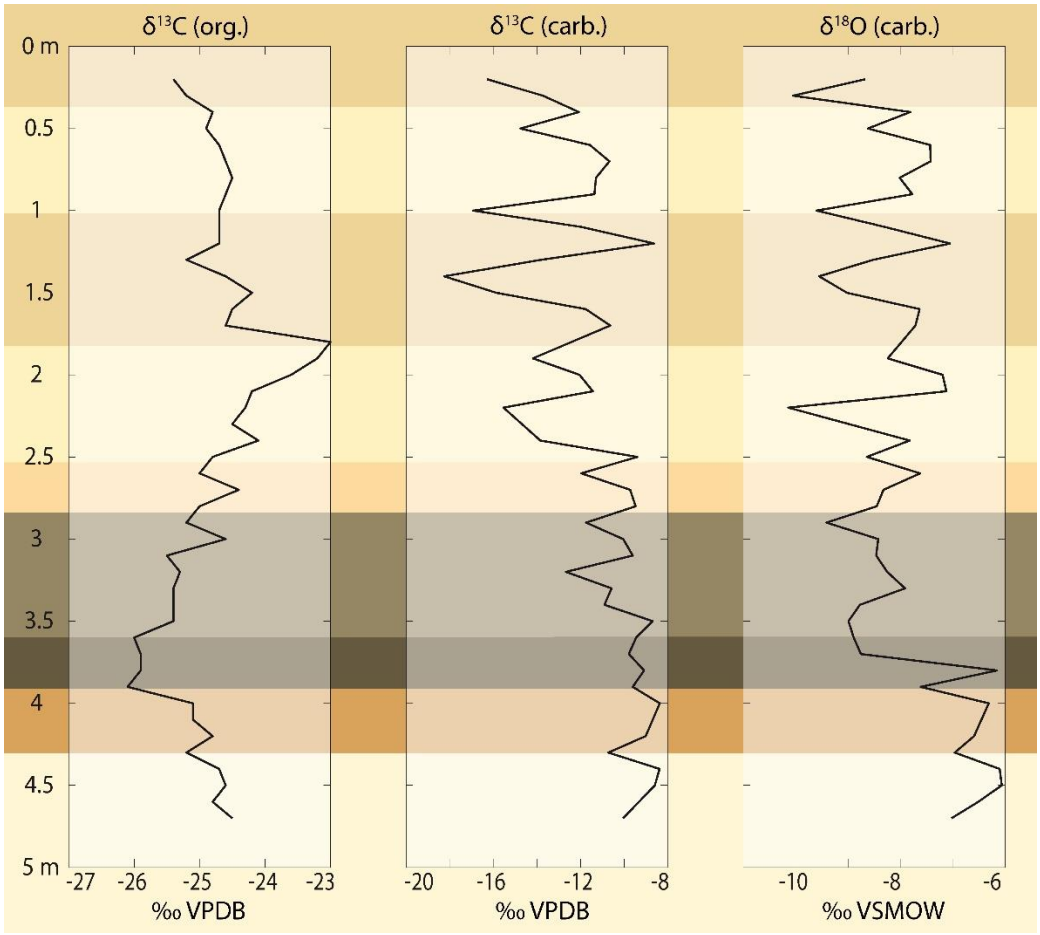

Figure 4.11: Stable isotopes composition of $\delta^{13}C$ and $\delta^{18}O$ in the Bůhzdař profile.

4.7. Total principal component analysis (total PCA)

The total PCA was calculated from variables selected from previous PCAs of grain size distribution, chemical composition (XRD), mineralogical composition (XRD), total organic carbon (TOC) and stable isotope $\delta^{13}C$ from the organic matter ($\delta^{13}C_{org}$). The chosen variables have the most diverse distribution in the correlation circles. The groups with similar distribution are represented by a single variable in the total PCA. The distribution of selected variables of the total PCA correlation circle is shown in the Figure 4.12.

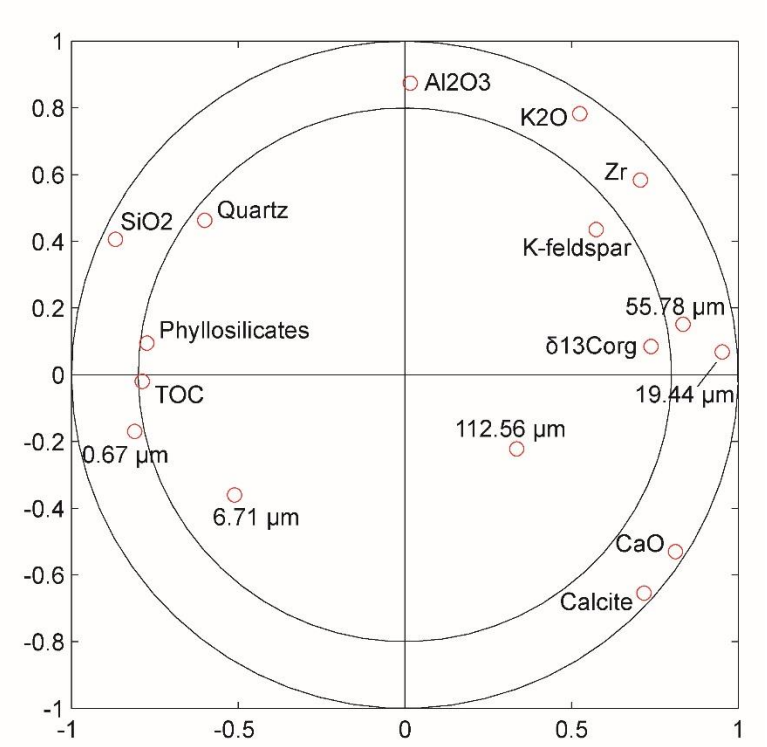

Figure 4.12: A correlation circle distributing the total PCA variables according to their similar distribution in the profile Bůhzdař.

The PCA divided samples into 7 groups (Fig. 4.13 and 4.14). The dendrogram in the Figure 4.13 has two main branches dividing samples into loess samples (0.2–2.4 m and 4.4–4.6 m) and paleosol samples (2.8–4.2 m). This division is also visible in Figure 4.14 where the loess samples are situated in the right half of the chart and the paleosol samples can be found in the left half. Group number 1 is marked by violet color in the charts and contains samples from the top part of the study profile 0.2–0.8 m (Recent soil and Loess I). Group number 2 (yellow color) contains samples from the depths between 1.2 m and 2.0 m that are part of the horizons of Loess II and the top part of Loess III. Group number 3 (pink color) is formed by two samples from the depths of 2.2 m and 2.4 m (Loess III) that are very rich in light loess dolls. Group number 4 is marked by brown color and is made up of samples from the transition between Loess IV and Chernozemic paleosol I (2.8 m and 3.0 m). Group number 5 consists of samples from depths between 3.2 m and 3.8 m (Chernozemic paleosol I and II) has the color green. Group number six marked by red color is a group of samples from the Paleosol/Loess horizon (4.0–4.2 m). The last group, group number 6, consists of samples from the deepest horizon of loess, Loess V (4.4–4.6 m).

Clearly visible is the fact that the samples from each group are predominantly distributed next to each other in Figure 4.14. This is a sign of similar distribution of the variables in each group and confirms the visual division into individual horizons.

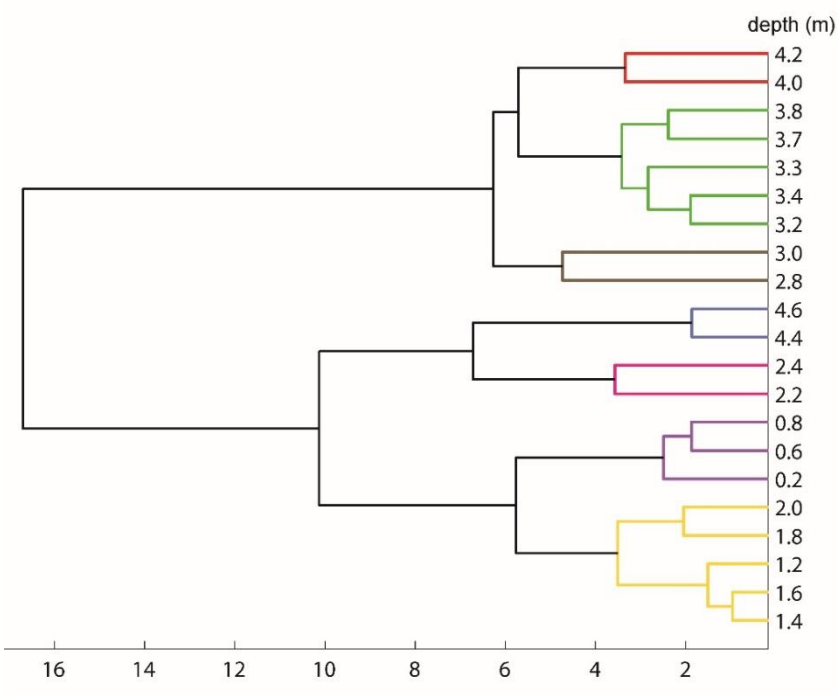

Figure 4.13: A PCA dendrogram dividing the samples into groups based on the similarity of variables distribution in the Bůhzdař profile.

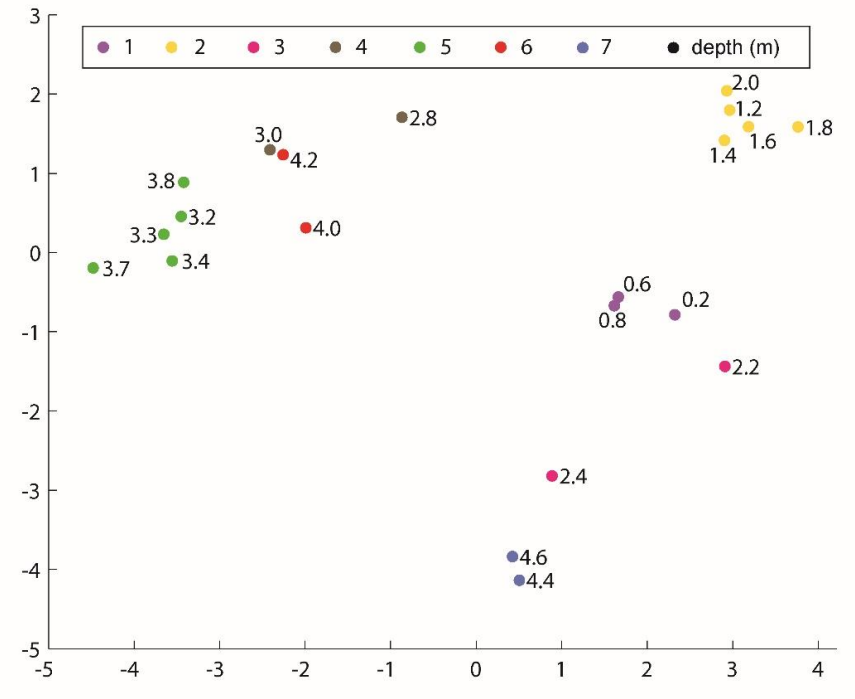

Figure 4.14: Distribution of samples based on the similarity of variables distribution in the Bůhzdař profile and their division into groups according to the PCA dendrogram.

4.8. Loess dolls

4.8.1. Color

Besides bulk material, $CaCO_3$ concretions, known as loess dolls, were also analyzed. The loess doll samples are denoted by the letter “C”). Loess dolls extracted from different depths of the study profile exhibit a different color (Tab. 4.3). It is noteworthy that the surface colors of loess dolls (outside color) have the same hue (10 YR) as all the bulk samples while the interior of loess dolls is much greyer and the hue is mostly 5 YR. The lightest recorded color is nearly white (10 YR 8/1) while the darkest color is nearly black (5 YR 4/1) (Fig. 4.15).

Figure 4.15: The lightest (10 YR 8/1) and the darkest (5 YR 4/1) loess dolls.

Table 4.3: Colors of loess dolls in the Bůhzdař profile.

Depth (m)	Ouside color	Inside color
C 1.6	10 YR 7/3	5 YR 6/1
C 2.4	10 YR 8/1	5 YR 8/1
C 3.6	10 YR 4/2	5 YR 4/1
C 4.5	10 YR 8/2	10 YR 6/1

.

4.8.2. Chemical and mineralogical composition

As it was presumed the loess dolls as the concretions of $CaCO_3$ contain large amounts of $CaCO_3$. The mineralogical analysis (XRD) of the light loess doll from the depth of 2.4 m demonstrated 99 % of calcite while the dark one in the depth of 3.6 m only contained 70 % of calcite (Tab. 4.4). The rest of the minerals is quartz. The chemical composition analyses (XRF) confirmed the mineralogical data with high content of CaO (49.33 % for the light loess doll and 40.23 % for the dark one) and CO_3 (40.05 % for the light loess doll and 34.02 % for the dark one). The amount of SiO_2 reaching 7.99–19.22 % is quite high as well (Tab. 4.4). The other major elements are insignificantly present. Although the trace elements are less present than the major ones, the difference from to the amount of trace elements in the bulk samples is not as significant as it is in the case of major elements. The dark loess doll is richer in all elements compared to the light one (Tab. 4.4).

Table 4.4: Chemical and mineralogical composition of loess dolls from the Bůhzdař profile.

Sample depth (m)	Major elements composition (% weight total)									Trace elements composition (ppm)							Calcite (%)	Quartz (%)
	SiO_2	TiO_2	Al_2O_3	Fe_2O_3	MgO	CaO	Na_2O	K_2O	CO_3	Mn	Rb	Sr	Zr	Ba	La	Ce		
C 2.4	7.99	0.08	1.13	0.41	0.63	49.33	0.05	0.17	40.05	94	12	143	32	74	14	7	99	1
C 3.6	19.22	0.25	3.28	1.23	0.68	40.23	0.16	0.53	34.02	465	37	266	79	209	19	21	70	30
C 4.5	17.04	0.14	2.29	0.81	0.67	42.87	0.09	0.38	35.52	-	-	-	-	-	-	-	-	-

4.8.3. Stable isotopes $\delta^{13}C$ and $\delta^{18}O$

The stable isotopes $\delta^{13}C$ and $\delta^{18}O$ were measured from the carbonate concretions. The results are very interesting because all the values are very similar (Tab. 4.5). The differences between the minimum and maximum of $\delta^{13}C_{carb}$ is only 1.32 ‰ (9.89 ‰ for the bulk samples) and 0.60 ‰ $\delta^{18}O_{carb}$ (4.08 for the bulk samples).

Table 4.5: Stable isotopes $\delta^{13}C$ and $\delta^{18}O$ of loess dolls in the Bůhzdař profile.

Depth	$\delta^{13}C_{carb}$	$\delta^{18}O_{carb}$
C 1.1	-9.61	-6.36
C 1.5	-9.47	-6.26
C 1.6	-9.53	-6.28
C 2.4	-9.18	-6.31
C 2.9	-9.22	-6.41
C 3.6	-8.83	-6.11
C 4.3	-8.88	-6.13
C 4.4	-8.89	-6.05
C 4.5	-8.29	-5.82
C 4.6	-8.98	-5.88

4.9. Paleoclimate transfer functions

Paleoclimate transfer functions reconstructing mean annual temperatures (MAT) and mean annual precipitation (MAP) were calculated by Sheldon et al. (2002), Hall and Penner (2013) and Tabor and Myers (2015) (Tab. 4.6). The mean annual precipitation estimates show differences between loess horizons (dryer) and paleosols horizons (more humid). The mean annual temperature estimates are do not exhibit much variety and do not show relevant differences between loess horizons and paleosols horizons.

Table 4.6: Approximations of mean annual precipitation (MAP) and mean annual temperatures (MAT) by the paleoclimate transfer functions based on data of XRF and $\delta^{13}C_{org.}$

		Loess I	**Loess II**	**Loess III**	**Loess IV**	**Cher. paleosol I**	**Cher. paleosol II**	**Loess/p.**	**Loess V**
XRF	**MAP1 (mm)**	376–392	397–431	357–485	521–564	605–670	536–666	695–711	276–381
	MAP2 (mm)	503–524	535–574	480–581	709–755	790–838	726–852	818–860	364-517
	MAP3 (mm)	416–459	481–552	386–543	797–902	992–1081	834–1097	1060–1162	230–441
	MAT1 (°C)	16.5–16.6	16.5–16.7	16.6–16.8	17.2–17.5	17.6–17.8	17.5.–17.7	17.5–17.8	16.2–16.6
	MAT2 (°C)	8.4–8.6	8.4–8.8	7.8–8.2	7.8–8.2	7.4–7.7	7.7–8.4	7.9–8.5	7.6–8.2
	MAT3 (°C)	11.0–11.7	10.7–11.3	10.8–12.6	12.6–12.7	12.5–12.6	12.3–12.6	12.7–13.1	12.0–12.4
δ13Corg	**MAP4 (mm)**	506–517	466–525	481–514	504–515	510–531	542–548	514–524	505–512
	MAT4 (°C)	7.5–7.9	7.5–8.7	7.7–8.4	7.6–7.9	7.4–7.8	7.0–7.2	7.5–7.7	7.8–7.9

5. Discussion

5.1. Grain size distribution

Muhs (2007) defines the grain size composition of loess as typically made of 60–90 % silt-sized particles (50–2 μm diameter) and measureable amounts of clay-sized particles (<2 μm) and sand-sized particles (>50 μm). However, European authors define the silt-sized particles as particles 63–2 μm in diameter (Rousseau et al., 2007; Antoine et al., 2009; Terhorst et al., 2009, 2015). The grain size division is not unified and authors differ not only on the upper size limit of silt but also on the lower limit. Hošek et al., 2015 define silt-sized particles as particles between 4 μm and 63 μm. For our study we used the most common European division of silt (63–2 μm) that is defined in Figure 3.12. Nevertheless, the amount of silt-sized particles in the loess samples is between 70.20 % and 82.26 % (61.29 % to 75.54 % for the samples of paleosols) in the Bůhzdař profile. This corresponds very well with other European loess profiles. The amount of silt-sized particles is generally approximately 60–80 % (Rousseau et al., 2007). The clay-sized content in the upper loess horizons (Loess I, II and III) is in accordance with the European average (>20 %, Rousseau et al., 2007) with values ranging from 11.47 % to 18.73 %. Slightly higher values were record in the samples from the lowest loess horizon (Loess V), between 21.50 % and 23.71 % of clay. On the other hand, the values of clay-sized particle content in the chernozemic paleosol samples are noticeably higher (24.21–35.33 %) than in the loess samples. The sample from the depth 4.0 m is noteworthy as it is depleted in clay (only 17.36 % compared to values over 23 % in ambient samples). This fact can be explained by leaching (Sheldon and Tabor, 2009) or by input of new aeolian material (Hradilová, 1994). Another sample worth attention is the one from the depth of 2.8 m (Loess IV) with a clay content of 27.38 %, which is too much to be included in to the loess. This sample is definitely part of the horizon of slow transition between forming loess and paleosol and it is closer to paleosol than to loess (Rousseau et al., 2007). Besides the samples rich in coarse particles, there are also samples without any coarser material content in the Bůhzdař profile. Those samples were found in the depths of 3.3 m and 3.7 m (Chernozemic paleosol I and II) and they do not contain any particles bigger than 20 μm. This can indicate low rates of sedimentation and no input of coarser aeolian material because of no close source of deflatable material (<30 km) (Muhs, 2013).

In general, grain size of aeolian material is associated with wind strength during the transportation of material (Pye, 1987; Muhs, 2007; Antoine et al., 2009). Stronger wind can move larger particles and the final grain size is coarser. This fact is widely used as the

connection between aeolian dynamics and climate changes (Shi et al., 2003; Porter, 2007; Antoine et al., 2009). Therefore, peaks of coarse particles (>63 μm) in grain size distribution correspond with times when the winds and transport of aeolian material strengthened (Antoine et al., 2009). Shi et al., 2003, who worked on the loess-paleosol sequence in Dolní Věstonice (Czech Republic), liken the peaks (up to 40 %) of coarse grain size distribution to the Heinrich events which are associated with large and rapid climate changes. Antione et al., 2013 resampled the study of Shi et al, 2003 and they correlated the peaks of coarse grain size distribution with a locality in Nussloch (Germany) and North GRIP $\delta^{18}O$ values (Fig. 5.1) that reflect climate changes.

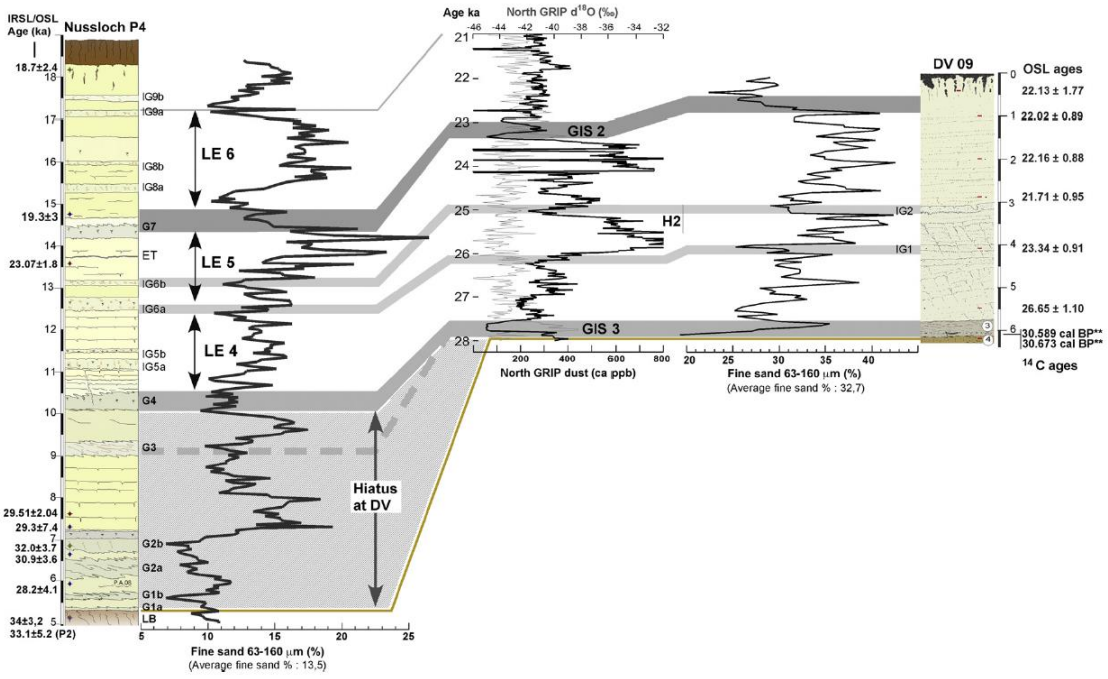

Figure 5.1: Comparison between coarse fraction (>63 μm) in loess profiles in Nussloch and Dolní Věstonice (DV) and NGRIP dust and $\delta^{18}O$ records. Source: Antoine et al., 2013.

Grain size distribution in Zeměchy, the closest well studied profile to Bůhzdař, was studied by Hošek et al. 2015. There are also apparent peaks in sand-sized particles (>63 μm) in the loess horizons (Fig. 5.2), over 25 % in Zeměchy and over 20 % in Dobšice (Czech Republic). Grain size is coarser in Zeměchy because of the presence of pellet sands (Hošek et al., 2015).

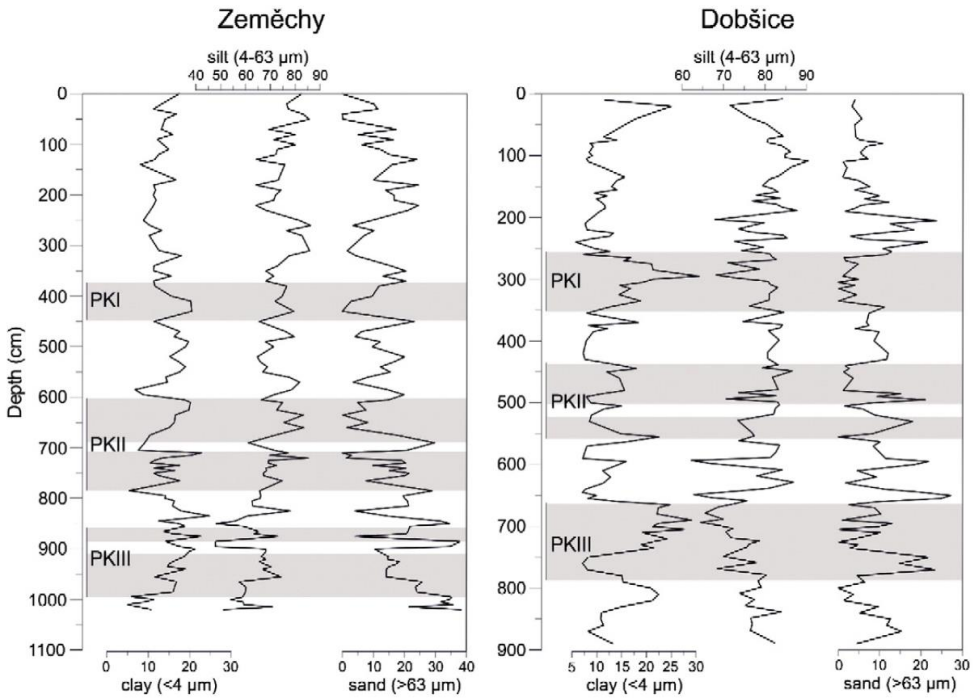

Figure 5.2: Grain size distribution of the Zeměchy profile, close to the Bůhzdař profile, and the Dobšice profile. Source: Hošek et al., 2015.

The peaks of coarser grains are can also be seen in the Bůhzdař profile (Fig. 5.3). The biggest peak is in the depth of 2.2 m (Loess III) and reaches up to 16.05 % of sand-sized particles. However, samples of grain size distribution in this thesis were extracted every 20 cm which is too low a resolution for further interpretation.

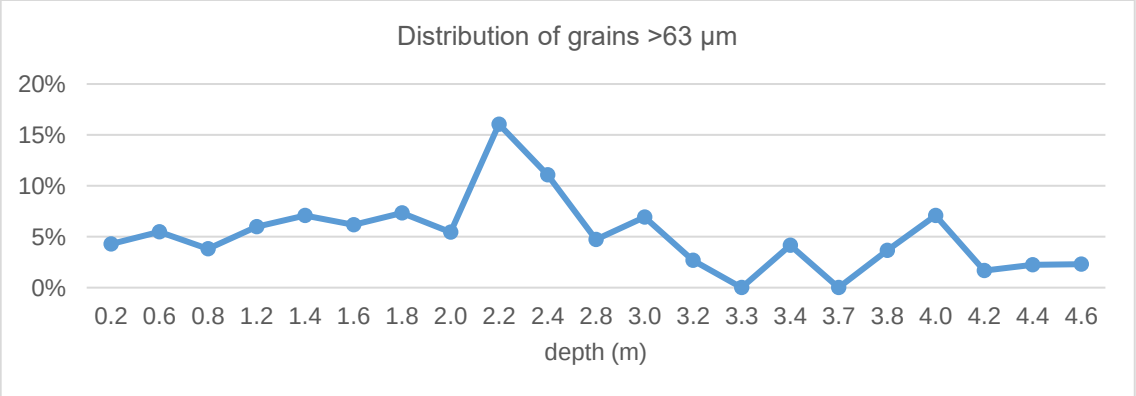

Figure 5.3: Distribution of sand-sized grains in the Bůhzdař profile.

5.2. Chemical composition (XRF) and mineralogical composition (XRD)

The most common mineral in loess is quartz, in European loess its amount ranges from 40 % to 80 %, followed by phyllosilicates (up to 30 %). Beside quartz and phyllosilicates, loess contains carbonates (calcite, dolomite) and feldspars (Rousseau et al., 2007). The

chemical composition is dependent on the mineralogical composition of loess. Loess is typically geochemically composed of dominant SiO_2 (55–65 %), Al_2O_3, Fe_2O_3, TiO_2, MgO and CaO (Muhs, 2007). The amount of Al_2O_3, Fe_2O_3 and TiO_2 depends on clay minerals content and the amount of CaO and MgO depends on the amount of carbonates (Muhs, 2007).

The mineralogical and geochemical composition of European loess corresponds well with the composition of the Bůhzdař profile. Quartz content is slightly lower in Bůhzdař, between 36.02 % and 49.72 %, the amount of phyllosilicates reaches up to 39.56 %. However, those values are not very indicative since XRD is primarly a qualitative method and the quantitative values merely an estimate. The chemical composition (XRF) of the Bůhzdař profile is far more precise, the values of SiO_2 content range between 56.90 % and 64.06 %, corresponding with the loess average by Muhs, 2007. The world average of geochemical composition by Újvari et al., 2008 (70.71 % of SiO_2) is not very relevant because the spatial distribution of studied loess regions is not particularly representative. Central Europe is represented just by samples from Hungary while Eastern Europe, with the largest loess cover in Europe (Frechen et al. 2003), is completely missing. However, the values recorded at the Bůhzdař profile (with average loess sample values 60.69 % of SiO_2 and 9.60 % of Al_2O_3) can be placed between Kaiserstuhl in Germany (59.90 % of SiO_2 and 7.88 % of Al_2O_3) and profiles in Hungary (63.87 % of SiO_2 and 12.41 % of Al_2O_3) as recorded by Újvari et al., 2008, which is consistent with its geographical location. The geochemical composition of paleosols is qualitatively the same as the loess composition but the proportions of individual components are different. This fact is caused mainly by leaching and other soil forming mechanisms (Sheldon and Tabor, 2009; Antoine et al., 2009; Drewink et al., 2014; Tabor and Myers, 2015). The paleosols differ from loess mostly in the values of SiO_2 that reach over 70 % in paleosols (around 50 % of quartz) and the amount of phyllosilicates (up to 44.02 %). The content of carbonates is lower in the paleosols (0–3.45 % of calcite) than in loess (up to 25.01 %).

Besides the principal minerals in the study profile, it is important to mention two more minerals that were found in some samples of the study profile: goethite and amphibole. Goethite wad detected in two samples of paleosols, in the depth of 3.8 m (Chernozemic paleosol I) and in the depth of 4.2 m (Loess/paleosol). Goethite is probably the product of weathering and can signalize higher acidity and oxidation in the soil during its formation (Tabor and Myers, 2015). Amphibole was detected in three loess samples in the horizon of Loess I (0.4 m, 0.8 m and 1.0 m) and in two paleosols samples in the depth of 3.5 m (Chernozemic paleosol I) and 3.9 m (Chernozemic paleosol II). Amphibole is a typical mineral for igneous rocks (Kachlík and Chlupáč, 1996). The presence of amphibole in

certain samples can indicate changes in material input. Localities with igneous rocks are located no less than 9 km W (Vinařická hora) and 11 NW (Slánská hora) of the Bůhzdař profile. Larger-scale areas of igneous rocks are situated 45 km N (Central Bohemian Uplands) of the study locality (Geologická mapa 1: 50 000, 2013). Thus, the presence of amphibole in certain samples can hint at changes in wind direction or intensity.

The presence of a higher amount of clay minerals (phyllosilicates) can signal pedogenesis in the past as the increased presence of clay-sized particles (Sheldon and Tabor, 2009). A significantly higher amount of phyllosilicates (over 33 %) is visible from the depth of 2.4 m (Loess III) in Figure 5.4. Between the depths of 2.4 m and 4.3 m the content of clay minerals fluctuates between 32.09 % and 44.23 %, twice more than in a number of loess samples. Except for the presence of goethite that signalizes higher oxidation rates and acidity in the paleosols (Tabor and Myers, 2015), we cannot confirm any other significant differences in the distribution of different clay minerals in the Bůhzdař profile because the results of mineralogical composition analysis are only tentative for the clay minerals. There seems to be a slightly higher proportion of chlorite in the samples between 2.3 m and 4.3 m that could suggest weak weathering (Tabor and Myers, 2015) and aridity (Khormali and Kehl, 2011). However, the higher proportion of chlorite may not be relevant because it was calculated from total proportion of phyllosilicates which is higher in those samples.

For a more precise explanation of pedogenic processes in the study profile it is necessary to use the results of the chemical composition analysis (XRF). The most significant differences between the loess and paleosol samples is the amount of more soluble compounds such as CaO, MgO, Na_2O and K_2O that are more abundant in loess than in the paleosols from where they were leached (Chesworth, 2008, Sheldon and Tabor, 2009). Al_2O_3 and Fe_2O_3 are distributed evenly in the study profile and do not show any noticeable differences between loess and chernozemic paleosols. This can be explained by high $CaCO_3$ content in the entire profile (calcified root cells are present in the whole profile) and low rates of leaching. However, Loess/paleosol has higher amount of Al_2O_3 and Fe_2O_3 (over 11 % of Al_2O_3 and over 4 % of Fe_2O_3) and a slight increase with depth was recorded in this horizon. This can indicate the presence of the process of illuviation in the past and the Loess/paleosol horizon could be described as a horizon of subsoil, B horizon of Luvisol (Chesworth, 2008, Huang et al., 2012). A comparison of clayeyness ratio Al/Si and clay sized particles shows a similarity of the curve in the bottom part of graph (Fig. 5.4), most notably peaks at the same depths, around 3.7 m and 4.2 m, that signify a high rate of pedogenesis. The increasing values between the depths of 3.9 and 4.2 m can probably be

attributed to illuviation (Sheldon and Tabor, 2009). The upper part of graph in Figure 5.4 is affected by loess input and does not reflect the clayeyness.

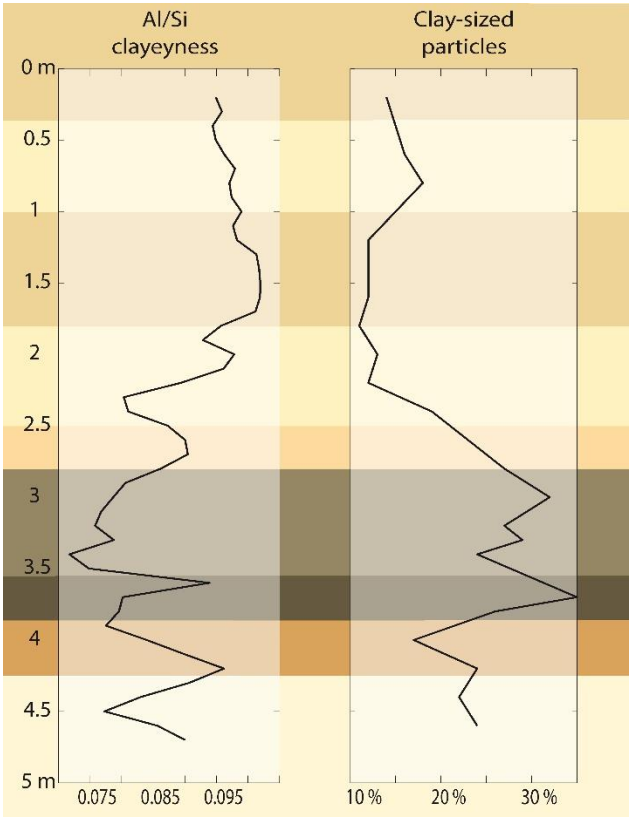

Figure 5.4: The molar ratio Al/Si representing the clayeyness and the distribution of clay-sized particles in the Bůhzdař profile.

Many authors of recent European papers containing XRF results (Bábek et al., 2011; Bokhorst et al., 2009; Buggle et al., 2011; Hošek et al., 2015; Obreht et al., 2015; Schatz et al., 2015) use element ratios for better clarity and representation of pedogenic processes, especially the chemical index of alteration (CIA) by Nesbitt and Young, 1982.

In this thesis, the molecular weathering and pedogenesis ratios by Sheldon and Tabor (2009) and chemical index of alteration (CIA) by Nesbitt and Young (1982) calculated by Babechuk et al. (2013) were used.

The comparison of the element ratios with other profiles is just illustrative. The chemical composition of loess differs by region and the amount of crucial elements that give the values of weathering ratios can be different within one locality (Újvari et al., 2008; Antoine et al., 2009). However, the weathering ratios representing leaching by proportion of mobile elements such as Sr or bases (Ca, Na, K, Mg) and stable elements such as Ba, Rb or Al show differences between loess horizons and paleosols horizons very well (Gallet et al.,

1996, 1998; Sheldon and Tabor, 2009). The most commonly used trace element ratios are Ba/Sr and Rb/Sr, both exhibit a similar shape of curve and both ratios express leaching intensity (Gallet et al., 1996; Chen et al., 1999; Zech et al., 2008; Sheldon and Tabor, 2009; Bábek et al., 2011; Buggle et al., 2011; Hošek et al., 2015; Obreht et al., 2015). As is visible in Figure 5.5, CIA and Ba/Sr or Rb/Sr ratios all have peaks in paleosols and minimums in loess horizons. The methods of CIA calculation are not unified (especially the values of CaO such as the Ca content of silicates) and results of CIA can be different (McLennan, 1993; Zech et al., 2008; Goldberg and Humayun, 2010). Therefore, it is not possible to compare the CIA values from different studies because the authors generally do not describe in detail the steps for solving the equation of chemical index alteration.

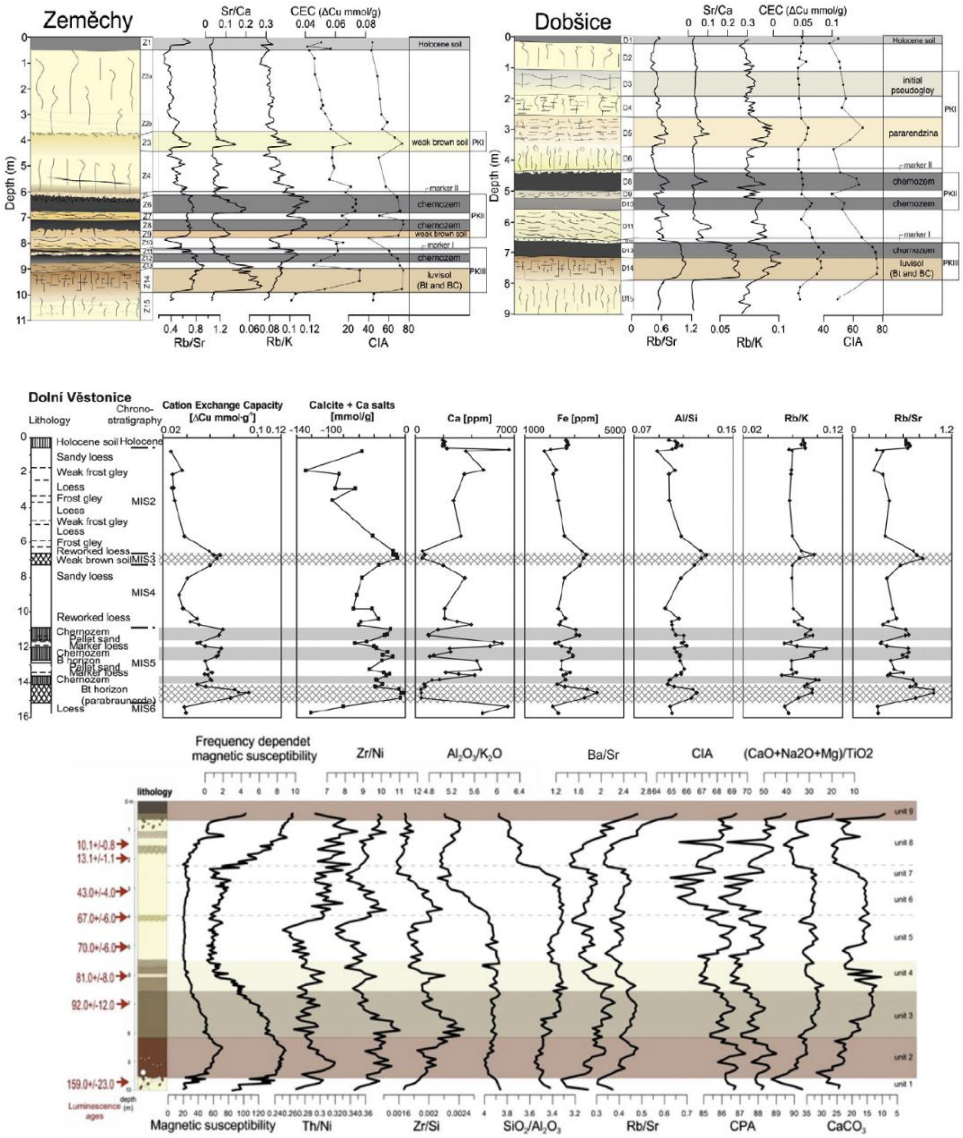

Figure 5.5: Loess/paleosols sequences in the Czech Republic and Serbia: a) Zeměchy and Dobšice, Czech Republic, by Hošek et al., 2015, b) Dolní Věstonice, Czech Republic, by Bábek et al., 2011, c) Orlovat, Serbia, by Obrecht et al., 2015

The Bůhzdař profile does not confirm the similarity of CIA and Ba/Sr curves. Ba/Sr ratio shows high values around the depth of 1.5 m (Loess II) that suggest leaching and possibly a presence of paleosol while the CIA graph shows higher values only in the horizons of paleosols (Chernozemic paleosol I and II and Paleosol/loess). Nevertheless, the horizon of Loess II has CIA values slightly higher than the surrounding loess and can represent a very slightly developed soil.

The similarity in minimal values of most of elements and peaks in amount of CaO between the Bůhzdař profile and Stary Kaydaky (Ukraine) studied by Buggle et al., 2011 (Fig. 5.6) seems very interesting. Those minimal values correspond with the presence of big loess dolls in the Bůhzdař profile. However, Buggle et al., 2011 do not mention $CaCO_3$ concretions at all. For further comparison a more detailed description of the Stary Kaydaky profile would be helpful.

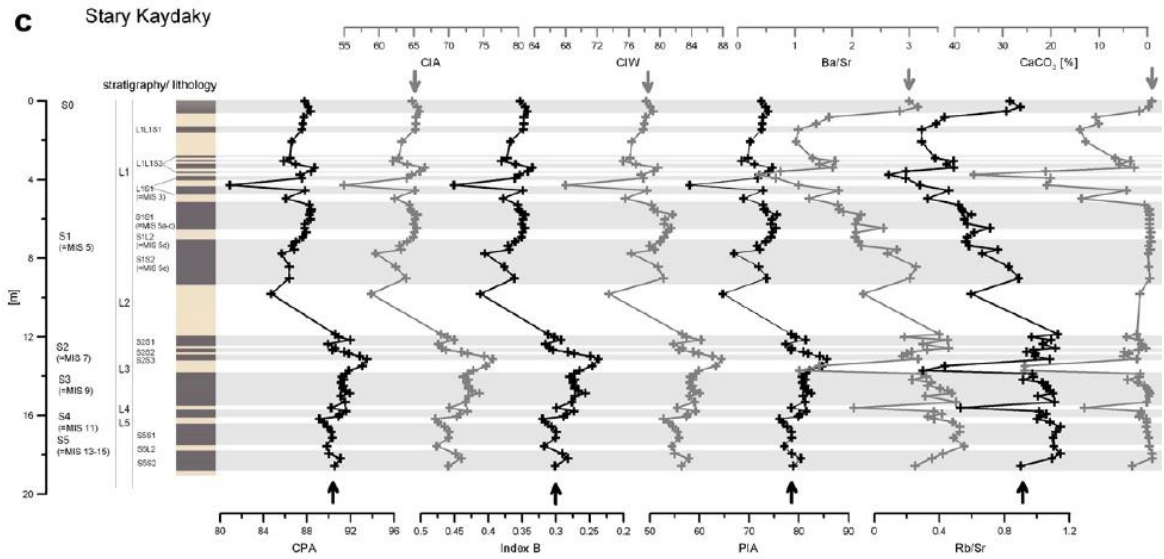

Figure 5.6: Stary Kaydaky (Ukraine) profile and the geochemical proxies. Source: Buggle et al., 2011.

5.3. Total organic carbon (color)

The values of total organic carbon (TOC) from the study profile occur between 0.27 % in the depth of 2.9 m and 0.71 % in the depth of 3.7 m, corresponding very well with the results of TOC content from other localities in the Czech Republic and western Slovakia. The fossil chernozems have TOC values between 0.3 to 1.0 % of total organic carbon in Central Europe (Vysloužilová et al., 2014). The values of other fossil chernozems are similar, around 0.5 % in Serbia (Hatté et al., 2013). The values of TOC in loess are very low in most

of profiles. In the Nussloch profile (Germany), the TOC value in loess is less than 0.1 % (Hatté et al., 2009), in the Dolní Věstonice profile (Czech Republic), the amount of TOC is lower than 0.1 % as well (Antoine et al., 2013). Slightly higher values (TOC content around 0.15 %) were recorded in the Surduk profile (Serbia), these values are still very low compared to fossil chernozem (Hatté et al., 2013). The values of TOC of the loess horizons Loess I, II, III and IV of the Bůhzdař profile (around 0.16 %) correspond well with the European loess profiles' values. The values of TOC of the horizon of Loess V are slightly higher, up to 0.27 %. It seems interesting that the horizon of Loess V has the lightest color (10 YR 8/2) but the TOC content is quite high (up to 0.27 %) compared to the dark horizons of Chernozemic paleosol I 10 YR 5/4–5/3) with a TOC content of around 0.41 %.

5.4. Stable isotopes $\delta^{13}C$ and $\delta^{18}O$

Stable isotope records from the loess/paleosol sequences are not very numerous. There is just one study describing the stable isotope $\delta^{13}C$ record from organic matter ($\delta^{13}C_{org}$) in the Dolní Věstonice profile in the Czech Republic by Antoine et al. (2013). The records of stable isotopes $\delta^{13}C$ and $\delta^{18}O$ from pedogenic carbonates are completely missing in the Czech Republic. The Bůhzdař profile has values of $\delta^{13}C_{org}$ ranging from -26.1 ‰ (Chernozemic paleosol II) to -23.0 ‰ (Loess III) which corresponds perfectly with $\delta^{13}C_{org}$ values of the Dolní Věstonice profile (from -26 ‰ in the fossil chernozems to -23 ‰ in the loess) that is situated 230 km SE of the study profile (Antoine et al., 2013). Those values correspond with another well studied profile, the Nussloch profile (Germany) with $\delta^{13}C_{org}$ values ranging from -24.9 ‰ in the paleosol to -23.5 ‰ in loess and with the highest measured value of $\delta^{13}C_{org}$ -25.8 ‰ in recent soil (Hatté et al., 1999). Similar values of $\delta^{13}C_{org}$ (mean value -24.5 ‰) were described by Hatté et al. (1998) in the Achenheim profile (Germany). It is generally assumed that vegetation is mostly composed of C3 plants in European temperate regions (Collins, 1986; Collatz et al., 1998) and the differences in amount of $\delta^{13}C$ in organic matter are caused by climate changes such as temperature, humidity, available soil water and amount of the atmospheric CO_2 (O'Leary, 1988; Hatté et al., 1999; Antoine et al., 2013; Obreht et al., 2014). The values of $\delta^{13}C_{org}$ in most cases inversely correspond with the values of TOC in the studied profiles (Hatté et al, 1998, 1999; Schatz et al., 2011; Antoine et al., 2013; Hatté et al., 2013; Obreht et al., 2014). However, some profiles that are located SE of the Czech Republic (Tokaj in Hungary, Crvenka in Serbia, Belotinac in Serbia) show slightly higher values of $\delta^{13}C_{org}$ in recent soils (around -23 ‰), possibly caused by a greater amount of C4 plants (Collins, 1986), than recent soils in the Czech and German profiles (Fig. 5.7). The amount of $\delta^{13}C_{org}$ in loess is around -24 ‰ in the Hungarian and Serbian profiles, comparable to other European and Chinese loess locations (Jiamao et al., 1996;

Porter et al., 2001; Li and Liu, 2003; Kaakinen et al., 2006; Ning et al., 2006; Schatz et al., 2011; Zech et al., 2013; Obreht et al., 2014; Rao et al., 2015). Nevertheless, the profiles from Serbia (Crvenka and Surduk) recording paleosols from the last interglacial show the lowest values of $\delta^{13}C_{org}$ (around -25.5 ‰) in these horizons of developed paleosols (Hatté et al., 2013; Zech et al, 2013). That hints at a predominance of C3 plants, similar to other European profiles. All the European profiles refer to an increasing amount of vegetation (higher TOC values) when the amount of $\delta^{13}C_{org}$ is low in the past. The developed paleosols (mostly fossil chernozems) reach the lowest $\delta^{13}C_{org}$ values while weakly developed soils do not show significant differences from the surrounding loess (Hatté et al., 1998, 1999; Anotine et al., 2013; Obreht et al., 2014).

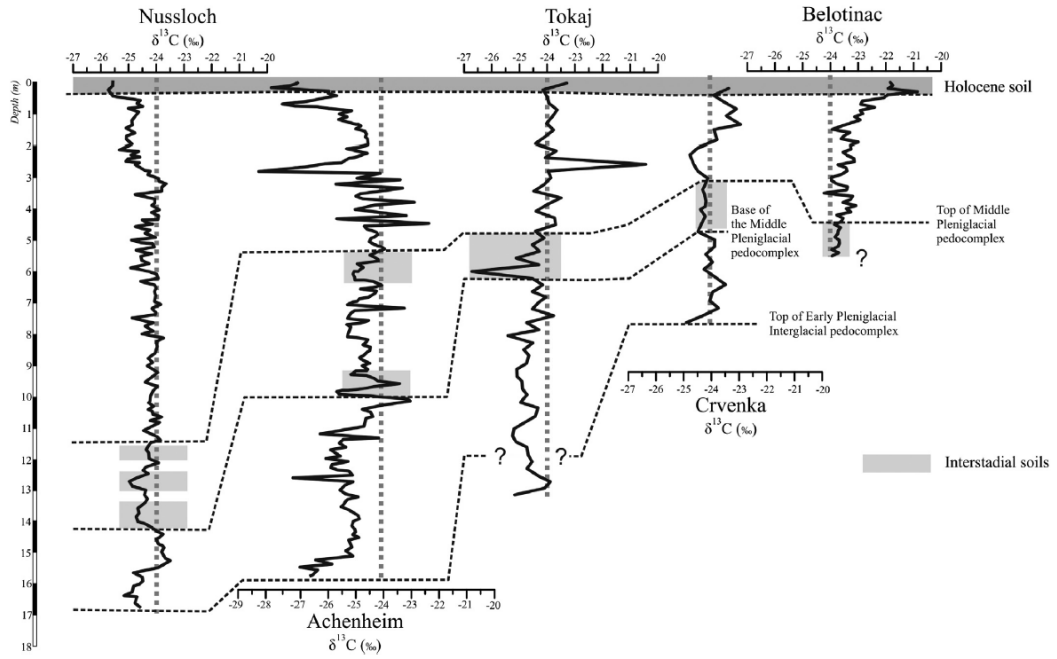

Figure 5.7: The $\delta^{13}C_{org}$ records in the European loess/paleosols sequences. Source: Obreht et al. (2014).

A different scenario can be found in Chinese loess profiles where the higher $\delta^{13}C_{org}$ (around -20 ‰) is characteristic for paleosols and indicates higher temperatures that are convenient for the expansion of C4 plants (Jiamao et al., 1996; Porter et al., 2001; Li and Liu, 2003; Kaakinen et al., 2006; Ning et al., 2006; Rao et al., 2015).

The studies recording the composition of stable isotopes $\delta^{13}C$ and $\delta^{18}O$ from pedogenic carbonates are completely missing in the Czech Republic. However, the results from this thesis can be compared with studies on loess carbonates from Ukraine by Boguckyj et al. (2006), from Poland by Lacka et al. (2009) and from the Nussloch profile (Germany) by

Gocke et al. (2010 and 2011). The Bůhzdař profile is unique in the continuous presence of calcified root cells or rhizoliths and several horizons with loess dolls in different depths. Boguckyj et al. (2006) and Lacka et al. (2009) report different values of stable isotopes of different pedogenic carbonates: rhizoliths from -11.5 ‰ to -8.5 ‰ of $\delta^{13}C$ and from –5.5 ‰ to -8.0 ‰ of $\delta^{18}O$, calcified root cells from -23 ‰ to -14 ‰ of $\delta^{13}C$ and -14 ‰ to -11 ‰ of $\delta^{18}O$. The isotopic composition of loess dolls (concretions) is only available for the Ukrainian location with quite a narrow range of values, from -10.1 ‰ to -8.7 ‰ of $\delta^{13}C$ and from -9.1 ‰ to -6.5 ‰ of $\delta^{18}O$ (Boguckyj et al., 2006). Those values of isotopic composition of loess dolls correspond well with the Bůhzdař loess doll samples (Tab. 4.5) with average values of -9.01 ‰ for $\delta^{13}C$ and -6.16 ‰ for $\delta^{18}O$. Only rhizoliths were reported in the Nussloch profile, with values around -10.9 ‰ of $\delta^{13}C$, similar to the isotope composition of rhizoliths in other profiles (Gocke et al., 2011).

It was expected that the isotopic composition of the calcified roots and rhizoliths would be reflecting the surrounding horizons (lower values in the paleosols and higher in the loess). Thus, the calcified root cells and the rhizoliths were not distinguished. However, the rhizoliths are more abundant in the deeper horizons (Chernozemic paleosol I and II, Paleosol/loess and Loess V) where the values of $\delta^{13}C$ and $\delta^{18}O$ are higher (Fig. 4.11).

The stable isotopes $\delta^{13}C$ and $\delta^{18}O$ record from pedogenic carbonates is not applicable for the reconstruction of paleoenvironment without dating of the pedogenic carbonates samples. The formation of pedogenic carbonates depends on the hydric conditions in the soil and most of the pedogenic carbonates were formed after the formation of surrounding material, especially in the paleosols (Gocke et al., 2010).

5.5. Paleoclimate transfer functions

The paleoclimate transfer functions reconstructing mean annual temperatures (MAT) and mean annual precipitation (MAP) published by Sheldon et al. (2002), Sheldon and Tabor (2009), Hall and Penner (2013) or Tabor and Myers (2015) are very useful and provide a clearer interpretation of geochemical data. However, these functions were conceived for a climate different from the prevailing climate in Central Europe. Unfortunately, most of those functions used in the Bůhzdař profile do not give reliable results, e.g. giving higher temperatures for the period of loess formation than during the period of paleosols formation (Tab. 4.6). The most relevant paleoclimate transfer function for the Bůhzdař profile seems to be a function conceived for the reconstruction of mean annual precipitation in the environment of Mollisols (MAP1) by Sheldon et al. (2002). Mollisols are in the USDA Soil Taxonomy equal to Chernozems in the World Reference Base and occur in a similar

environment (Vysloužilová et al., 2016). The approximation of mean annual precipitation according to this function is 276–439 mm per year for loess and 605–711 mm per year for paleosols. The results of the function transferring the $\delta^{13}C_{org}$ values into mean annual temperature and precipitation by Hall and Penner (2013) are appropriate only for paleosols (MAT 7.3 °C and MAP 533 mm) with similar $\delta^{13}C_{org}$ values as now days because this function was conceived for the environment of New Mexico (USA) where warmer and dryer periods are connected with C4 plant occurrence. C4 plants have distinctly higher $\delta^{13}C_{org}$ values than the C3 plants dominating in Central Europe. Therefore, the results of MAT are inverse (Tab. 4.6) and the estimates of MAT and MAP during the formation of loess and paleosols show little difference. Nevertheless, Schatz et al. (2015) used the paleoclimate transfer functions based on XRF and $\delta^{13}C_{org}$ values for the reconstruction of paleoclimate during the formation of both loess and paleosols in the Tokaj profile (Hungary).

6. Conclusion

The data from multiproxy evidence provided valuable information about paleoenvironment changes. The variable analyses coincide and confirm the main signs of evidence, namely loess and paleosols, of the two most different paleoenvironments in the Late Pleistocene. The grains are coarser in the loess than in the paleosols. The paleosols contain more SiO_2 (quartz and phyllosilicates) and less CaO (calcite and dolomite) than the loess. The amount of total organic carbon is higher in the paleosols than in the loess and the amount of stable isotope $\delta^{13}C$ from organic matter is lower in the paleosols than in the loess.

Using a comparison with other loess/paleosol sequences, the Bůhzdař profile can be conclusively divided into 8 different horizons, confirming the division expected after a preliminary visual inspection (Fig. 6.1). Nevertheless, two loess horizons (Loess II and Loess IV) display signs of slightly developed soils and can be interpreted as initial soils, according to Reuter (2000) as the paleo-relict Leptosols. The main part of the paleosol of the horizon of Loess II (paleo-relict Leptosol I) was probably eroded (Ložek VIII. 2016, in verb). In the horizon of Loess IV (paleo-relict Leptosol II) the measured values are continuously changing from values typical for loess to values typical for chernozemic paleosol. This can be interpreted as a gradual change of environment with probable fluctuations as can be seen in the stable isotope $\delta^{13}C$ record from organic matter. Unfortunately, the measured data did not permit to determine if the Chernozemic paleosol I was formed as a colluvium or as a Chernozem under different conditions than the Chernozemic paleosol II that shows characteristics of the paleo-relict Chernozem. It is possible to classify the Chernozemic paleosol I as a paleo-relict Chernozemic soil and the Chernozemic paleosol II as a paleo-relict Chernozem (Reuter, 2000). The underlying horizon named as Loess/paleosol has signs of more intensive alteration than the other paleosols and slight signs of illuviation, thus it can be indicated as a paleo-relict Luvisol (Reuter, 2000). However, those paleosols were definitely affected by erosion that was present also during the glaciation (presence of ice wedges, cryoturbation or layers of marl flakes arranged in layers probably caused by solifluction) because the study profile is situated in a gentle slope. Compared to the other studied profiles in Europe (Hatté et al, 1998 and 1999; Antoine et al., 2013; Hatté et al., 2013; Zech et al, 2013; Obrecht et al., 2014; Hošek et al., 2015), it is possible to find parallels between the Bůhzdař profile horizons and the generally accepted paleosols, the pedocomplexes (PK), defined by Kukla (1977). The Leptosol (Loess II) is likely equal to PK I, the Chernozemic paleosol I and II and the Luvisol (Loess/paleosol) can be equal to the PK II–PK III. Further dating would be helpful for the final profile description because the Bůhzdař profile was definitely affected by the erosion in the past.

With the help of the paleoclimate transfer functions using the data from XRF it is possible to estimate paleo-precipitation using the XRF data. For the period of loess formation the precipitation was around 300 mm per year and for the period of formation paleo-relict Leptosol 400–500 mm per year, for the paleo-relict Chernozem around 600 mm per year and for the paleo-relict Luvisol around 700 mm per year. However, the estimates of precipitation amount reflect mostly the water availability in the soil and the real precipitation could be lower caused by lower evaporation from the soil during the cold periods. From the results of the stable isotope $\delta^{13}C$ record from organic matter it is possible to determine that the temperatures during the formation of paleo-relict Chernozem were similar to recent temperatures. Those results correspond well with investigation and paleomalacofauna analysis by Ložek (1952).

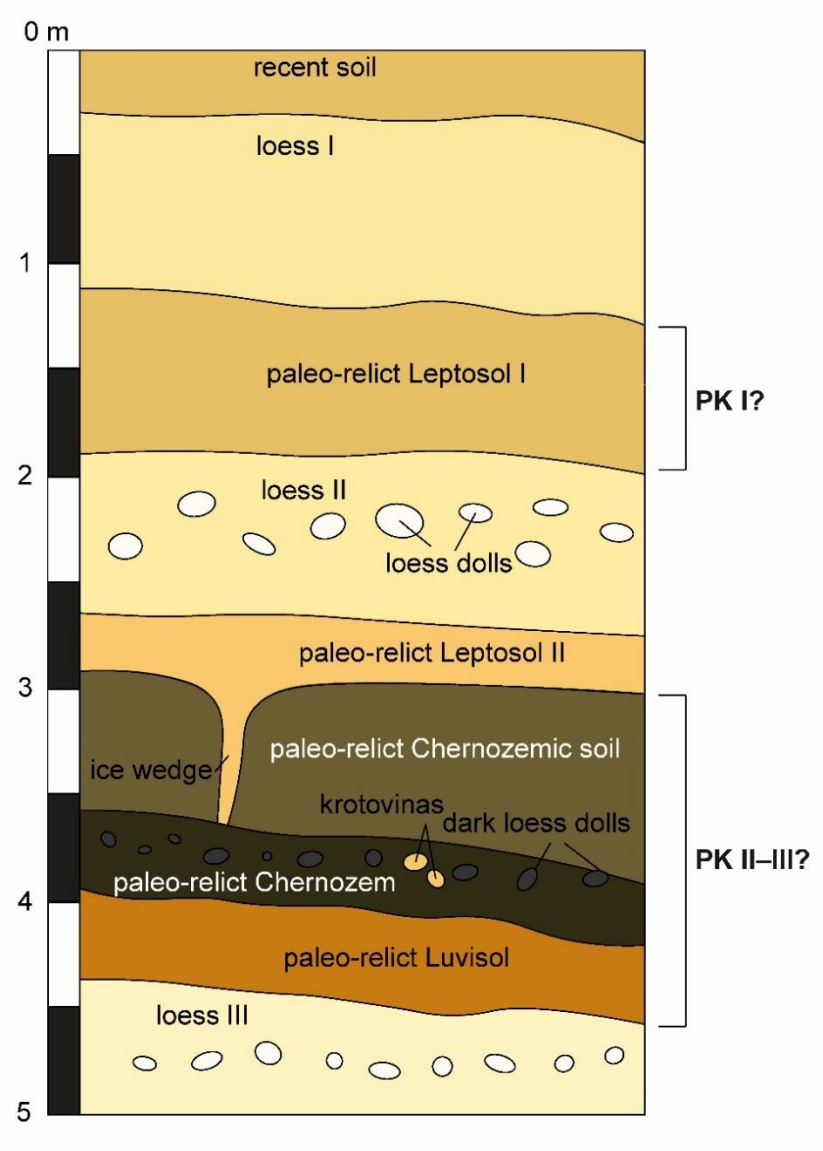

Figure 6.1: Final description of the Bůhzdař profile with determined paleosols and pedocomplexes (PK).

7. References

7.1. Literature

ANTOINE, P., ROUSSEAU, D.-D., DEGEAI, J.-P., MOINE, O., LAGROIX, F., KREUTZER, S., FUCHS, M., HATTÉ, C., GAUTHIER, C., SVOBODA, J. and LISÁ, L. (2013): High-resolution record of the environmental response to climatic variations during the Last Interglacial–Glacial cycle in Central Europe: the loess-palaeosol sequence of Dolní Věstonice (Czech Republic). Quaternary Science Reviews, 67, p. 17–38.

ANTOINE, P., ROUSSEAU, D.-D., MOINE, O., KUNESCH, S., HATTÉ, C., LANG, A., TISSOUX, H. and ZÖLLER, L. (2009): Rapid and cyclic aeolian deposition during the Last Glacial in European loess: a high-resolution record from Nussloch, Germany. Quaternary Science Reviews, 28, no. 25–26, p. 2955–2973.

BALATKA, B. and KALVODA, J. (2006): Geomorfologické členění reliéfu Čech. Kartografie Praha, Praha, 79 p.

BARTA, G. (2011): Secondary carbonates in loess-paleosoil sequences: a general review. Open Geosciences, 3, no. 2.

BARTA, G. (2014): Paleoenvironmental reconstruction based on the morphology and distribution of secondary carbonates of the loess-paleosol sequence at Süttő, Hungary. Quaternary International, 319, p. 64–75.

BERTRAN, P. et al. (2014): Distribution and chronology of Pleistocene permafrost features in France: Database and first results: Pleistocene permafrost features in France. Boreas, 43, no. 3, p. 699–711.

BRINDLEY, G. W. (1952): Identification of Clay Minerals by X-ray Diffraction Analysis. Clays and Clay Minerals, 1, no. 1, p. 119–129.

BUSACCA, A. J. and SWEENEY, M. R. (2005): LOESS. In: Encyclopedia of Soils in the Environment. Elsevier, p. 364–373.

CHEN, J., AN, Z. and HEAD, J. (1999): Variation of Rb/Sr Ratios in the Loess-Paleosol Sequences of Central China during the Last 130,000 Years and Their Implications for Monsoon Paleoclimatology. Quaternary Research, 51, no. 3, p. 215–219.

CHESWORTH, W. ed. (2008): Encyclopedia of soil science: [glossary terms included]. Springer, Dordrecht, 902 p.

CHLUPÁČ, I. (2002): Geologická minulost České republiky. Academia, Praha, 436 p.

CILEK, V. (2001): The loess deposits of the Bohemian Massif: silt provenance, palaeometeorology and loessification processes. Quaternary International, 76–77, p. 123–128.

COLLATZ, G. J., BERRY, J. A. and CLARK, J. S. (1998): Effects of climate and atmospheric CO 2 partial pressure on the global distribution of C 4 grasses: present, past, and future. Oecologia, 114, no. 4, p. 441–454.

COLLINS, R. P. and JONES, M. B. (1986): The influence of climatic factors on the distribution of C4 species in Europe. Vegetatio, 64, no. 2–3, p. 121–129.

DEMEK, J., MACKOVČIN, P. and BALATKA, B. (2006): Hory a nížiny: zeměpisný lexikon ČR. AOPK ČR, Brno.

DODONOV, A. E. (2013): LOESS RECORDS | Central Asia. In: Encyclopedia of Quaternary Science. Elsevier, p. 585–594.

DREWNIK, M., SKIBA, M., SZYMAŃSKI, W. and ŻYŁA, M. (2014): Mineral composition vs. soil forming processes in loess soils — A case study from Kraków (Southern Poland). CATENA, 119, p. 166–173.

ELIAS, S. A. (2007): Encyclopedia of Quaternary science. Elsevier, Amsterdam, Netherlands; Boston [Mass.

FRECHEN, M. (2003): Loess in Europe—mass accumulation rates during the Last Glacial Period. Quaternary Science Reviews, 22, no. 18–19, p. 1835–1857.

FRECHEN, M., ZANDER, A., CÍLEK, V. and LOŽEK, V. (1999): Loess chronology of the Last Interglacial/Glacial cycle in Bohemia and Moravia, Czech Republic. Quaternary Science Reviews, 18, no. 13, p. 1467–1493.

GALLET, S., JAHN, B. and TORII, M. (1996): Geochemical characterization of the Luochuan loess-paleosol sequence, China, and paleoclimatic implications. Chemical Geology, 133, no. 1–4, p. 67–88.

GALLET, S., JAHN, B., VAN VLIET LANOË, B., DIA, A. and ROSSELLO, E. (1998): Loess geochemistry and its implications for particle origin and composition of the upper continental crust. Earth and Planetary Science Letters, 156, no. 3–4, p. 157–172.

GHAFARPOUR, A., KHORMALI, F., BALSAM, W., KARIMI, A. and AYOUBI, S. (2016): Climatic interpretation of loess-paleosol sequences at Mobarakabad and Aghband, Northern Iran. Quaternary Research, 86, no. 1, p. 95–109.

GOLDBERG, K. and HUMAYUN, M. (2010): The applicability of the Chemical Index of Alteration as a paleoclimatic indicator: An example from the Permian of the Paraná Basin, Brazil. Palaeogeography, Palaeoclimatology, Palaeoecology, 293, no. 1–2, p. 175–183.

HAN, J., KEPPENS, E., LIU, T., PAEPE, R. and JIANG, W. (1997): Stable isotope composition of the carbonate concretion in loess and climate change. Quaternary International, 37, p. 37–43.

HASINGER, O., SPANGENBERG, J. E., MILLIÈRE, L., BINDSCHEDLER, S., CAILLEAU, G. and VERRECCHIA, E. P. (2015): Carbon dioxide in scree slope deposits: A pathway from atmosphere to pedogenic carbonate. Geoderma, 247–248, p. 129–139.

HATTÉ, C., FONTUGNE, M., ROUSSEAU, D.-D., ANTOINE, P., ZÖLLER, L., LABORDE, N. T. and BENTALEB, I. (1998): δ13C variations of loess organic matter as a record of the vegetation response to climatic changes during the Weichselian. Geology, 26, no. 7, p. 583.

HATTÉ, C., GAUTHIER, C., ROUSSEAU, D.-D., ANTOINE, P., FUCHS, M., LAGROIX, F., MARKOVI&CACUTE;, S. B., MOINE, O. and SIMA, A. (2013): Excursions to C4 vegetation recorded in the Upper Pleistocene loess of Surduk (Northern Serbia): an organic isotope geochemistry study. Climate of the Past, 9, no. 3, p. 1001–1014.

HILLEL, D. and HATFIELD, J. L. eds. (2005): Encyclopedia of soils in the environment. Elsevier/Academic Press, Oxford, UK ; Boston, 4 p.

HOŠEK, J., HAMBACH, U., LISÁ, L., GRYGAR, T. M., HORÁČEK, I., MESZNER, S. and KNÉSL, I. (2015): An integrated rock-magnetic and geochemical approach to loess/paleosol sequences from Bohemia and Moravia (Czech Republic): Implications for the Upper Pleistocene paleoenvironment in central Europe. Palaeogeography, Palaeoclimatology, Palaeoecology, 418, p. 344–358.

HRADILOVÁ, J. (1994): New micromorphological knowledge of the last Pleistocene glacial cycle in the loess profile at Praha-Sedlec. Journal of the Czech Geological Society, 39, no. 4, p. 319–329.

HRNČIAROVÁ, T., MINISTERSTVO ŽIVOTNÍHO PROSŤREDÍ ČESKÉ REPUBLIKY (PRAHA) and VÝZKUMNY ÚSTAV SILVA TAROUCY PRO KRAJINU A OKRASNÉ ZAHRADNICTVÍ (PRŮHONICE) (2009): Atlas krajiny České republiky = Landscape atlas of the Czech Republic. Ministerstvo životního prostředí České republiky [etc., Praha [etc.

HUANG, P. M., LI, Y. and SUMNER, M. E. eds. (2012): Properties and processes. CRC Press, Boca Raton, Fla., 1442 p.

KAAKINEN, A., SONNINEN, E. and LUNKKA, J. P. (2006): Stable isotope record in paleosol carbonates from the Chinese Loess Plateau: Implications for late Neogene paleoclimate and paleovegetation. Palaeogeography, Palaeoclimatology, Palaeoecology, 237, no. 2–4, p. 359–369.

KACHLÍK, V., CHLUPÁČ, I., UNIVERZITA KARLOVA, PŘÍRODOVĚDECKÁ FAKULTA and KATEDRA GEOLOGIE (1996): Základy geologie. Karolinum, Praha.

KALM, V. E., RUTTER, N. W. and ROKOSH, C. D. (1996): Clay minerals and their paleoenvironmental interpretation in the Baoji loess section, Southern Loess Plateau, China. CATENA, 27, no. 1, p. 49–61.

KHORMALI, F. and KEHL, M. (2011): Micromorphology and development of loess-derived surface and buried soils along a precipitation gradient in Northern Iran. Quaternary International, 234, no. 1–2, p. 109–123.

KŘÍŽEK, M., NYPLOVÁ, P. and KYSILKA, T. (2011): Ledové klíny a jejich vztah ke klimatu. Geografické rozhledy, 20, no. 5, p. 28–29.

KUBIENA, W. L. (1953): Bestimmungsbuch und Systematik der Böden Europas. Enke, Stuttgart, 392 p.

KUBIENA, W. L. and LOŽEK, V. (no date): Survey of Czechoslovak Quaternary: Soils.

KUKLA, G. J. (1969): The cause of the Holocene climate change. Geolie en Mijnbouw, 48, no. 3, p. 307–334.

KUKLA, G. J. (1975): Loess Stratigraphy of Central Europe. In: Butzer, K. W. and Isaac, G. L. (eds.): After the Australopithecines. DE GRUYTER MOUTON, Berlin, New York.

KUKLA, G. J. (1977): Pleistocene land—sea correlations I. Europe. Earth-Science Reviews, 13, no. 4, p. 307–374.

LI, Y. and LIU, T. (2003): δ13C values of the loess-paleosol sequence in Dali area, Shaanxi Province, China, and paleoenvironmental implications. Chinese Science Bulletin, 48, no. 9, p. 902.

LISÁ, L. and UHER, P. (2006): Provenance of Wurmian loess and loess-like sediments of Moravia and Silesia (Czech Republic): a study of zircon typology and cathodoluminiscence. Geologica carpatica, 57, no. 5, p. 397–403.

LOŽEK, V. (1964): Quartarmollusken der Tschechoslowakei. Praha, 374 p.

LOŽEK, V. (1973): Příroda ve čtvrtohorách. Academia, Praha, 372 p.

LOŽEK, V. (2007): Zrcadlo minulosti: česká a slovenská krajina v kvartéru. Dokořán, Praha, 198 p.

LOŽEK, V. (2011): Po stopách pravěkých dějů: O silách, které vytvářely naši krajinu. Dokořán, Praha, 181 p.

LOŽEK, V., CÍLEK, V. and KUBÍKOVÁ, J. eds. (2003): Střední Čechy: příroda, člověk, krajina. Dokořán, Praha, 127 p.

LYONS, H. A., THOMAS, J. S., HEURICH, A. E., SHEPHERD, D. A. and WETMORE, S. D. (1976): Efficacy of doxycycline in acute infections of the lower respiratory tract. Current Therapeutic Research, Clinical and Experimental, 19, no. 1, p. 24–31.

MACKOVČIN, P. and MUDRA, P. eds. (2005): Střední Čechy. AOPK ČR [u.a.], Praha, 902 p.

MANFRED FRECHEN (2011): Loess in Europe.

MARKOVIĆ, S. B., BOKHORST, M. P., VANDENBERGHE, J., MCCOY, W. D., OCHES, E. A., HAMBACH, U., GAUDENYI, T., JOVANOVIĆ, M., ZÖLLER, L., STEVENS, T. and MACHALETT, B. (2008): Late Pleistocene loess-palaeosol sequences in the Vojvodina region, north Serbia. Journal of Quaternary Science, 23, no. 1, p. 73–84.

MARKOVIĆ, S., B., KOSTIĆ, N., S. and OCHES, E. A. (2004): Paleosols in the Ruma loess section (Vojvodina, Serbia). Revista Mexicana de Ciencias Geológicas, 2004, no. 21, p. 79–87.

MAŠEK, J. (1990): Vysvětlivky k základní geologické mapě ČSSR l:25000, l2-232 Buštěhrad.- Ústř.úst.geol. Praha.

MCCANN, T. (2008): The geology of central Europe: Volume 1: Precambrian and Paleozoic. Geological Society, London.

MCLENNAN, S. M. (1993): Weathering and Global Denudation. The Journal of Geology, 101, no. 2, p. 295–303.

MUHS, D. R. (2007): LOESS DEPOSITS, ORIGINS AND PROPERTIES. In: Encyclopedia of Quaternary Science. Elsevier, p. 1405–1418.

MUHS, D. R. (2013): The geologic records of dust in the Quaternary. Aeolian Research, 9, p. 3–48.

NĚMEČEK, J., SMOLÍKOVÁ, L. and KUTÍLEK, M. (1990): Pedologie a paleopedologie. Academia, Praha, 546 p.

NESBITT, H. W. and YOUNG, G. M. (1982): Early Proterozoic climates and plate motions inferred from major element chemistry of lutites. Nature, 299, no. 5885, p. 715–717.

NING, Y., LIU, W. and AN, Z. (2006): Variation of soil Δδ 13C values in Xifeng loess-paleosol sequence and its paleoenvironmental implication. Chinese Science Bulletin, 51, no. 11, p. 1350–1354.

OBREHT, I., BUGGLE, B., CATTO, N., MARKOVIČ, S. B., BÖSEL, S., VANDENBERGHE, D. A. G., HAMBACH, U., SVIRČEV, Z., LEHMKUHL, F., BASARIN, B., GAVRILOV, M. B. and JOVIĆ, G. (2014): The Late Pleistocene Belotinac section (southern Serbia) at the southern limit of the European loess belt: Environmental and climate reconstruction using grain size and stable C and N isotopes. Quaternary International, 334–335, p. 10–19.

O'LEARY, M. H. (1988): Carbon Isotopes in Photosynthesis. BioScience, 38, no. 5, p. 328–336.

PELÍŠEK, J. (1936): O moravských černozemích. Příroda, XXIX, no. 10, p. 294–289.

POKORNÝ, P. (2011): Neklidné časy: kapitoly ze společných dějin přírody a lidí. Dokořán, Praha, 369 p.

PORTER, S. C. (2007): LOESS RECORDS | China. In: Encyclopedia of Quaternary Science. Elsevier, p. 1429–1440.

PYE, K. (1987): Aeolian dust and dust deposits. Academic Press, London ; Orlando, 334 p.

PYE, K. (1995): The nature, origin and accumulation of loess. Quaternary Science Reviews, 14, no. 7–8, p. 653–667.

RAO, Z., GUO, W., XIE, L., HUANG, C., LIU, X., HUA, H. and CHEN, F. (2015): High resolution δ13CTOC and magnetic susceptibility data from the late Early Pleistocene southern margins of the Chinese Loess Plateau. Organic Geochemistry, 87, p. 78–85.

REUTER, G. (2000): A logical system of paleopedological terms. CATENA, 41, no. 1–3, p. 93–109.

ROBERTS, H. M., MUHS, D. R. and BETTIS, E. A. (2007): LOESS RECORDS | North America. In: Encyclopedia of Quaternary Science. Elsevier, p. 1456–1466.

ROUSSEAU, D.-D., DERBYSHIRE, E., ANTOINE, P. and HATTÉ, C. (2007): LOESS RECORDS | Europe. In: Encyclopedia of Quaternary Science. Elsevier, p. 1440–1456.

ŠANTRŮČEK, J., ŠANTRŮČKOVÁ, H., KAŠTOVSKÁ, E., KVĚTOŇ, J. and TAHOVSKÁ, K. (2014): Stabilní izotopy a jejich použití v biologii a ekologii. Jihočeská univerzita v Českých Budějovicích, České Budějovice, 111 p.

SCHULZE, D. G. (2005): CLAY MINERALS. In: Encyclopedia of Soils in the Environment. Elsevier, p. 246–254.

SHELDON, N. D., RETALLACK, G. J. and TANAKA, S. (2002): Geochemical Climofunctions from North American Soils and Application to Paleosols across the Eocene-Oligocene Boundary in Oregon. The Journal of Geology, 110, no. 6, p. 687–696.

SHELDON, N. D. and TABOR, N. J. (2009): Quantitative paleoenvironmental and paleoclimatic reconstruction using paleosols. Earth-Science Reviews, 95, no. 1–2, p. 1–52.

SHI, C., ZHU, R., GLASS, B. P., LIU, Q., ZEMAN, A. and SUCHÝ, V. (2003): Climate variations since the last interglacial recorded in Czech loess. Geophysical Research Letters, 30, no. 11.

SMALLEY, I., MARKOVIĆ, S. B. and SVIRČEV, Z. (2011): Loess is [almost totally formed by] the accumulation of dust. Quaternary International, 240, no. 1–2, p. 4–11.

TABOR, N. J. and MYERS, T. S. (2015): Paleosols as Indicators of Paleoenvironment and Paleoclimate. Annual Review of Earth and Planetary Sciences, 43, no. 1, p. 333–361.

TAYLOR, S. ., MCLENNAN, S. . and MCCULLOCH, M. . (1983): Geochemistry of loess, continental crustal composition and crustal model ages. Geochimica et Cosmochimica Acta, 47, no. 11, p. 1897–1905.

VYSLOUŽILOVÁ, B., DANKOVÁ, L., ERTLEN, D., NOVÁK, J., SCHWARTZ, D., ŠEFRNA, L., DELHON, C. and BERGER, J.-F. (2014): Vegetation history of chernozems in the Czech Republic. Vegetation History and Archaeobotany, 23, no. S1, p. 97–108.

VYSLOUŽILOVÁ, B., ERTLEN, D., SCHWARTZ, D. and ŠEFRNA, L. (2016): Chernozem. From concept to classification: a review. AUC GEOGRAPHICA, 51, no. 1, p. 85–95.

VYSLOUŽILOVÁ, B., ERTLEN, D., ŠEFRNA, L., NOVÁK, T., VIRÁGH, K., RUÉ, M., CAMPANER, A., DRESLEROVÁ, D. and SCHWARTZ, D. (2015): Investigation of vegetation history of buried chernozem soils using near-infrared spectroscopy (NIRS). Quaternary International, 365, p. 203–211.

ŽEBERA, K. (1958): Československo ve starší době kamenné. Nakladatelství Československé akademie věd, Praha, 214 p.

ZECH, M., ZECH, R., ZECH, W., GLASER, B., BRODOWSKI, S. and AMELUNG, W. (2008): Characterisation and palaeoclimate of a loess-like permafrost palaeosol sequence in NE Siberia. Geoderma, 143, no. 3–4, p. 281–295.

ZECH, R., ZECH, M., MARKOVIĆ, S., HAMBACH, U. and HUANG, Y. (2013): Humid glacials, arid interglacials? Critical thoughts on pedogenesis and paleoclimate based on multi-proxy analyses of the loess–paleosol sequence Crvenka, Northern Serbia. Palaeogeography, Palaeoclimatology, Palaeoecology, 387, p. 165–175.

7.2. Other sources

BABECHUK, M., WIDDOWSON, M. and KAMBER, B. S. (2013): Chemical weathering index calculations spreadsheet. [electronic resource] https://www.tcd.ie/Geology/assets/doc/WeatheringIndexCalculations.xlsx (downloaded on 7th of July 2016)

BLOTT, S. J. and PYE, K. (2001): GRADISTAT: a grain size distribution and statistics package for the analysis of unconsolidated sediments. Earth Surface Processes and Landforms, 26, no. 11, p. 1237–1248. [electronic resource] http://doi.wiley.com/10.1002/esp.261 (downloaded on 7th of July 2016)

DIBAVOD (2013): Digitální báze vodohospodářských dat, VÚV TGM, [electronic resource] URL:http://www.dibavod.cz

Geologická mapa 1 : 50 000: Czech Geological Survey, [electronic resource] http://www.geologicke-mapy.cz (downloaded on 7th of January 2016)

Geologická mapa 1 : 500 000: Czech Geological Survey, [electronic resource] http://www.geologicke-mapy.cz (downloaded on 7th of January 2016)

Klimadiagramme weltweit. [electronic resource] http://www.Klimadiagramme.de (downloaded on 7th of June 2016)

Mapy.cz. [electronic resource] http://www.Mapy.cz (downloaded on 7th of June 2016)

Obec Zájezd. [electronic resource] http://www.obeczajezd.iprostor.cz , (downloaded on 7th of June 2016)

Souhrnné mapy VÚMOP. [electronic resource] http://www.Mapy.VÚMOP.cz (downloaded on 7th of June 2016)

ZM 200: Základní mapa ČR 1: 200 000, ČÚZK, dostupné na URL: http://geoportal.cenia.cz (downloaded on 7th of January 2016)

7.3. Software

ESRI (2010): ArcMap 10.0

MATLAB 7.8.0 (2009)

Microsoft (2010): Excel 2010

8. Appendix

Appendix 1

```
 Varia=char('Ca','Fe','Mg','Mn','Sr'); % les noms des variables
D=VERCORS(:,3:7); % les data quantitatives
plotmatrix(Data);

M = Data;
%%
Z=zscore(M);
R=corrcoef(Z);
[V,la]=eig(R); % V : vectuers propres; la : valeurs propres

%%
la=diag(la);
Tableau=[(flipud(la))./20 cumsum(flipud(la)./20)];
disp(Tableau);

%% Projection des points sur axes 1 et 2
CPn=Z*V;
figure(4)
plot(CPn(:,end),CPn(:,end-1),'+r');

%% Cercle des correlations
figure(5);
x=0:0.1:(2*pi)+0.1;
plot(sin(x),cos(x),'-k');
axis square
hold on;
plot(0.8*sin(x),0.8*cos(x),'-k');
plot([-1 1],[0 0],'-k');
plot([0 0],[-1 1],'-k');

%% Calcul et projection des correlations entre CP et variables
K=repmat(la,1,20)';
rCP=sqrt(K).*V;
plot(rCP(:,end),rCP(:,end-1),'or');
gname(Varia)

%% Classification
Y=pdist(CPn);
%Dend=linkage(Y,'single');
Dend10=linkage(Y,'ward');
%dendrogram(Dend,0);
%figure(1)
%dendrogram(Dend,0,'orientation','left','colorthreshold',21);
figure(5)
dendrogram(Dend10,0,'orientation','left','colorthreshold',6,'labels',Nom);
%Coph=[cophenet(Dend,Y) cophenet(Dend2,Y)]

%% Groupes pour ACP
T10=cluster(Dend10,'maxclust',5);
figure
gscatter(CPn(:,end),CPn(:,end-1),T10);% prendre les derniere et avant-derniere colonnes↙
des coef ACP (CPn)
```